

JW 288

NSWC/WOL/TR 75-162

NSWC/WOL/TR 75-162

NSWC **TECHNICAL** **REPORT** **WOL**

WHITE OAK LABORATORY

S.E.R.A. X. THE AZIALLY SLOTTED INFINITE CYLINDER — INTERNAL AND NEAR APERTURE FIELDS: SURFACE CURRENT, APERTURE FIELD AND B.S.C.S. FOR INTERMEDIATE SLOT ANGLES

JANUARY 1976

**NAVAL SURFACE WEAPONS CENTER
WHITE OAK LABORATORY
SILVER SPRING, MARYLAND 20910**

- Approved for public release; distribution unlimited

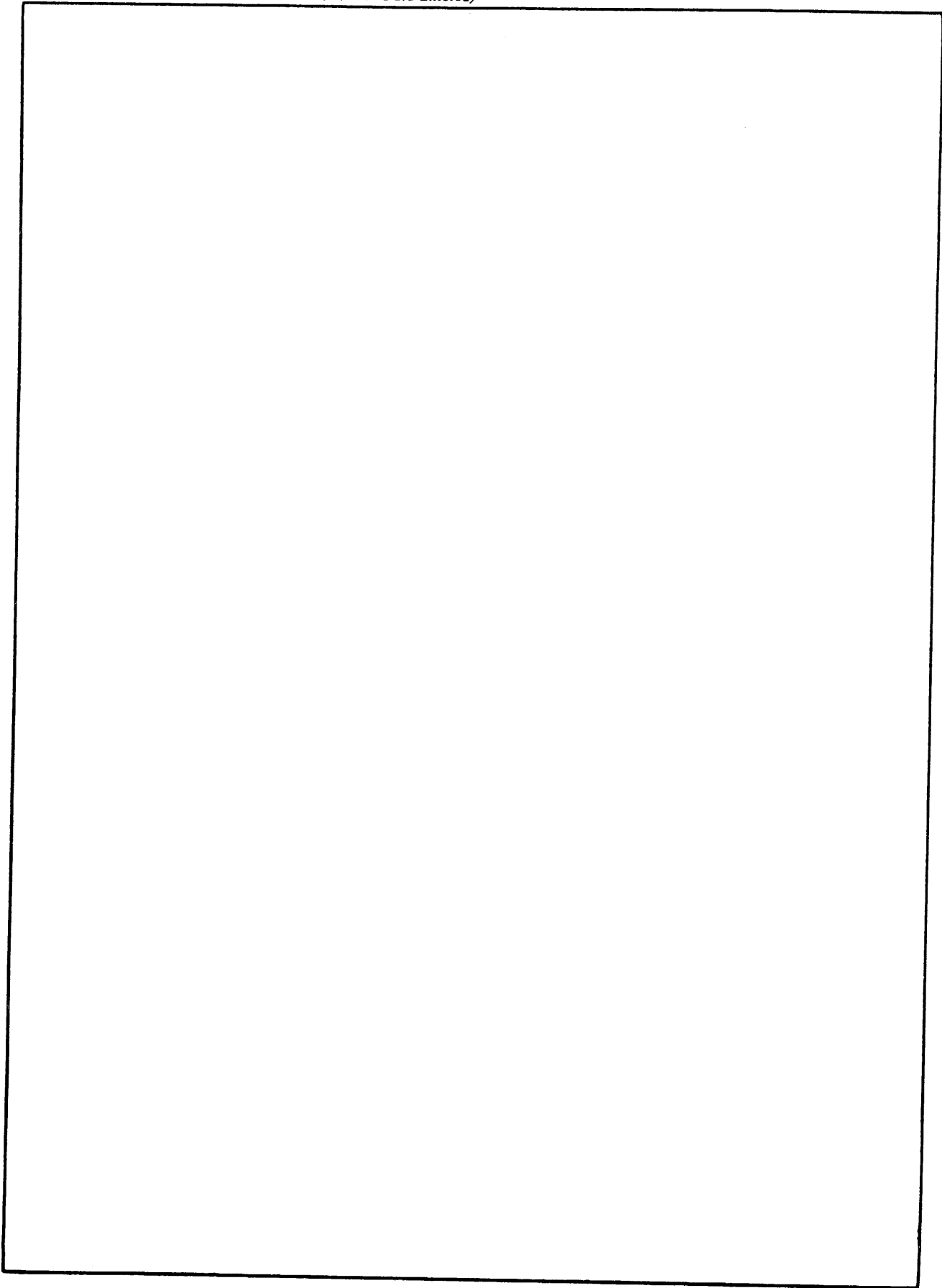
**NAVAL SURFACE WEAPONS CENTER
WHITE OAK, SILVER SPRING, MARYLAND 20910**

UNCLASSIFIED

SECURITY CLASSIFICATION OF THIS PAGE (When Data Entered)

REPORT DOCUMENTATION PAGE		READ INSTRUCTIONS BEFORE COMPLETING FORM
1. REPORT NUMBER NSWC/WOL/TR 75-162	2. GOVT ACCESSION NO.	3. RECIPIENT'S CATALOG NUMBER
4. TITLE (and Subtitle) "S.E.R.A. X. The Axially Slotted Infinite Cylinder - Internal and Near Aperture Fields. Surface current, Aperture Field and B.S.C.S. For Intermediate Slot Angles"		5. TYPE OF REPORT & PERIOD COVERED Topical Report
		6. PERFORMING ORG. REPORT NUMBER
7. AUTHOR(s) L. F. Libelo, A. G. Henney, J. N. Bombardt, F. S. Libelo		8. CONTRACT OR GRANT NUMBER(s)
9. PERFORMING ORGANIZATION NAME AND ADDRESS Naval Surface Weapons Center White Oak Laboratory Silver Spring, Maryland 20910		10. PROGRAM ELEMENT, PROJECT, TASK AREA & WORK UNIT NUMBERS NMAT-03L-000/ZR011-01-01 DNA-EB088-52 HDL-E052E6 Subtask EB-088
11. CONTROLLING OFFICE NAME AND ADDRESS		12. REPORT DATE January 1976
		13. NUMBER OF PAGES 96
14. MONITORING AGENCY NAME & ADDRESS (if different from Controlling Office)		15. SECURITY CLASS. (of this report) UNCLASSIFIED
		15a. DECLASSIFICATION/DOWNGRADING SCHEDULE
16. DISTRIBUTION STATEMENT (of this Report) Approved for public release, distribution unlimited		
17. DISTRIBUTION STATEMENT (of the abstract entered in Block 20, if different from Report)		
18. SUPPLEMENTARY NOTES The effort was funded jointly by NSWC/WOL under the IR program and the Defense Nuclear Agency. Work was performed in collaboration with the Harry Diamond Laboratories, Washington, D.C.		
19. KEY WORDS (Continue on reverse side if necessary and identify by block number) Axially Slotted Conducting Cylinder Electromagnetic Scattering Interior Electric Field Distribution Exterior Near Electric Field Distribution Extension to Intermediate Slot Angles		
20. ABSTRACT (Continue on reverse side if necessary and identify by block number) The calculated interior electric field distributions and the near field region exterior to the slot field distributions are presented in this report. These are the fields for the infinite circular cylinder with an axial slot irradiated at normal, symmetric incidence. In addition results for aperture field, surface current and back-scattering cross-sections are given for intermediate size slot angles.		

SECURITY CLASSIFICATION OF THIS PAGE(When Data Entered)




SECURITY CLASSIFICATION OF THIS PAGE(When Data Entered)

30 January 1976

NSWC/WOL/TR 75-162

SCATTERING OF ELECTROMAGNETIC RADIATION BY APERTURES X. THE AXIALLY SLOTTED INFINITE CYLINDER-INTERNAL AND NEAR APERTURE FIELDS. SURFACE CURRENT, APERTURE FIELD AND B.S.C.S. FOR INTERMEDIATE SLOT ANGLES.

This report contains formal and numerical results of research into an electromagnetic diffraction problem. The study was performed jointly at the Naval Surface Weapons Center/White Oak and at the Harry Diamond Laboratories. These efforts were supported at the Naval Surface Weapons Center/White Oak partly by the Defense Nuclear Agency under Task DNA-EB088-52, and partly by the Independent Research Program (Task Number MAT-03L-000/ZR011-01-01). The Harry Diamond Laboratory effort was supported by the Defense Nuclear Agency under HDL Project: E052E6 under Subtask EB-088. In addition contributions to the study were made independently by one of the co-authors (F. S. Libelo). This document is for information only.



LEMMUEL L. HILL

TABLE OF CONTENTS

	Page
LIST OF FIGURES	3
LIST OF TABLES	5
I. INTRODUCTION	10
II. DERIVATION OF THE ELECTRIC FIELD INSIDE AND IN THE NEIGHBORHOOD OF THE SLOT	14
III. CALCULATED INTERIOR AND EXTERIOR ELECTRIC FIELDS	19
1. Radial Distribution Along the Symmetry Diameter Through the Slot	19
2. Radial Distribution Along An Asymmetric Ray Through the Slot	31
3. Radial Distribution Along the $\phi=90^\circ$ Ray.	35
4. Radial Distribution Along A Ray Inside But Just Beyond the Slot Edge, $\phi \approx \phi_0$	39
5. Radial Distribution Along An Asymmetric Ray Toward the Back Wall	43
IV. APERTURE ELECTRIC FIELD, SURFACE CURRENTS AND BACK-SCATTERING CROSS-SECTION	72
1. Aperture Electric Field and Surface Currents	72
2. Electric Field In the Slot At Resonance.	87
3. Back-Scattering Cross-Section.	89
V. COMMENTS ON THE COMPUTER PROGRAM	91
VI. CONCLUSIONS AND DISCUSSION	94
LIST OF REFERENCES.	96

LIST OF FIGURES

Figure	Title	Page
1	Geometry of the Scattering Problem for the Axially Slotted Cylinder	13
2	Radial Distribution of Electric Field Along $\phi=0^\circ$ Ray for $\gamma=1.000$ and Half Slot Angle ϕ_0 .	25
3	Radial Distribution of Electric Field Along $\phi=0^\circ$ Ray for $\gamma=2.000$ and Half Slot Angle ϕ_0 .	26
4	Radial Distribution of Electric Field Along $\phi=0^\circ$ Ray for $\gamma=3.830$ and Half Slot Angle ϕ_0 .	27
5	Radial Distribution of Electric Field Along $\phi=180^\circ$ Ray for $\gamma=1.00$ and Half Slot Angle ϕ_0 .	28
6	Radial Distribution of Electric Field Along $\phi=180^\circ$ Ray for $\gamma=2.00$ and Half Slot Angle ϕ_0 .	29
7	Radial Distribution of Electric Field Along $\phi=180^\circ$ Ray for $\gamma=3.830$ and Half Slot Angle ϕ_0 .	30
8	Radial Distribution of Electric Field For Ray Through Aperture, $\gamma=1.00$, Half Slot Angle ϕ_0 .	32
9	Radial Distribution of Electric Field For Ray Through Aperture, $\gamma=2.00$, Half Slot Angle ϕ_0 .	33
10	Radial Distribution of Electric Field For Ray Through Aperture, $\gamma=3.83$ and Half Slot Angle ϕ_0 .	34
11	Radial Distribution of Electric Field Along The $\phi=90^\circ$ Ray for $\gamma=1.000$ and Half Slot Angle ϕ_0 .	36
12	Radial Distribution of Electric Field Along $\phi=90^\circ$ Ray for $\gamma=2.00$ and Half Slot Angle ϕ_0 .	37
13	Radial Distribution of Electric Field Along The $\phi=90^\circ$ Ray for $\gamma=3.83$ and Half Slot Angle ϕ_0 .	38
14	Radial Distribution of Electric Field Along Ray Inside Cylinder, $\phi \neq \phi_0$, For $\gamma=1.000$ and Half Slot Angle ϕ_0 .	40
15	Radial Distribution of Electric Field Along Ray Inside Cylinder, $\phi \neq \phi_0$, For $\gamma=2.00$ and Half Slot Angle ϕ_0 .	41

LIST OF FIGURES (Contd)

Figure	Title	Page
16	Radial Distribution of Electric Field Along Ray Inside Cylinder, $\phi \approx \phi_0$, For $\gamma=3.83$ and Half Slot Angle ϕ_0	42
17	Radial Distribution of Electric Field Along $\phi=135^\circ$ Ray For $\gamma=1.00$ and Half Slot Angle ϕ_0	45
18	Radial Distribution of Electric Field Along $\phi=135^\circ$ Ray For $\gamma=2.00$ and Half Slot Angle ϕ_0	46
19	Radial Distribution of Electric Field Along The $\phi=135^\circ$ Ray For $\gamma=3.83$ and Half Slot Angle ϕ_0	47
20	Electric Field in the Slot, Surface Current on the Conductor; $\gamma=1.00$, $\phi_0=20^\circ$	76
21	Electric Field in the Slot, Surface Current on the Conductor; $\gamma=2.00$, $\phi_0=20^\circ$	77
22	Electric Field in the Slot, Surface Current on the Conductor; $\gamma=3.83$, $\phi_0=20^\circ$	78
23	Electric Field in the Slot, Surface Current on the Conductor; $\gamma=1.000$, $\phi_0=25^\circ$	79
24	Electric Field in the Slot, Surface Current on the Conductor; $\gamma=2.00$, $\phi_0=25^\circ$	80
25	Electric Field in the Slot, Surface Current on the Conductor; $\gamma=3.830$, $\phi_0=25^\circ$	81
26	Real and Imaginary Parts of the Slot Electric Field Near Resonance	88
27	Back-Scattering Cross-Section, $\phi_0=30^\circ$	90

LIST OF TABLES

TABLE	Title	Page
1	Radial Distribution of Electric Field, $ E_z / E_o $, Along the $\phi=0^\circ$ Ray For Half Slot Angle $\phi_o=20^\circ$ and Circumference to Wavelength Ratios, $\gamma=1.000, 2.000$ and 3.830	48
2	Radial Distribution of Electric Field, $ E_z / E_o $, Along The $\phi=0^\circ$ Ray For Half Slot Angle $\phi_o=25^\circ$ and Circumference to Wavelength Ratios, $\gamma=1.000, 2.000$ and 3.830	49
3	Radial Distribution of Electric Field, $ E_z / E_o $, Along the $\phi=0^\circ$ Ray For Half Slot Angle $\phi_o=30^\circ$ and Circumference to Wavelength Ratios, $\gamma=1.000, 2.000$ and 3.830	50
4	Radial Distribution of Electric Field, $ E_z / E_o $, Along the $\phi=0^\circ$ Ray For Half Slot Angle $\phi_o=45^\circ$ and Circumference to Wavelength Ratios, $\gamma=1.000, 2.000$ and 3.830	51
5	Radial Distribution of Electric Field, $ E_z / E_o $, Along the $\phi=0^\circ$ Ray For Half Slot Angle $\phi_o=60^\circ$ and Circumference to Wavelength Ratios, $\gamma=1.000, 2.000$ and 3.830	52
6	Radial Distribution of Electric Field, $ E_z / E_o $, Along the $\phi=0^\circ$ Ray For Half Slot Angle $\phi_o=90^\circ$ and Circumference to Wavelength Ratios, $\gamma=1.000, 2.000$ and 3.830	53
7	Radial Distribution of Electric Field, $ E_z / E_o $, Along the $\phi=10^\circ$ Ray For Half Slot Angle $\phi_o=20^\circ$ and Circumference to Wavelength Ratios, $\gamma=1.000, 2.000$ and 3.830	54
8	Radial Distribution of Electric Field, $ E_z / E_o $, Along the $\phi=10^\circ$ Ray For Half Slot Angle $\phi_o=25^\circ$ and Circumference to Wavelength Ratios, $\gamma=1.000, 2.000$ and 3.830	55

LIST OF TABLES (Contd)

TABLE	Title	Page
9	Radial Distribution of Electric Field, $ E_z / E_o $, Along the $\phi=15^\circ$ Ray For Half Slot Angle $\phi_o=30^\circ$ and Circumference to Wavelength Ratios, $\gamma=1.000, 2.000$ and 3.830	56
10	Radial Distribution of Electric Field, $ E_z / E_o $, Along the $\phi=22^\circ$ Ray For Half Slot Angle $\phi_o=45^\circ$ and Circumference to Wavelength Ratios, $\gamma=1.000, 2.000$ and 3.830	57
11	Radial Distribution of Electric Field, $ E_z / E_o $, Along the $\phi=30^\circ$ Ray For Half Slot Angle $\phi_o=60^\circ$ and Circumference to Wavelength Ratios, $\gamma=1.000, 2.000$ and 3.830	58
12	Radial Distribution of Electric Field, $ E_z / E_o $, Along the $\phi=45^\circ$ Ray For Half Slot Angle $\phi_o=90^\circ$ and Circumference to Wavelength Ratios, $\gamma=1.000, 2.000$ and 3.830	59
13	Radial Distribution of Electric Field, $ E_z / E_o $, Along the $\phi=30^\circ$ Ray For Half Slot Angle $\phi_o=20^\circ$ and Circumference to Wavelength Ratios, $\gamma=1.000, 2.000$ and 3.830	60
14	Radial Distribution of Electric Field $ E_z / E_o $, Along the $\phi=35^\circ$ Ray For Half Slot Angle $\phi_o=25^\circ$ and Circumference to Wavelength Ratios, $\gamma=1.000, 2.000$ and 3.830	60
15	Radial Distribution of Electric Field, $ E_z / E_o $, Along the $\phi=40^\circ$ Ray For Half Slot Angle $\phi_o=30^\circ$ and Circumference to Wavelength Ratios, $\gamma=1.000, 2.000$ and 3.830	61
16	Radial Distribution of Electric Field, $ E_z / E_o $, Along the $\phi=56^\circ$ Ray For Half Slot Angle $\phi_o=45^\circ$ and Circumference to Wavelength Ratios, $\gamma=1.000, 2.000$ and 3.830	61

LIST OF TABLES (Contd)

TABLE	Title	Page
17	Radial Distribution of Electric Field, $ E_z / E_o $, Along the $\phi=70^\circ$ Ray For Half Slot Angle $\phi_o=60^\circ$ and Circumference to Wavelength Ratios, $\gamma=1.000, 2.000$ and 3.830	62
18	Radial Distribution of Electric Field, $ E_z / E_o $, Along the $\phi=113^\circ$ Ray For Half Slot Angle $\phi_o=90^\circ$ and Circumference to Wavelength Ratios, $\gamma=1.000, 2.000$ and 3.830	62
19	Radial Distribution of Electric Field, $ E_z / E_o $, Along the $\phi=90^\circ$ Ray For Half Slot Angle $\phi_o=20^\circ$ and Circumference to Wavelength Ratios, $\gamma=1.000, 2.000$ and 3.830	63
20	Radial Distribution of Electric Field, $ E_z / E_o $, Along the $\phi=90^\circ$ Ray For Half Slot Angle $\phi_o=25^\circ$ and Circumference to Wavelength Ratios, $\gamma=1.000, 2.000$ and 3.830	63
21	Radial Distribution of Electric Field, $ E_z / E_o $, Along the $\phi=90^\circ$ Ray For Half Slot Angle $\phi_o=30^\circ$ and Circumference to Wavelength Ratios, $\gamma=1.000, 2.000$ and 3.830	64
22	Radial Distribution of Electric Field, $ E_z / E_o $, Along the $\phi=90^\circ$ Ray For Half Slot Angle $\phi_o=45^\circ$ and Circumference to Wavelength Ratios, $\gamma=1.000, 2.000$ and 3.830	64
23	Radial Distribution of Electric Field, $ E_z / E_o $, Along the $\phi=90^\circ$ Ray For Half Slot Angle $\phi_o=60^\circ$ and Circumference to Wavelength Ratios, $\gamma=1.000, 2.000$ and 3.830	65
24	Radial Distribution of Electric Field, $ E_z / E_o $, Along the $\phi=135^\circ$ Ray For Half Slot Angle $\phi_o=20^\circ$ and Circumference to Wavelength Ratios, $\gamma=1.000, 2.000$ and 3.830	65

LIST OF TABLES (Contd)

TABLE	Title	Page
25	Radial Distribution of Electric Field, $ E_z / E_o $, Along the $\phi=135^\circ$ Ray For Half Slot Angle $\phi_o=25^\circ$ and Circumference to Wavelength Ratios, $\gamma=1.000, 2.000$ and 3.830	66
26	Radial Distribution of Electric Field, $ E_z / E_o $, Along the $\phi=135^\circ$ Ray For Half Slot Angle $\phi_o=30^\circ$ and Circumference to Wavelength Ratios, $\gamma=1.000, 2.000$ and 3.830	66
27	Radial Distribution of Electric Field, $ E_z / E_o $, Along the $\phi=135^\circ$ Ray For Half Slot Angle $\phi_o=45^\circ$ and Circumference to Wavelength Ratios, $\gamma=1.000, 2.000$ and 3.830	67
28	Radial Distribution of Electric Field, $ E_z / E_o $, Along the $\phi=135^\circ$ Ray For Half Slot Angle $\phi_o=60^\circ$ and Circumference to Wavelength Ratios, $\gamma=1.000, 2.000$ and 3.830	67
29	Radial Distribution of Electric Field, $ E_z / E_o $, Along the $\phi=135^\circ$ Ray For Half Slot Angle $\phi_o=90^\circ$ and Circumference to Wavelength Ratios, $\gamma=1.000, 2.000$ and 3.830	68
30	Radial Distribution of Electric Field, $ E_z / E_o $, Along the $\phi=180^\circ$ Ray For Half Slot Angle $\phi_o=20^\circ$ and Circumference to Wavelength Ratios, $\gamma=1.000, 2.000$ and 3.830	68
31	Radial Distribution of Electric Field, $ E_z / E_o $, Along the $\phi=180^\circ$ Ray For Half Slot Angle $\phi_o=25^\circ$ and Circumference to Wavelength Ratios, $\gamma=1.000, 2.000$ and 3.830	69
32	Radial Distribution of Electric Field, $ E_z / E_o $, Along the $\phi=180^\circ$ Ray For Half Slot Angle $\phi_o=30^\circ$ and Circumference to Wavelength Ratios, $\gamma=1.000, 2.000$ and 3.830	69

LIST OF TABLES (Contd)

TABLE	Title	Page
33	Radial Distribution of Electric Field, $ E_z / E_o $, Along the $\phi=180^\circ$ Ray For Half Slot Angle $\phi_o=45^\circ$ and Circumference to Wavelength Ratios, $\gamma=1.000, 2.000$ and 3.830	70
34	Radial Distribution of Electric Field, $ E_z / E_o $, Along the $\phi=180^\circ$ Ray For Half Slot Angle $\phi_o=60^\circ$ and Circumference to Wavelength Ratios, $\gamma=1.000, 2.000$ and 3.830	70
35	Radial Distribution of Electric Field, $ E_z / E_o $, Along the $\phi=180^\circ$ Ray For Half Slot Angle $\phi_o=90^\circ$ and Circumference to Wavelength Ratios, $\gamma=1.000, 2.000$ and 3.830	71
36	The Distribution of the Electric Field Over The Aperture for Half Slot Angle $\phi_o=20^\circ$	82
37	The Distribution of the Electric Field Over The Aperture for Half Slot Angle $\phi_o=25^\circ$	83
38	Morse-Feshbach Electrostatic Approximation to the Amplitude of the Aperture Electric Field Normalized to the Theoretical Value at the Slot Center for Half Slot Angles $\phi_o=20^\circ$ and $\phi_o=25^\circ$	84
39	Normalized Constants $A(\gamma, \phi_o)$ for the Morse- Feshbach Electrostatic Approximation to the Slot Electric Field	84
40	Surface Current Distribution Around Conductor for Half Slot Angle $\phi_o=20^\circ$	85
41	The Surface Current Distribution Around the Conductor for Half Slot Angle $\phi_o=25^\circ$	86

I. INTRODUCTION

This report constitutes another in our series of investigations of the characteristic effects of the presence of finite size apertures in conducting bodies subjected to irradiation by electromagnetic waves. Essentially this publication is a companion piece to the earlier report by Bombardt and Libelo¹ on the infinite, slotted, conducting circular cylinder. In the earlier paper we presented the tangential aperture electric field, the surface current distribution, and the back-scattering cross-sections for normal symmetric incidence on an axially slotted circular cylinder for slot angles from 60° on up and for circumference to wavelength ratios from 1 to 5.

We publish in this report our numerical results for the electric field distribution inside, basically, the same axially slotted cylinder. The same field component outside and in the neighborhood of the slot has also been evaluated and is included in this paper. Figure 1 displays in a plane normal to the cylinder axis the geometry involved in the study.

Results are displayed both graphically and in tabular form for the electric field distributions obtained inside and outside of the slotted cylinder. Particular emphases have been placed on studying the off-symmetry radial distribution through the aperture, the radial distribution inside just beyond the slot and the inside rear region of the axially slotted cylinder. Slots subtending total angles of 40°, 50°, 60°, 90°, and 180° have been considered. In each case results have been obtained for values of the circumference to wavelength ratio parameter $\gamma=2\pi a/\lambda$ equal to 1, 2 and 3.83. (The reader is asked to bear with us with regard to notation. In the earlier companion paper we denoted this parameter by $\eta=2\pi a/\lambda$.)

1. J. N. Bombardt (HDL) and L. F. Libelo "Scattering of Electromagnetic Radiation by Apertures: \bar{V} Surface Current, Tangential Aperture Electric Field, and Back-Scattering Cross-Section For the Axially Slotted Cylinder at Normal, Symmetric Incidence." Hereafter referred to as S.E.R.A. \bar{V}

We also include in this report additional results for narrower slots than in the earlier paper S.E.R.A. \bar{V} .¹ These are the tangential aperture electric field the surface current density, and the back-scattering cross-section for 40° and 50° slots for circumference to wavelength ratios $\gamma=1, 2, \text{ and } 3.83$.

Prior to the development of the necessary analysis itself we first present a cursory review of the earlier work of others on determining the interior and exterior field distributions. The earliest known attempt at solution is that of Sommerfeld.² He formulated the internal and external fields in terms of series expansions. Application of the boundary conditions to these series expansions failed to lead to explicit evaluation of the unknown coefficients in these series. Hence Sommerfeld attempted approximate solutions. For this purpose he restricted the problem to the case where the slot arc-length is small in comparison to the wavelength of the incident radiation. Via the method of least squares he derived analytic expressions for the coefficients in this asymptotic limit. It is well known now, however, that he failed to report any numerical results he may have obtained. Furthermore if he obtained any experimental results he never published the data. It should be noted that in the results we report below we are not constrained to the asymptotic limit of very small slots. Morse and Feshbach³ also assumed series expansions for the fields. In their investigation they expressed the unknown series expansion coefficients in terms of an integral of the unknown electric field over the slot. They then approximately solved this integral equation by assuming that the distribution of the field over the slot in the cylinder is proportional to the electrostatic field distribution over the slot in an infinite plane. They were able to derive at the midpoint of the slot an analytic result for the constant of proportionality.

1. "S.E.R.A." \bar{V} op cit.

2. A. Sommerfeld, "Partial Differential Equations" p. 29-31 Academic Press, New York, NY 1949.

3. P. M. Morse and Feshbach, "Methods of Theoretical Physics" Part II, p. 1387-1398, McGraw-Hill Book Co., New York, NY 1953.

Unfortunately they also failed to report any numerical or experimental results. In the previous paper¹ we attempted to present a comprehensive review of the earlier investigations into the diffraction and scattering characteristics of the infinite circular cylinder with an infinite axial slot. Reference to that paper will reveal that except for the very narrow slot⁴ there is a glaring dearth of both calculated fields and measurements inside the slotted cylinder. The bulk of the effort seems to have been devoted to determining the back-scattering cross-section. We shall be content with merely referring the reader back to the earlier paper S.E.R.A. \bar{V} for a more complete discussion of the history of the problem. An appropriate summary of the problem to date is that basically numerical and experimental results for the internal fields are practically non-existent. This paper is meant to partially fill this gap in knowledge and thereby to provide a reference point for future work. It will also provide an ideal situation to be used for comparison purposes in discussing the extensive experimental data we have accumulated and shall be reporting on in subsequent reports in this series. In the case of the very narrow slot in the conducting infinite circular cylinder we omit from this report any discussion of the analytic portion of the study we have effected as well as the experimental results we have available. As we have stated in the past this situation is of sufficient interest and significance to merit a separate publication. This we are preparing and shall publish and disseminate in the near future.

To make this report somewhat self-contained we shall briefly develop the theory necessary to calculate the interior and near slot exterior fields. We then present the corresponding results and discuss them. Following this we then present the results extending the earlier work in "S.E.R.A. \bar{V} " to smaller slot angles and the corresponding discussion of these.

1. "S.E.R.A." \bar{V} op cit.

4. V. N. Koshparenok and V. P. Shestopalov, "Diffraction of a Plane Electromagnetic Wave by a Circular Cylinder with a Longitudinal Slot" Zh. Vychisl. i Mat. Fiz., 11 719-737 (1971).

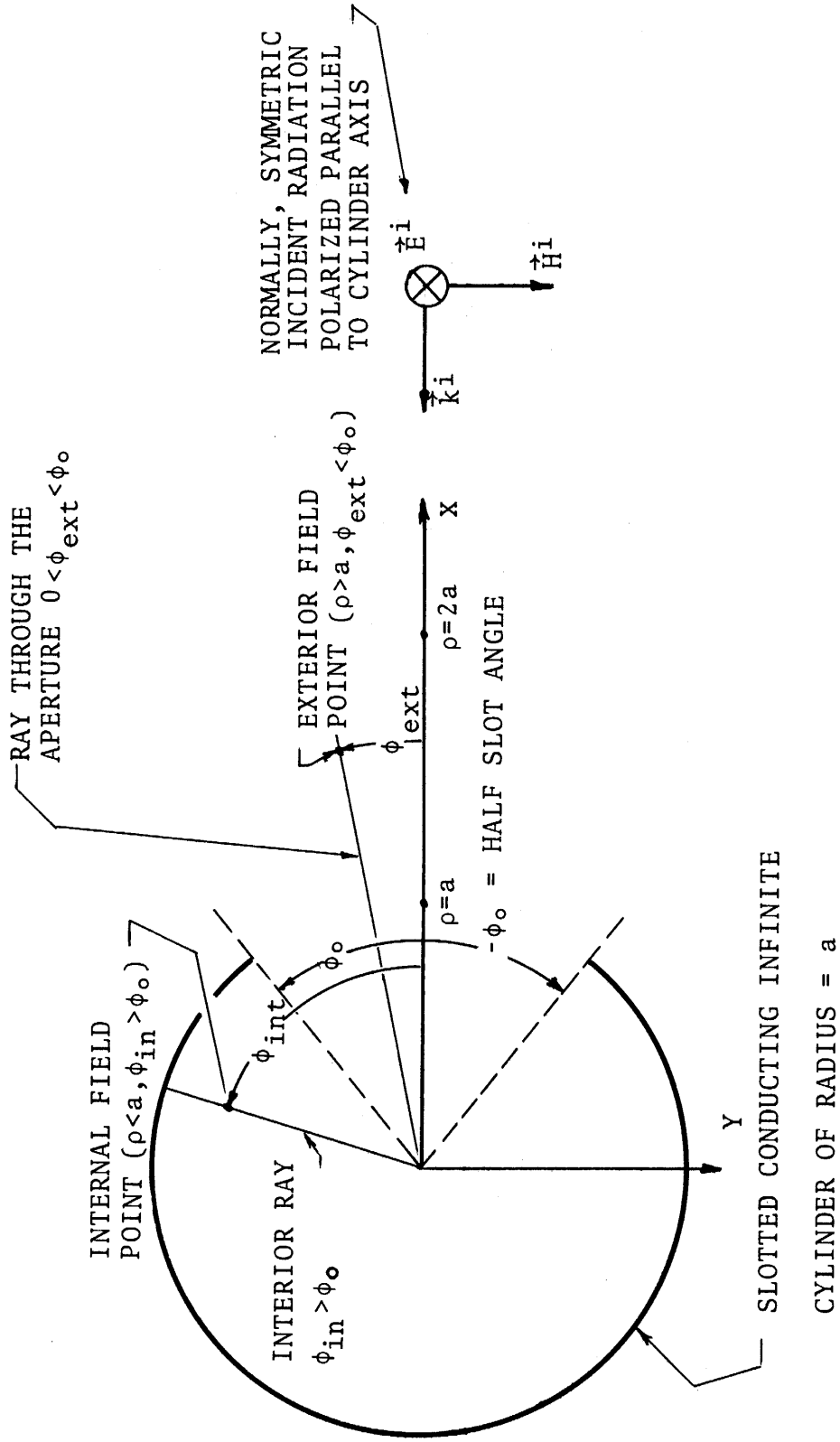


FIGURE 1. GEOMETRY OF THE SCATTERING PROBLEM FOR THE AXIALLY SLOTTED CYLINDER

II. DERIVATION OF THE ELECTRIC FIELD INSIDE AND IN THE NEIGHBORHOOD OF THE SLOT

In Figure 1 can be found all the necessary details of the geometry of the problem. Clearly the scattering problem is two-dimensional. The monochromatic, plane, linearly polarized electromagnetic wave is shown incident normal to the cylinder axis and simultaneously symmetric with respect to the longitudinal slot in the cylinder. We are considering the case of E-polarization, namely the electric field in the incident radiation is assumed parallel to the axis of the slotted cylinder which we take as the z-axis in our coordinate system. Harmonic time dependence of the form $e^{-i\omega t}$ is assumed. However, we suppress the appearance of the explicit time exponential from the following equations.

Then the incident electric field is given by

$$(1) \quad \vec{E}^i(\vec{r}) = E_z^i(\rho, \phi) \vec{e}_z = E_0 e^{-i\kappa \cos\phi} \vec{e}_z$$

and the incident magnetic field by

$$(2) \quad \vec{H}^i(\vec{r}) = H_y^i(\rho, \phi) \vec{e}_y = H_0 e^{-i\kappa \rho \cos\phi} \vec{e}_y$$

where we have as usual defined the quantity

$$(3) \quad \kappa \equiv \omega/c = 2\pi/\lambda$$

and of course \vec{e}_z and \vec{e}_y are respectively unit vectors along the positive Z and Y axes. Working in MKS units we have the following relation between the amplitudes of the electric and magnetic fields in the incident wave

$$(4) \quad E_0 = \sqrt{\mu_0/\epsilon_0} H_0$$

where ϵ_0 and μ_0 are respectively the electric permittivity and magnetic permeability of free space.

There is only a z-component of electric field in this problem and this field at a source free point satisfies the homogeneous scalar Helmholtz wave equation

$$(5) \quad \nabla^2 E_z(\vec{r}) + k^2 E_z(\vec{r}) = 0$$

In polar cylindrical coordinates then we have only the magnetic field components H_ρ and H_ϕ to consider and these are given in terms of the axial electric field via the pair of relations

$$(6) \quad H_\rho(\rho, \phi) = -(1/i\omega\mu_0 \rho) \frac{\partial E_z(\rho, \phi)}{\partial \phi}$$

$$(7) \quad H_\phi(\rho, \phi) = 1(1/i\omega\mu) \frac{\partial E_z(\rho, \phi)}{\partial \rho}$$

As a consequence of the symmetry of the problem the electric field is an even function of the angle ϕ . This in turn implies that H_ϕ is also an even function of ϕ while H_ρ is an odd function of the angle ϕ .

In the interior region of the cylinder of radius a we assume the form of the electric field to be

$$(8) \quad E_z^{(1)}(\rho, \phi) = \sum_{m=0}^{\infty} A_m \frac{J_m(\gamma\rho/a)}{J_m(\gamma)} \cos m\phi \quad \text{for } \rho < a$$

Note that we have used the superscript (1) to denote the region of space for $\rho < a$. In eq. (8) the A_m are unknown expansion coefficients.

In the region exterior to the slotted cylinder the electric field is assumed formally to be composed of two parts. One is the well known field that would be present if there were no slot in the cylinder.⁵⁻⁷ This is the first sum in eq. (9) immediately below. The second part is a contribution to the field due solely to the

-
5. J. J. Bowman, T. B. A. Senior and P. L. E. Uslenghi, eds., "Electromagnetic and Acoustic Scattering by Simple Shapes" p 92-93 North Holland Publishing Co., Amsterdam, The Netherlands, 1969
 6. R. F. Harrington, "Time Harmonic Electromagnetic Fields" p 232-234 McGraw-Hill Book Co., New York 1961
 7. M. Kerker, "The Scattering of Light and Other Electromagnetic Radiation" Ch. 6, Academic Press, New York 1969

presence of the slot. This is the second sum in eq. (9). Thus in the exterior region i.e. for $\rho > a$ which we denote by the superscript (2) we have

$$(9) \quad E_z^{(2)}(\rho, \phi) = E_0 \sum_{m=0}^{\infty} \epsilon_m (-i)^m \left[J_m(\gamma\rho/a) - \frac{J_m(\gamma)}{H_m^{(1)}(\gamma)} H_m^{(1)}(\gamma\rho/a) \right] \cdot \\ \cdot \cos m\phi + \sum_{m=0}^{\infty} A_m \frac{H_m^{(1)}(\gamma\rho/a)}{H_m^{(1)}(\gamma)} \cos m\phi \quad \text{for } \rho > a$$

This field satisfies the scalar Helmholtz equation at source free points in the exterior region. Furthermore the set of expansion coefficients A_m that appear in the exterior solution are identical with those appearing in the interior solution. This follows from the requirements that the interior and exterior fields be identical over the slot and that each separately vanish over the conducting portion of the cylinder of radius a . The quantity ϵ_m in eq. (9) is defined by

$$(10) \quad \epsilon_m = \begin{cases} 1 & m = 0 \\ 2 & m = 1, 2, 3, \dots \end{cases}$$

Consistent with the notation of our earlier paper¹ we denote the electric field in the slot by $\mathcal{E}(\phi)$ where then we can write

$$(11) \quad E_z(a, \phi) = E_z^{(1)}(a, \phi) = E_z^{(2)}(a, \phi) = \begin{cases} \mathcal{E}(\phi) & -\phi_0 < \phi < \phi_0 \\ 0 & \phi_0 < \phi < -\phi_0 \end{cases}$$

Equivalently we have

$$(12) \quad \sum_{m=0}^{\infty} A_m \cos m\phi = \begin{cases} \mathcal{E}(\phi) & -\phi_0 < \phi < \phi_0 \\ 0 & \phi_0 < \phi < -\phi_0 \end{cases}$$

Inverting eq. (12) we then can express the expansion coefficients in terms of the electric field distribution over the slot as follows

$$(13) \quad A_m = \frac{\epsilon_m}{2\pi} \int_{-\phi_0}^{\phi_0} d\phi \mathcal{E}(\phi) \cos m\phi$$

1. J. Bombardt, L. Libelo, "S.E.R.A.V", Ibid p 21

Using eq. (13) just obtained for the expansion coefficients we can then write the following expression for the interior electric field in terms of the electric field over the aperture

$$(14) \quad E_Z^{(1)}(\rho, \phi) = \sum_{m=0}^{\infty} \frac{J_m(\gamma\rho/a)}{J_m(\gamma)} \frac{\epsilon_m}{\pi} \cos m\phi \int_0^{\phi_0} d\phi' \mathcal{E}(\phi') \cos m\phi' \quad \text{for } \rho < a$$

Similarly substituting for the A_m in the exterior field expression, eq. (9), we obtain an expression for the electric field outside the cylinder in terms of the distribution of the electric field over the slot, namely

$$(15) \quad E_Z^{(2)}(\rho, \phi) = E_0 \sum_{m=0}^{\infty} \epsilon_m (-i)^m \left[J_m(\gamma\rho/a) - \frac{J_m(\gamma)}{H_m^{(1)}(\gamma)} H_m^{(1)}(\gamma\rho/a) \right] \\ + \sum_{m=0}^{\infty} \frac{\epsilon_m}{\pi} \frac{H_m^{(1)}(\gamma\rho/a)}{H_m^{(1)}(\gamma)} \cos m\phi \int_0^{\phi_0} d\phi' \mathcal{E}(\phi') \cos m\phi' \quad \text{for } \rho > a$$

Equations (14) and (15) are the formulations used to obtain the radial dependences of E_Z inside, and outside (but in the vicinity of the slot) of the cylinder of radius a .

In S.E.R.A.V¹ we derived an integral equation for the surface current density on the conductor which we shall merely repeat here.

$$(16) \quad \frac{\gamma}{4} \sqrt{\frac{\mu_0}{\epsilon_0}} \int_{\phi_0}^{2\pi-\phi_0} d\phi' \mathcal{K}(\phi') H_0^{(1)} \left(2\gamma \left| \sin \left(\frac{\phi-\phi'}{2} \right) \right| \right) = E_Z^i(a, \phi)$$

$$\text{for } \phi_0 < \phi < 2\pi - \phi_0$$

where $\mathcal{K}(\phi)$ is the surface current distribution on the conductor. We refer the reader back to that paper for the details of the derivation. In part IV of that report we showed how to determine $\mathcal{K}(\phi)$, the surface current on the conducting portion of the cylinder.

1. J. N. Bombardt and L. F. Libelo "S.E.R.A.V" Ibid, p 30

In an earlier paper⁸ a derivation was given of a connective integral equation between the slot electric field and the surface current density. We only give this relation here and refer the reader to that paper for the details of this simple derivation. We have in fact

$$(17) \quad \mathcal{E}(\phi) = E_z^i(a, \phi) - \frac{\gamma}{4} \sqrt{\frac{\mu_0}{\epsilon_0}} \int_{\phi_0}^{2\pi - \phi_0} d\phi' \mathcal{K}(\phi') H_0^{(1)}\left(2\pi \left| \sin\left(\frac{\phi - \phi'}{2}\right) \right| \right)$$

for $2\pi - \phi_0 < \phi < \phi_0$.

With the solution for $\mathcal{K}(\phi)$ in hand from eq. (16) we can then immediately determine $\mathcal{E}(\phi)$ using eq. (17). Then, in turn, with this aperture electric field distribution we can determine the electric field anywhere in the interior of the slotted cylinder using eq. (14). Similarly we can determine the electric field distribution anywhere in the exterior region using eq. (15).

The necessary modifications of the earlier computer program are discussed later on in this report. Having essentially completed the presentation of all the pertinent theoretical development we shall next proceed to the results obtained.

8. J. N. Bombar dt and L. F. Libelo, "S.E.R.A.:III. An Alternative Integral Equation With Analytic Kernels for the Slotted Cylinder Problem" HDL-TR-1588 Harry Diamond Laboratory, Washington, DC August 1972

III. CALCULATED INTERIOR AND EXTERIOR ELECTRIC FIELDS

a) Radial Distribution Along the Symmetry Diameter Through the Slot

The radial distribution of the amplitude of the electric field is shown in Figure 2 along the symmetry ray i.e. for $\phi=0^\circ$. In this figure the circumference to wavelength ratio is $\gamma = 2\pi a/\lambda = 1$. Results are shown in graphical form from inside at the center of the slot and out beyond the cylinder to a distance equal to the cylinder radius. Radial distributions for the fixed value of circumference to wavelength ratio $\gamma = 1$ are simultaneously displayed for half slot angles $\phi_0 = 20^\circ, 25^\circ, 30^\circ, 45^\circ, 60^\circ$ and 90° . It should be noted that for all these slot angles the case $\gamma = 1$ clearly is beyond cutoff for the slotted cylinder. This is rather noteworthy since the smallest slot angle represents a cylinder with $2\phi_0/360 = 1/9$ of the conductor removed whereas the largest slot angle corresponds to the situation where only half the cylinder remains. Nevertheless we observe that at $\gamma = 1$ we find the internal field merely decreases monotonically from the value at the center of the slot as we proceed inward to the center for all slot angles under consideration. Not surprisingly we note that the larger the slot angle the greater the degree of penetration of the electric field. That is for the fixed value $\gamma = 1$, beyond cutoff, increasing ϕ_0 presents a larger aperture to the incident radiation allowing the field inside to build up over that for a smaller opening. Furthermore, if we consider the radial distributions along the backward symmetry ray, i.e. for $\phi = 180^\circ$, from the center of the cylinder to the conducting wall itself we find that for $\gamma = 1$ the same diffusive type monotonic falloff of electric field persists for all the slot angles. The results are shown in Figure 5. Note that in all cases the decrease is to zero as it should be at the backwall of the cylinder, and the larger the slot angle the larger the field in the interior.

Outside the cylinder $\rho = a$, for $\gamma = 1$ the electric field in the near region, at least to $\rho = 2a$, increases in a continuous fashion from a minimum value at the slot center for half slot angle $\phi_0 = 20^\circ$. This characteristic persists as ϕ_0 increases. The electric field

outside is larger the greater the slot angle up to about $\phi_0 \approx 60^\circ$. For $\phi_0 = 60^\circ$ a maximum occurs at about $\rho = 1.7a$ and a slow decrease is seen thereafter to $\rho = 2a$. For $\phi_0 = 45^\circ$ a maximum occurs quite close to $\rho = 2a$. The inescapable fact that we have only half a cylinder is clearly evident for $\phi_0 = 90^\circ$. The corresponding curve in Figure 2 shows a maximum at about $\rho = 1.3a$ and a monotonic decrease to $\rho = 2a$. Note that the electric field near $\rho = 2a$ is not markedly different for $\gamma = 1$ for all slot angles considered.

Figure 3 gives the radial distribution of electric field for $\gamma = 2$ along the same symmetry ray that bisects the slot, i.e. $\phi = 0^\circ$. In this figure we can see the distribution of electric field from the axis of the cylinder to the slot itself and outside back toward the source over an additional distance equal to the cylinder radius. Figure 6 gives the complete picture of the electric field along this symmetry ray by extending its range in the direction inside away from the source all the way through to the inside back wall. For the circumference to wavelength ratio $\gamma = 2$ we are essentially dealing with a wavelength half that for $\gamma = 1$ for a cylinder of the same radius. Alternatively if we assume the wavelength is the same, the radius for $\gamma = 2$ is twice that for $\gamma = 1$. For the circular cylindrical waveguide both alternatives would in fact be identically the same situation. Before investigating the comparable situations with a slotted cylinder we first note the $\gamma = 2$ behavior of electric field. Inside the cylinder we can clearly discern that for $\gamma = 2$ we are still beyond cutoff for all the slot angles chosen. For the three smaller slot angles the radial distribution of electric field along the symmetry diameter displays a monotonic decrease from the value at the center of the slot and ultimately vanishes at the inside back conducting wall. For the larger slot angles a maximum for the electric field occurs inside the cylinder on the source side of the axis. The larger the slot angle the closer to the axis this maximum occurs. Proceeding further in along the symmetry diameter reveals the characteristic monotonic falloff in amplitude to zero at the back wall. Note the interesting difference in character displayed near the slot for $\gamma = 2$ as seen in Figure 3, when compared to the $\gamma = 1$

results shown in Figure 2. For $\gamma = 2$ we find the slot-center electric field amplitude increases as ϕ_0 increases until about $\phi_0 = 45^\circ$ (total slot angle $2\phi_0 = 90^\circ$). Thereafter, unlike the $\gamma = 1$ characteristic at the slot center, for $\gamma = 2$ further increase in slot angle produces a relatively marked decrease in amplitude in the electric field. Thus for example at the slot center we find the electric field amplitude for $\phi_0 = 45^\circ$ is about four times that for $\phi_0 = 20^\circ$. For $\phi_0 = 90^\circ$ and for $\phi_0 = 20^\circ$ the amplitudes at the slot center are approximately equal. Further interesting behavior manifests itself in Figure 3 for $\gamma = 2$ and $\phi = 0^\circ$. It should be noted that the maximum field inside increases from $\phi_0 = 45^\circ$ to $\phi_0 = 60^\circ$ and somewhere thereafter decreases with increasing slot angle as it simultaneously shifts toward the axis of the cylinder. Comparison of the $\phi_0 = 60^\circ$ and $\phi_0 = 90^\circ$ cases clearly reveals this behavior.

Next let us examine the behavior of the electric field amplitude outside the cylinder from the center of the slot to a distance away equal to the radius of the cylinder. We first observe that an oscillatory behavior is plainly present. The first minimum occurs furthest away from the smallest slot angle. Then as the slot angle increases we observe that the corresponding minimum of the field continuously shifts toward the slot center. At the same time the maximum in the field amplitude seen outside the slot for $\phi_0 = 20^\circ$ can be seen to be gradually rising and shifting toward the cylinder as the slot angle increases to $\phi_0 = 30^\circ$. Inspection of Figure 3 indicates quite clearly that this behavior continues as ϕ_0 increases until the first maximum eventually moves through the aperture somewhere between $\phi_0 = 30^\circ$ and $\phi_0 = 45^\circ$. Further increase in ϕ_0 then gives the behavior discussed above. Figure 3 shows quite vividly the evolution of the electric field radial distribution along the symmetry diameter through the slot as the slot angle continuously increases from a small ϕ_0 to the extreme case where only half the cylinder is left, $\phi_0 = 90^\circ$.

Let us return to the question raised earlier concerning the effect on the electric field distribution in the presence of a slot if the radius is kept fixed and the wavelength is halved or

alternatively the wavelength is maintained and the radius is doubled. Consider the latter cylinders first. For $\gamma = 2$ the rectangular area of the ϕ_0 ($\gamma = 2$) slot presented to the incident radiation equals that of the $\gamma = 1$ slot of twice that central angle. Of course ϕ_0 must be limited to $\pi/4$ or less for this to hold. For larger ϕ_0 we obviously have no simple correspondence between electric field distributions except in the limit of very large slots or equivalently very narrow cylindrical ribbons. This can be seen by examining the narrow strip results in S.E.R.A.V.¹ Since the slot for $\gamma = 1$ is a larger fraction of the entire cylinder than the corresponding slot for the $\gamma = 2$ cylinder we shouldn't expect any simple correspondence between the radial distributions of the electric field for anything but "small" apertures. Indeed inspection of Figures 2, 3, 5 and 6 do display this feature. Quite surprising however for $\phi_0 \cong 25^\circ$ we find the two field distributions are not greatly different. This is apparently the manifestation of some upper limit on intermediate sized slot behavior for the given wavelength. The corresponding discussion in the limit of very small slots will be presented in a separate subsequent report. We again note that we are at a value of γ that is beyond cutoff for all the slot angles considered. Now consider two cylinders of equal radii but with the incident radiation in one case of wavelength twice that of the other corresponding respectively to $\gamma = 1$ and $\gamma = 2$. A slot angle ϕ_0 in the first will present the same aperture area to the incident radiation as the slot angle $\frac{1}{2}\phi_0$ in the second cylinder. For slot angles of $\phi_0 \cong 35^\circ$ and smaller we discover that the electric field distributions are again pretty much the same in both cases. Once again we point out that discussion of the very narrow slot problem is omitted from this report. For the other extreme of very large slots or equivalently very narrow cylindrical ribbons or strips we expect the electric field distributions to be nearly the same. We have been comparing $\gamma = 1$ and $\gamma = 2$ results to this point with the same slot areas presented to the

1. J. Bombardt, L. Libelo S.E.R.A.V op.cit.

incident radiation. Now consider two $\gamma = 2$ situations. The first is a cylinder of radius $2a$ irradiated by an incident wave of wavelength λ . The second is a cylinder of radius a and the incident radiation is of wavelength $\lambda/2$. Note the extremely important result that the electric field distributions are exactly the same for both cases when the slot angle is the same in both cylinders. In retrospect this linear behavior is what must follow directly from the Maxwell equations. A further point to note is that the same effective aperture is presented to the incident radiation in both cases. We thus state that our axially slotted infinite cylinder is for a given slot angle, ϕ_0 , fixed by prescribing the one parameter γ . Nevertheless changing ϕ_0 does result in significant changes for any given value of γ . Thus the slotted cylinder we are considering is in fact a two parameter problem.

Figures 4 and 7 together display for $\gamma = 3.830$ the radial distributions of the electric field amplitude along the symmetry diameter through the slot center for all the slot angles ϕ_0 studied. Observe that for no slot the second interior circular waveguide mode TM_{11} occurs at $\gamma = 3.832$. Consequently we find from Figures 4 and 7 which display the characteristics of the TM_{11} mode that the existence of the infinite axial slot of half angle ϕ_0 appears to cause the interior resonance to shift to a slightly lower frequency. Although we have not explicitly shown it for the lowest mode the same behavior does accompany the presence of a slot. The shift is even smaller for the TM_{01} mode. If we study the relative locations of the maxima of the interior fields we note a number of interesting characteristics. First for all the slot angles the maximum occurs at the same radial distance from the center or axis of the cylinder on the $\phi = 180^\circ$ ray. The maxima are all located at about $\rho/a = 0.52$. On the other hand consider the maxima on the $\phi = 0^\circ$ ray. For $\phi_0 = 20^\circ$ the electric field maximum occurs at about $\rho/a = 0.50$. This indicates a slight shift toward the center on the side nearest the aperture. Increasing the slot angle ϕ_0 results in a further shift in the location of the electric field maximum on the slot side of the cylinder axis. Thus we observe that for $\phi_0 = 90^\circ$, the half-cylinder, this maximum occurs

at about $\rho/a = 0.44$. This behavior is evidently a consequence of the increasing size of the opening in the cylindrical shield that is presented to the incident radiation, which allows the energy to move further into the cylinder. It is interesting to note that as the angle ϕ_0 increases the slot edges also move further away from the slot center.

So much for the locations of the maxima within the slotted cylinder. Let us now focus our attention on their heights at the second resonance. Along the $\phi=180^\circ$ ray, as can be easily seen in Figure 7, the peaks become progressively flatter as the slot angle increases and finally includes half the cylinder at $\phi_0=90^\circ$. Although it is not quite as easily discernible in Figure 4 this also occurs at the maxima on the $\phi=0^\circ$ ray. Increasing the slot angle results in decreasing the peak height at resonance on both the $\phi=0^\circ$ and $\phi=180^\circ$ rays. We further observe from Figures 4 and 7 that for $\phi_0 \leq 30^\circ$ the peaks on the $\phi=180^\circ$ ray are at nearly the same height as those on the $\phi=0^\circ$ ray. Further increase in the slot angle results in the peak closer to the slot dropping faster than the more distant one on the $\phi=180^\circ$ ray. If we examine the ratio of height to width we find that as the slot angle increases this ratio decreases. Thus we can summarize the general behavior as displayed along the symmetry diameter at the resonance as follows: as the slot angle is increased from $\phi_0=20^\circ$, where we still can safely consider our system as essentially that of a circular cylinder, this becomes less realistic at the larger angles, say at $\phi_0 \geq 60^\circ$ where about one-third or more of the cylinder is missing. Obviously at $\phi_0=90^\circ$ when half the cylinder is gone the greatest deviation from the characteristics of the circular cylindrical waveguide should and does indeed become manifest.

Note that as a result of the aperture the electric field does not vanish on the cylinder axis. Actually the amplitude is quite small until the slot angle becomes about equal to or larger than $\phi_0=60^\circ$. It is interesting to observe in Figure 4 that for the half cylinder, $\phi_0=90^\circ$, the minimum field occurs away from the center and lies closer to the slot. Another interesting feature is the behavior of the electric field at the slot center for $\gamma=3.830$. Note that for

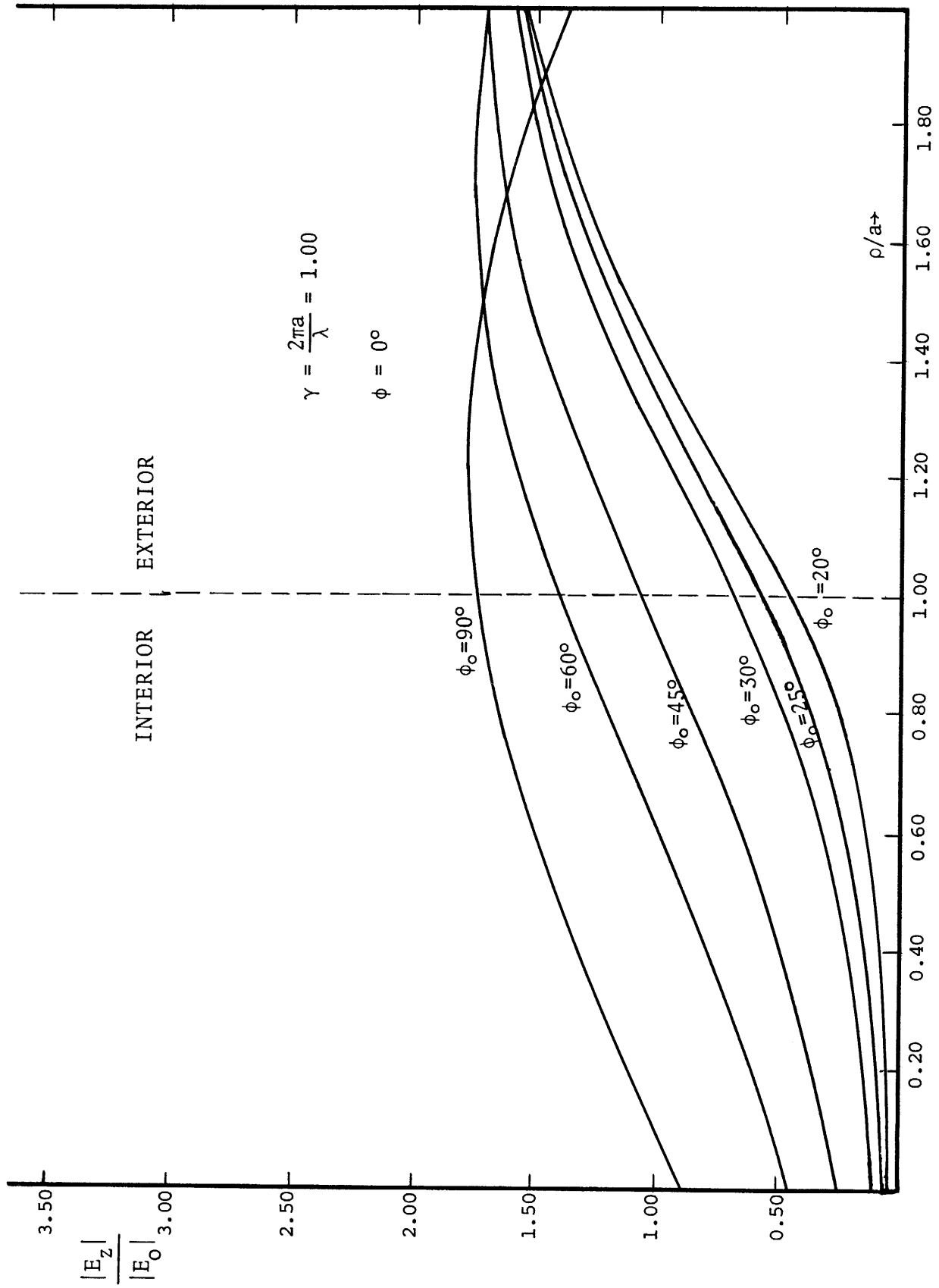


FIGURE 2. RADIAL DISTRIBUTION OF ELECTRIC FIELD ALONG $\phi = 0^\circ$ RAY FOR $\gamma = 1.000$ AND HALF SLOT ANGLE ϕ_0

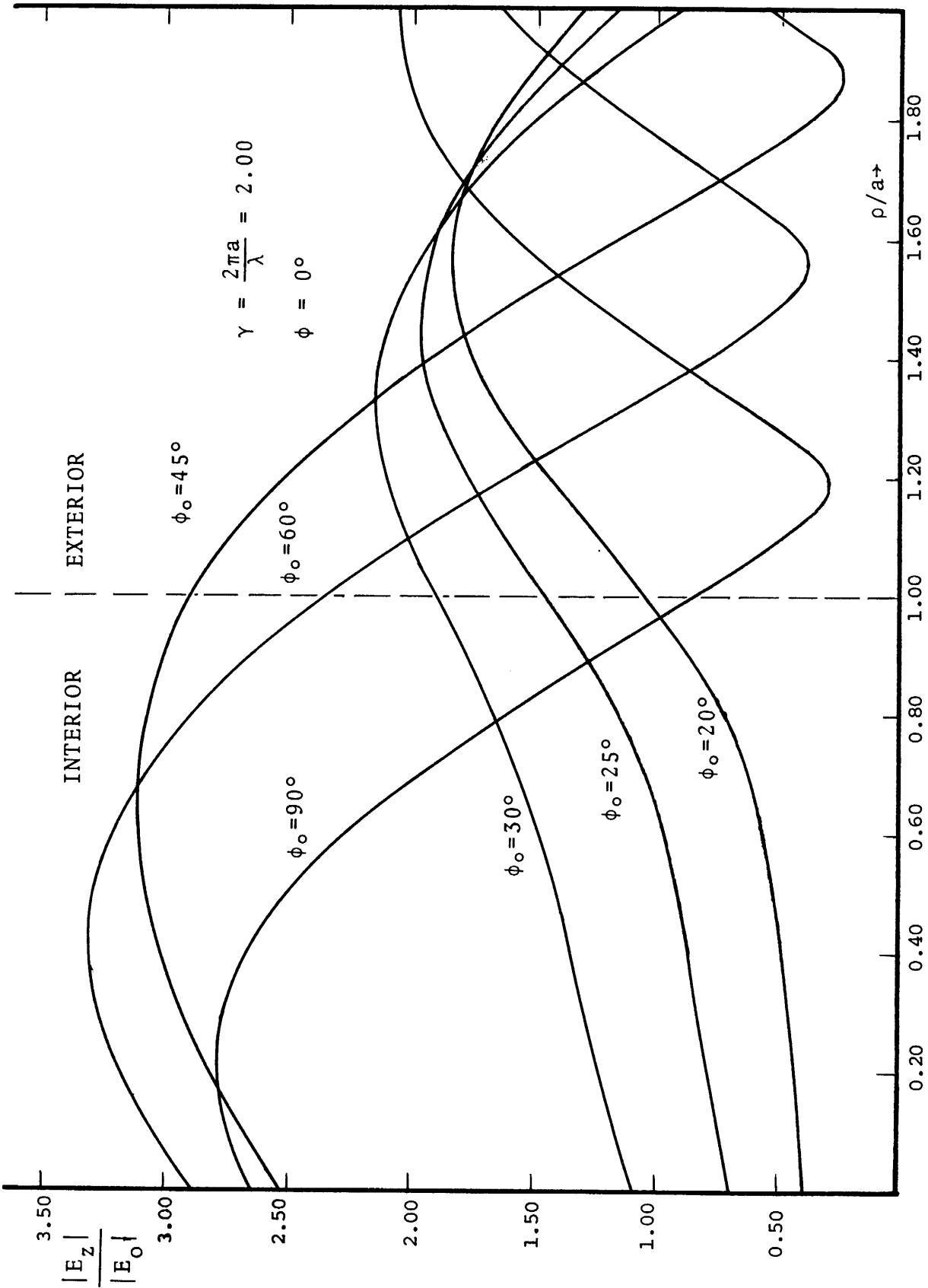


FIGURE 3. RADIAL DISTRIBUTION OF ELECTRIC FIELD ALONG $\phi=0^\circ$ RAY FOR $\gamma=2.000$ AND HALF SLOT ANGLE ϕ_0

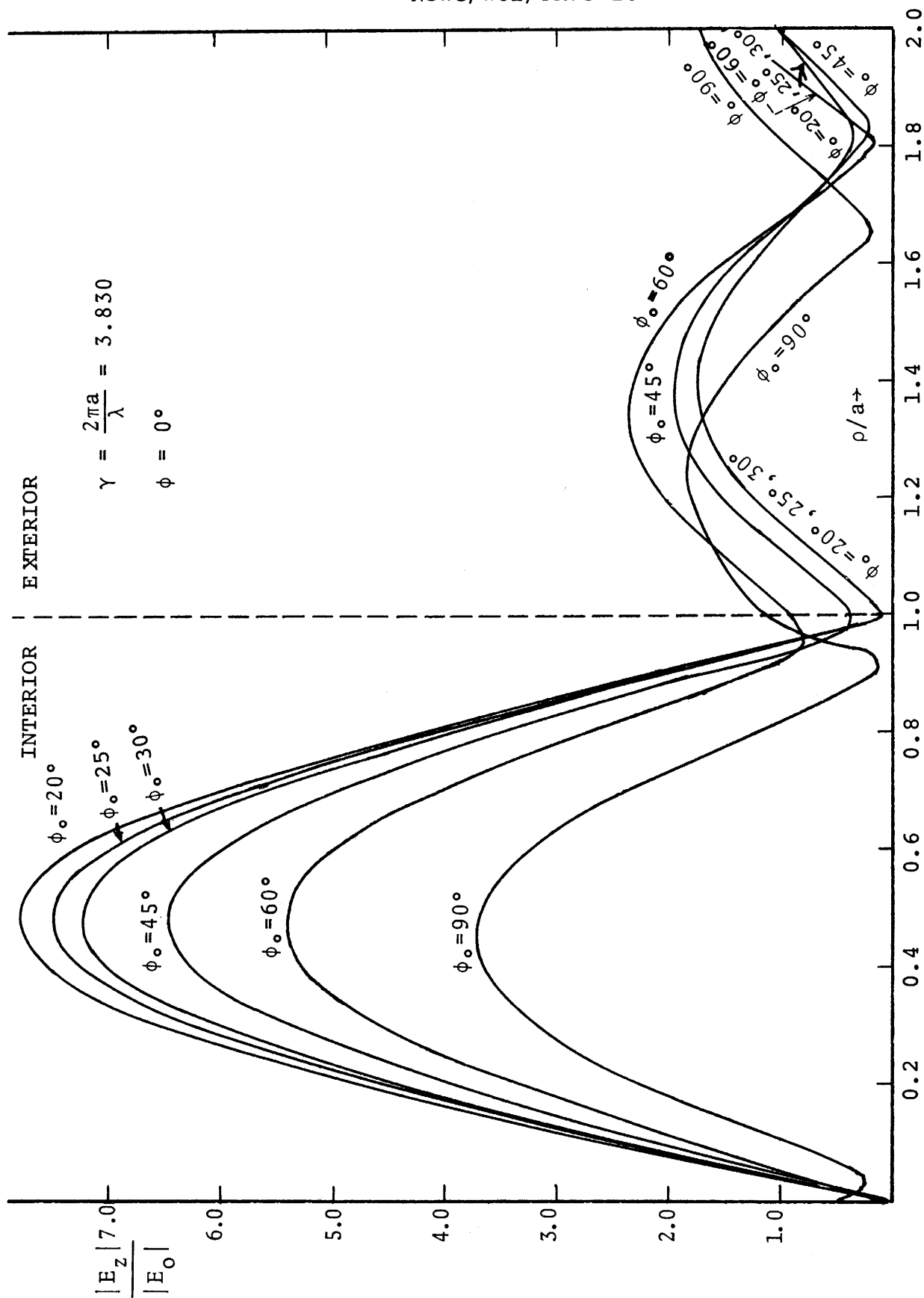


FIGURE 4. RADIAL DISTRIBUTION OF ELECTRIC FIELD ALONG $\phi=0^\circ$ RAY FOR $\gamma=3.830$ AND HALF SLOT ANGLE ϕ_0 .

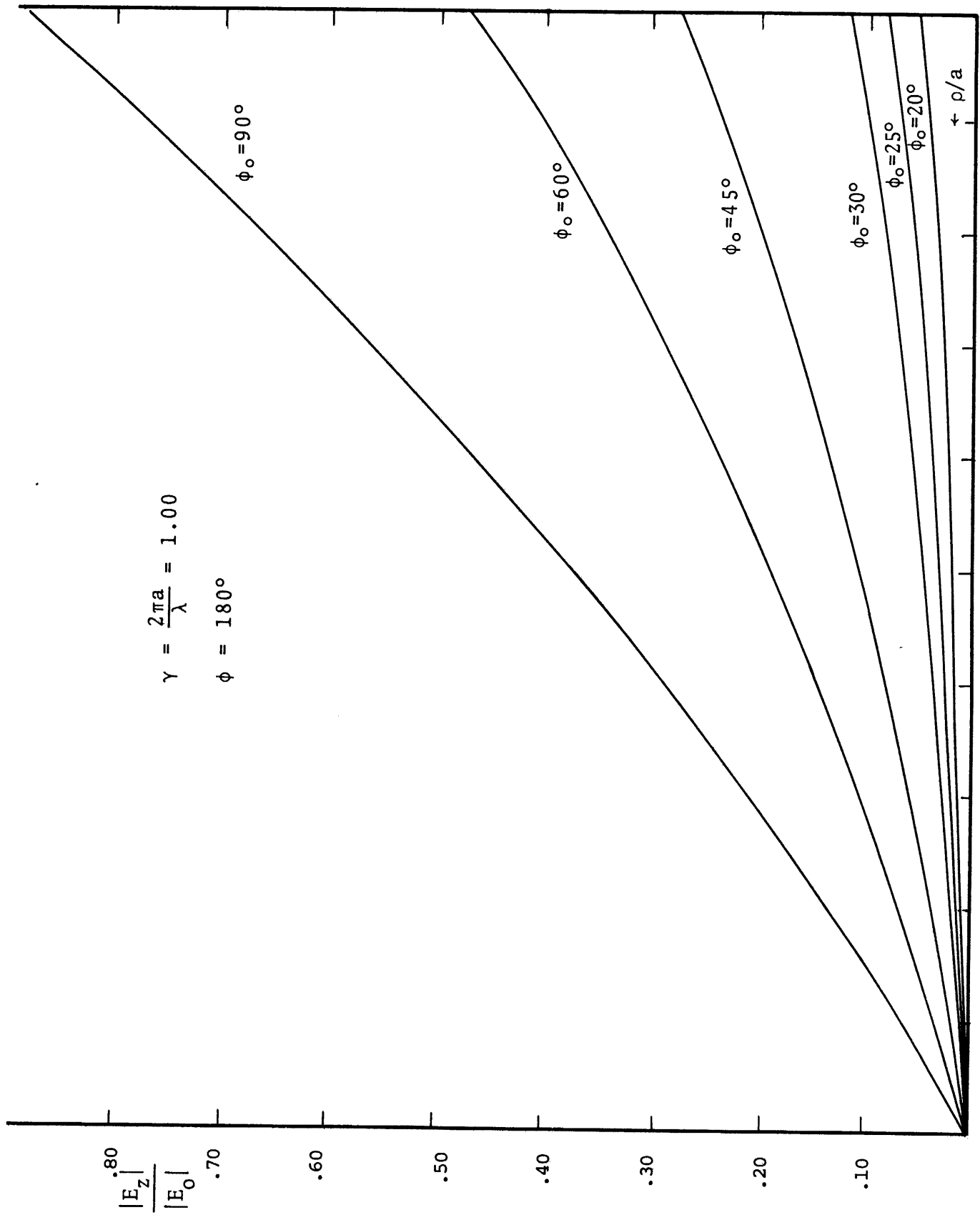


FIGURE 5. RADIAL DISTRIBUTION OF ELECTRIC FIELD ALONG $\phi=180^\circ$ RAY FOR $\gamma=1.00$ AND HALF SLOT ANGLE ϕ_0

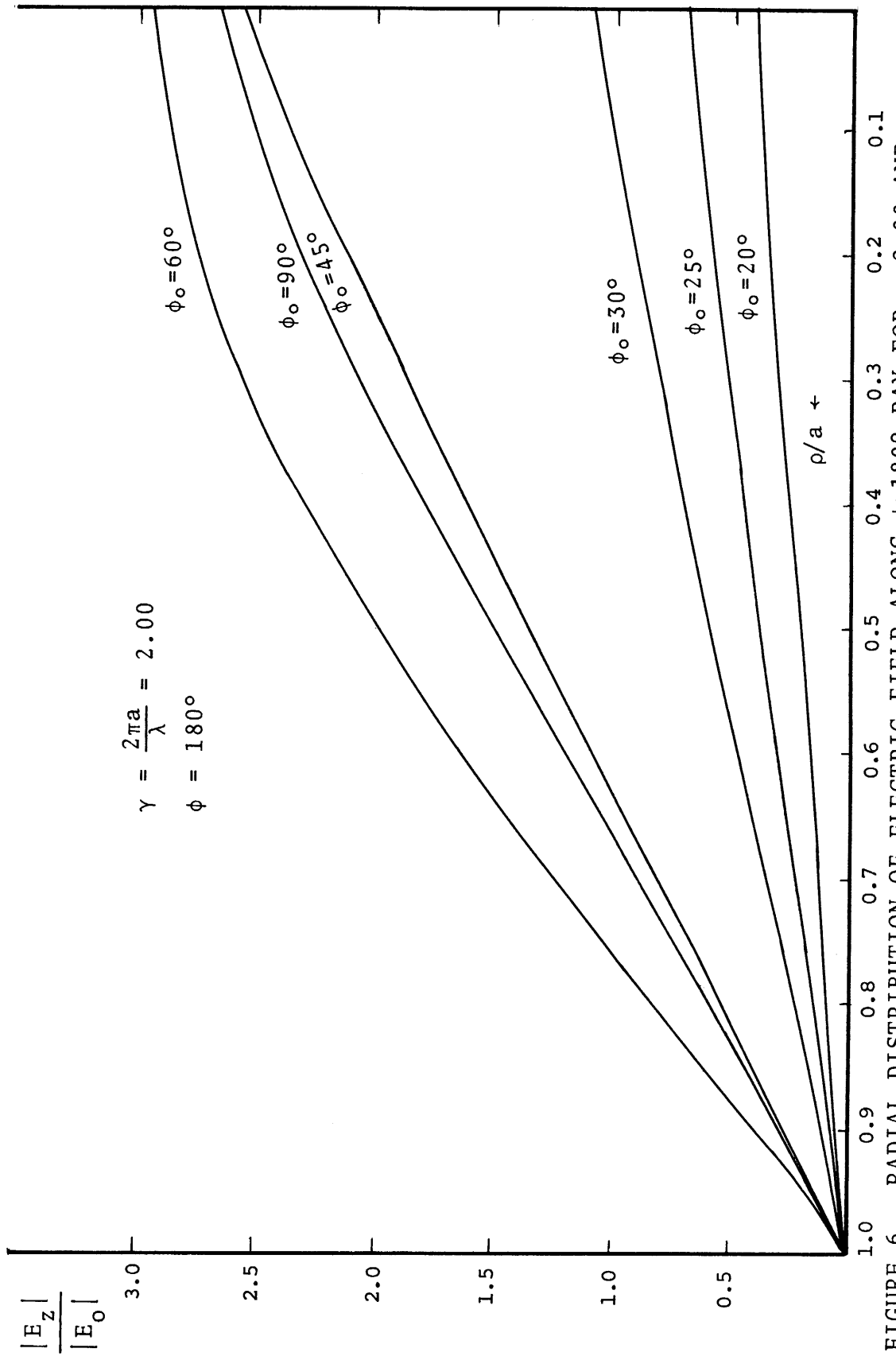


FIGURE 6. RADIAL DISTRIBUTION OF ELECTRIC FIELD ALONG $\phi=180^\circ$ RAY FOR $\gamma=2.00$ AND HALF SLOT ANGLE ϕ_0 .

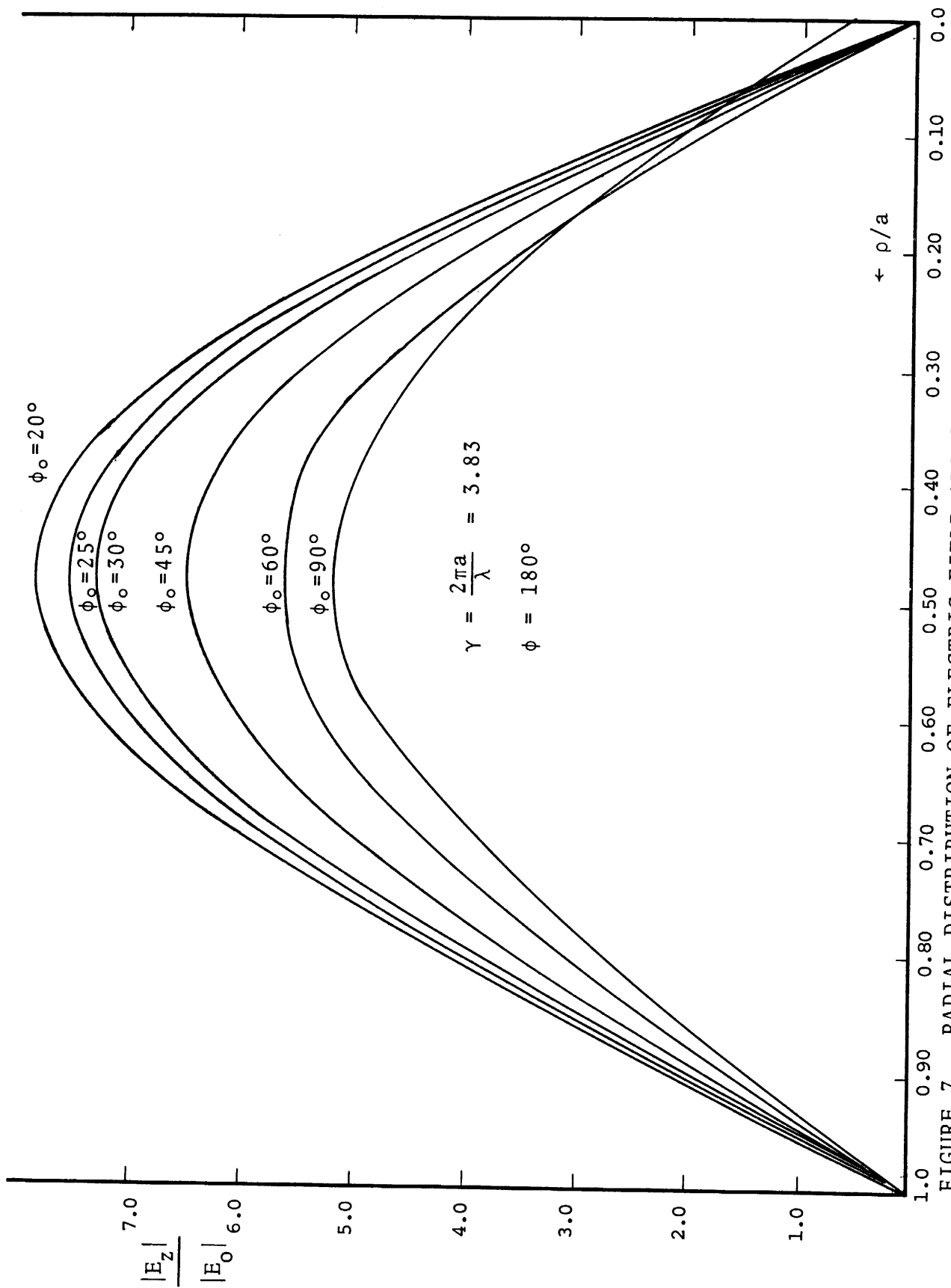


FIGURE 7. RADIAL DISTRIBUTION OF ELECTRIC FIELD ALONG $\phi=180^\circ$ RAY FOR $\gamma=3.830$ AND HALF SLOT ANGLE ϕ_0

the smaller slot angles a minimum occurs either at the slot center or near it. Thus for $\phi_0=20^\circ$, 25° and 30° this minimum occurs extremely close to the center of the slot. Actually this minimum moves inward toward the center or axis of the cylinder as ϕ_0 increases. The field at this minimum increases in amplitude with increasing ϕ_0 until about $\phi_0=60^\circ$. At some point beyond this size slot angle the amplitude reverses its behavior and decreases as ϕ_0 increases. At the slot-center the fields for $\gamma=3.830$ are slightly smaller than those for $\gamma=1.000$ and considerably smaller than those for $\gamma=2.000$. Roughly speaking the electric field at the center of the slot increases as γ increases toward a resonance and then quite abruptly falls in value at the resonance. This has been observed experimentally⁹ for a related problem. A subsequent report in this series will discuss that study in considerable detail.

In the exterior region just beyond the slot center the radial distribution of the electric field oscillates in amplitude in much the same manner as was observed in Figure 3 for $\gamma=2.000$.

b) Radial Distribution Along An Asymmetric Ray Through the Slot

Comparison of the curves in Figures 2 and 8 for $\gamma=1.000$ reveals that the radial distribution of the E-field along the $\phi=0^\circ$ ray is very much the same as that along an asymmetric ray through the aperture for $\phi \approx \frac{1}{2} \phi_0$. In fact if one examines Tables 1 and 7 which numerically display the radial distributions for $\phi_0=20^\circ$ and the two rays $\phi=0^\circ$ and $\phi=10^\circ$ we find that for $\gamma=1.000$ the latter differs from the former by only about 1 percent.

We pause at this point to indicate that the numerical results for the E-field amplitudes along each ray for each slot angle have been tabulated and displayed to show the γ -variations. These results are contained in Tables 1 through 35.

Returning to the line of discussion we note that for $\gamma=2.000$ and also for $\gamma=3.830$ with $\phi_0=20^\circ$ the radial distributions along the $\phi=0^\circ$ ray are almost identical to those along the $\phi=10^\circ$ ray. The only

9. "Coupling of Plane-Polarized Electromagnetic Waves to Cylindrical Modes" C. L. Andrews, L. F. Libelo, D. P. Margolis and R. S. Dunbar, Optics News, page 25, Sep 1975.

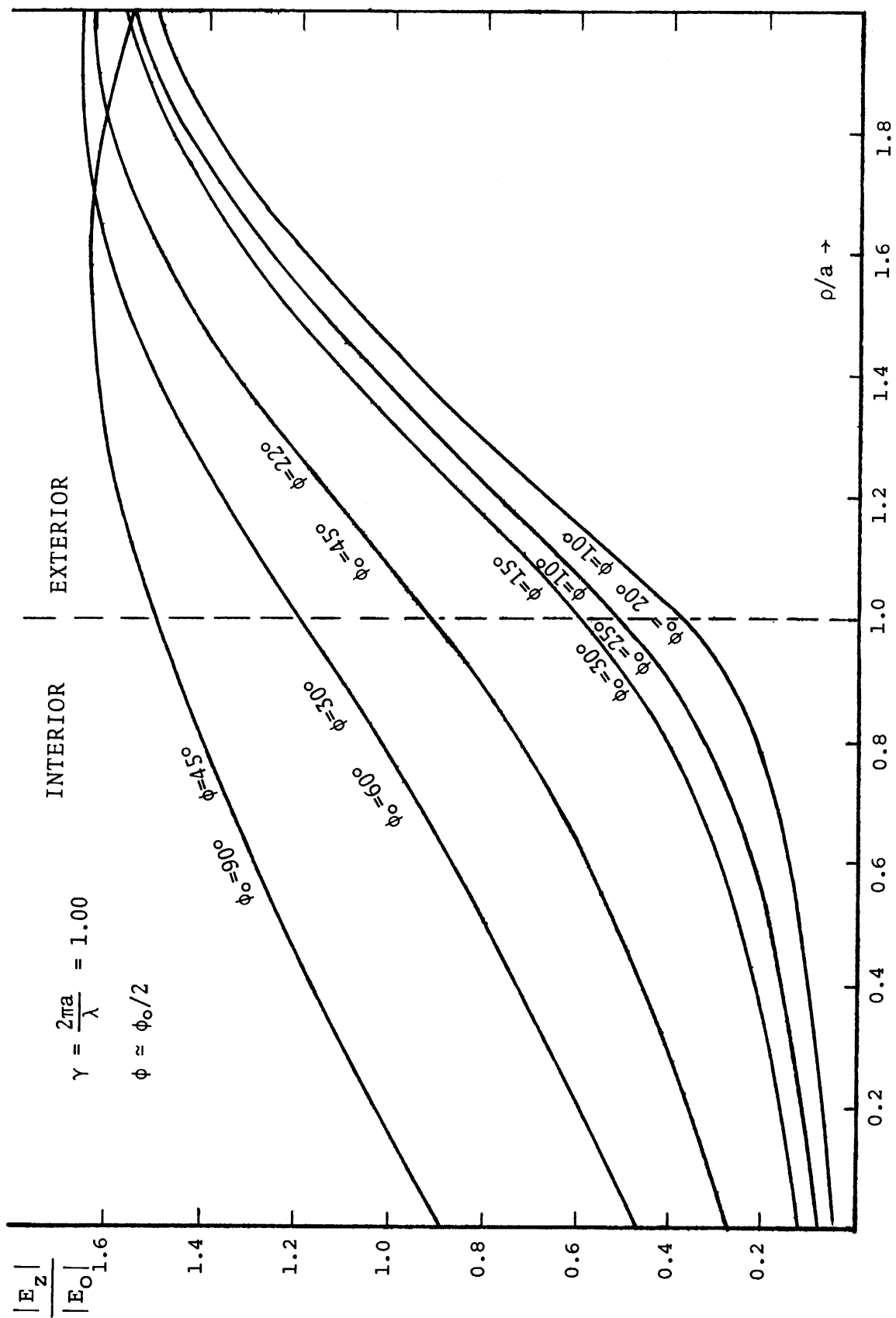


FIGURE 8. RADIAL DISTRIBUTION OF ELECTRIC FIELD FOR RAY THROUGH APERTURE, $\gamma=1.00$, HALF SLOT ANGLE ϕ_0

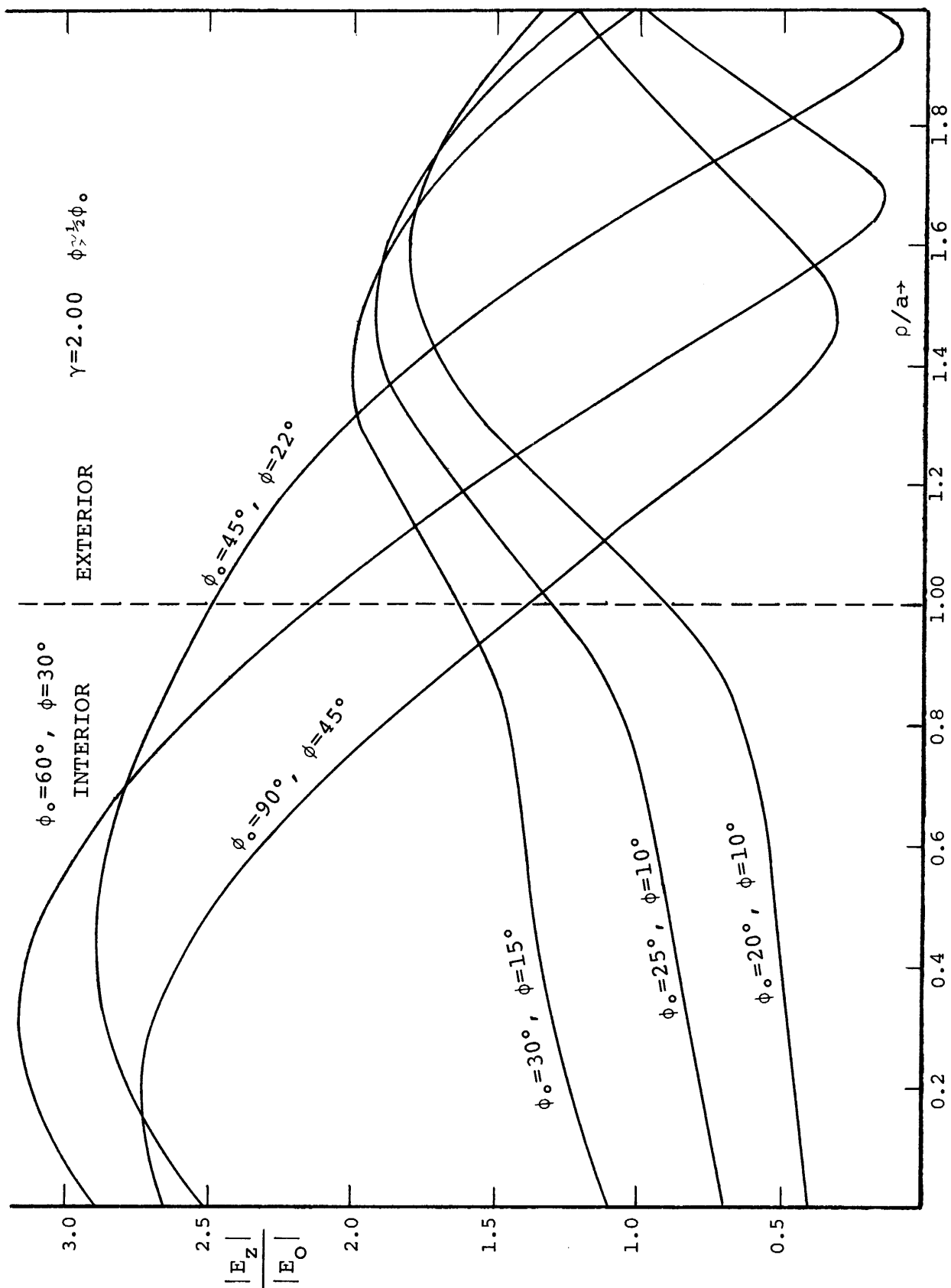


FIGURE 9. RADIAL DISTRIBUTION OF ELECTRIC FIELD FOR RAY THROUGH APERTURE, $\gamma=2.00$, HALF SLOT ANGLE ϕ_o .

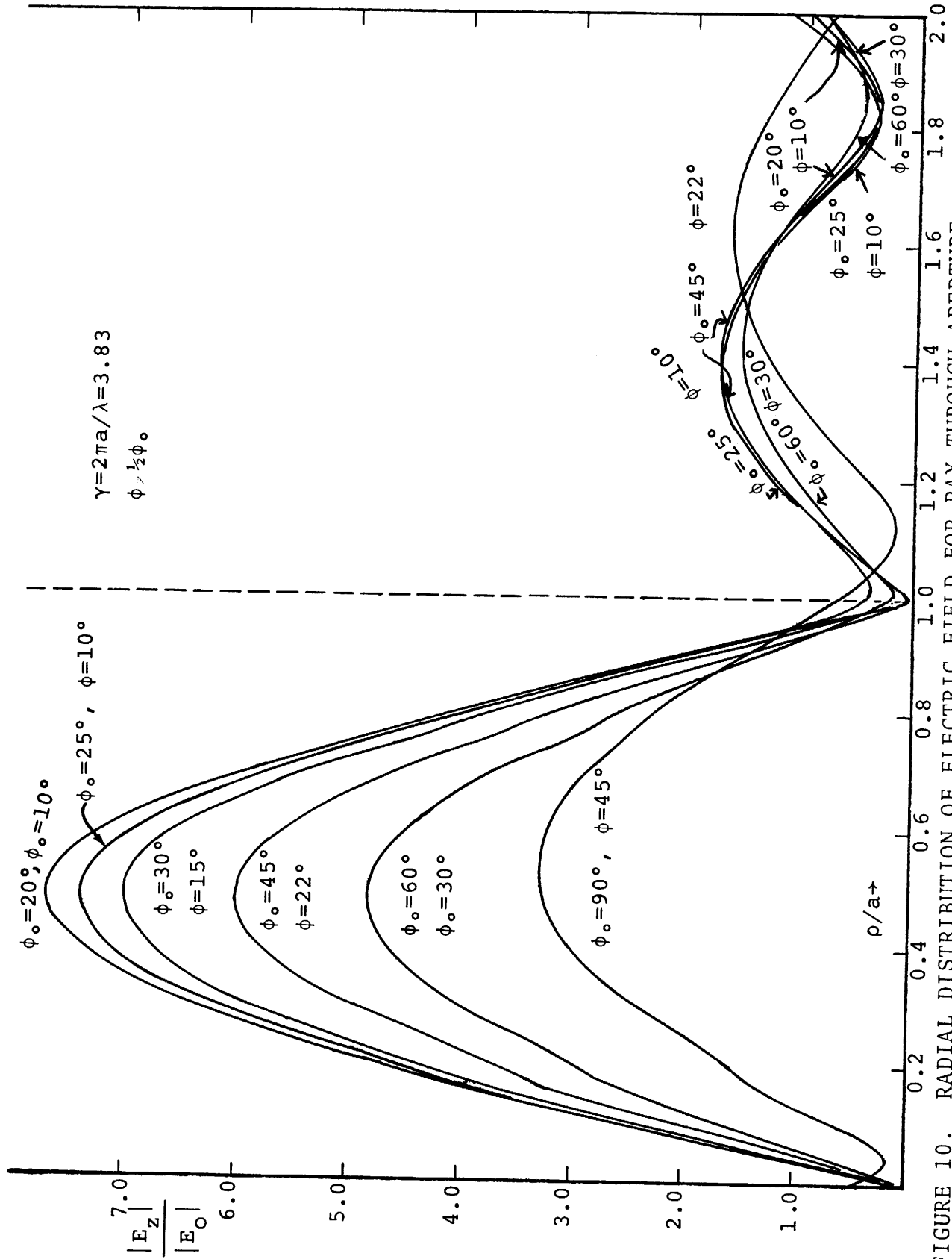


FIGURE 10. RADIAL DISTRIBUTION OF ELECTRIC FIELD FOR RAY THROUGH APERTURE
 $\gamma = 3.83$, HALF SLOT ANGLE ϕ_0 .

real difference is that the former values in general exceed the latter ones by only at most 3-4 percent. For $\phi_0=25^\circ$ about the same situation obtains for the $\phi=0^\circ$ and $\phi=10^\circ$ rays for $\gamma=1.000$, 2.000 and 3.830 . However for the resonance γ the field for $\phi=0^\circ$ is somewhat larger than that for $\phi=10^\circ$ at the larger distances from the slot. These observations can be made by either examining Tables 2 and 8 or Figures 2,3, 4 and Figures 8, 9 and 10. From these figures or from Tables 3 and 9 we note that the same relations hold for $\phi_0=30^\circ$ along the rays $\phi=0^\circ$ and $\phi=15^\circ$. The same comparable behavior is exhibited by the cylinder with a $\phi_0=45^\circ$ slot along the $\phi=0^\circ$ ray and the $\phi=22^\circ$ ray although the deviations are somewhat larger. For $\gamma=3.830$ this latter characteristic is due to the fact that along the $\phi \approx \frac{1}{2} \phi_0$ ray the minima in the vicinity of the slot move outward from the slot as ϕ_0 is increased from 20° . This feature is especially notable with $\gamma=3.830$ for $\phi_0=60^\circ$, along the $\phi=0^\circ$ and $\phi=30^\circ$ rays and for $\phi_0=90^\circ$, along the $\phi=0^\circ$ and $\phi=45^\circ$ rays. In summary then the radial distributions of electric field along rays through the center of the ϕ_0 slot are pretty much the same at least as far off symmetry as the $\phi \cong \frac{1}{2} \phi_0$ ray. There is however one very fascinating difference that can easily be discerned by comparing Figures 4 and 10 for the resonance case. This is the fact that the radial distributions off the symmetry ray exhibit shoulders on either side of the peak for the maxima closer to the slot.

c) Radial Distribution Along The $\phi=90^\circ$ Ray

Next we move around and consider the radial distribution of the electric field inside the slotted cylinder but along the direction perpendicular to the symmetry diameter. This is along the $\phi=90^\circ$ ray. Comparing Figures 11 and 12 we first note that at $\gamma=1.000$ and $\gamma=2.000$, beyond cutoff, the radial distributions for all slot angles depict monotonic falloffs from the field values at the cylinder axis to ultimately vanish at the conducting wall. For each γ we note that the larger the slot angle the greater the field amplitude, reflecting the fact that the larger aperture permits a higher degree of penetration of the incident radiation. Similarly the larger amplitudes for $\gamma=2.000$ relative to those of $\gamma=1.000$ illustrate the fact that beyond

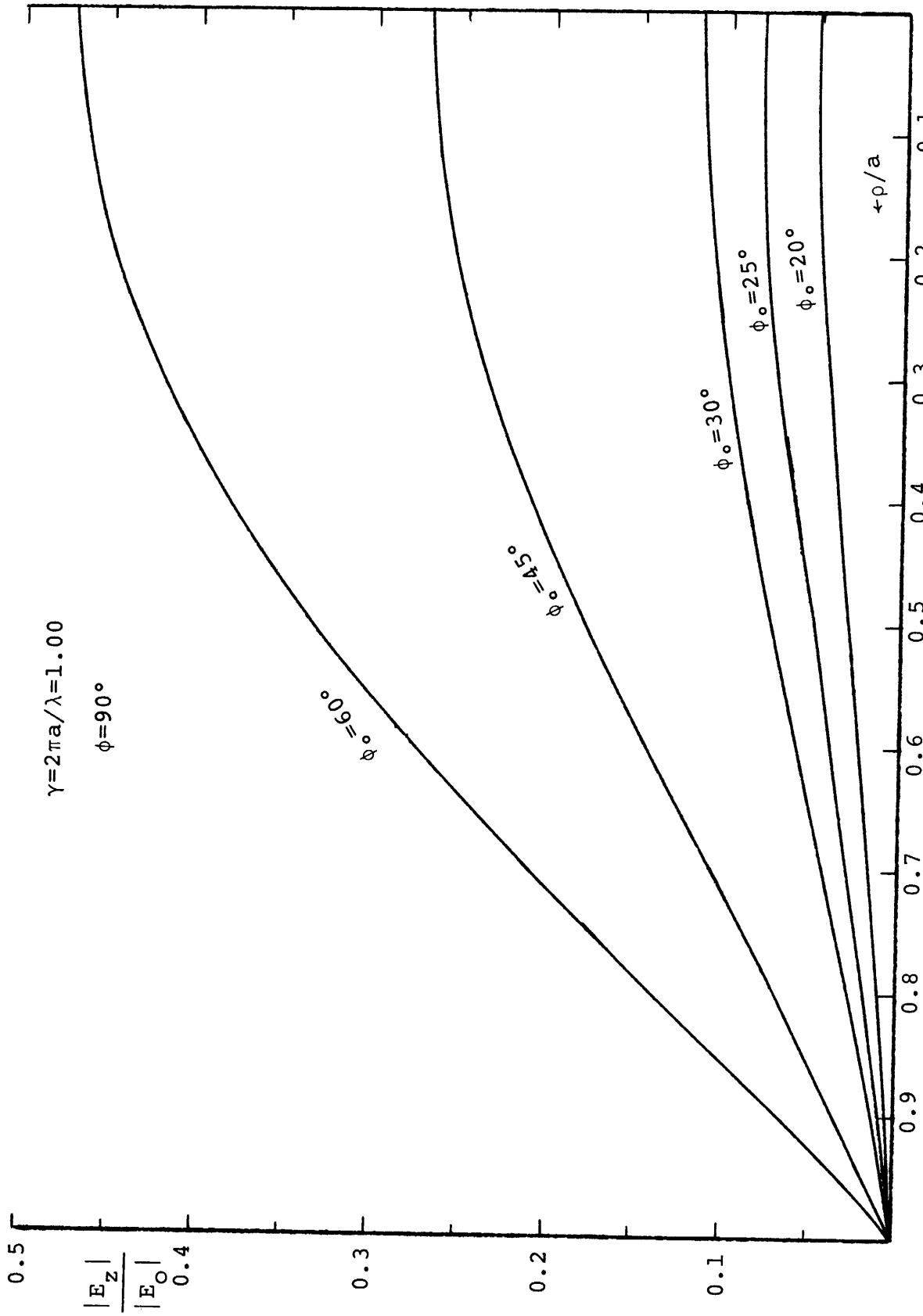


FIGURE 11. RADIAL DISTRIBUTION OF ELECTRIC FIELD ALONG THE $\phi = 90^\circ$ RAY FOR $\gamma = 1.000$ AND HALF SLOT ANGLE ϕ_0 .

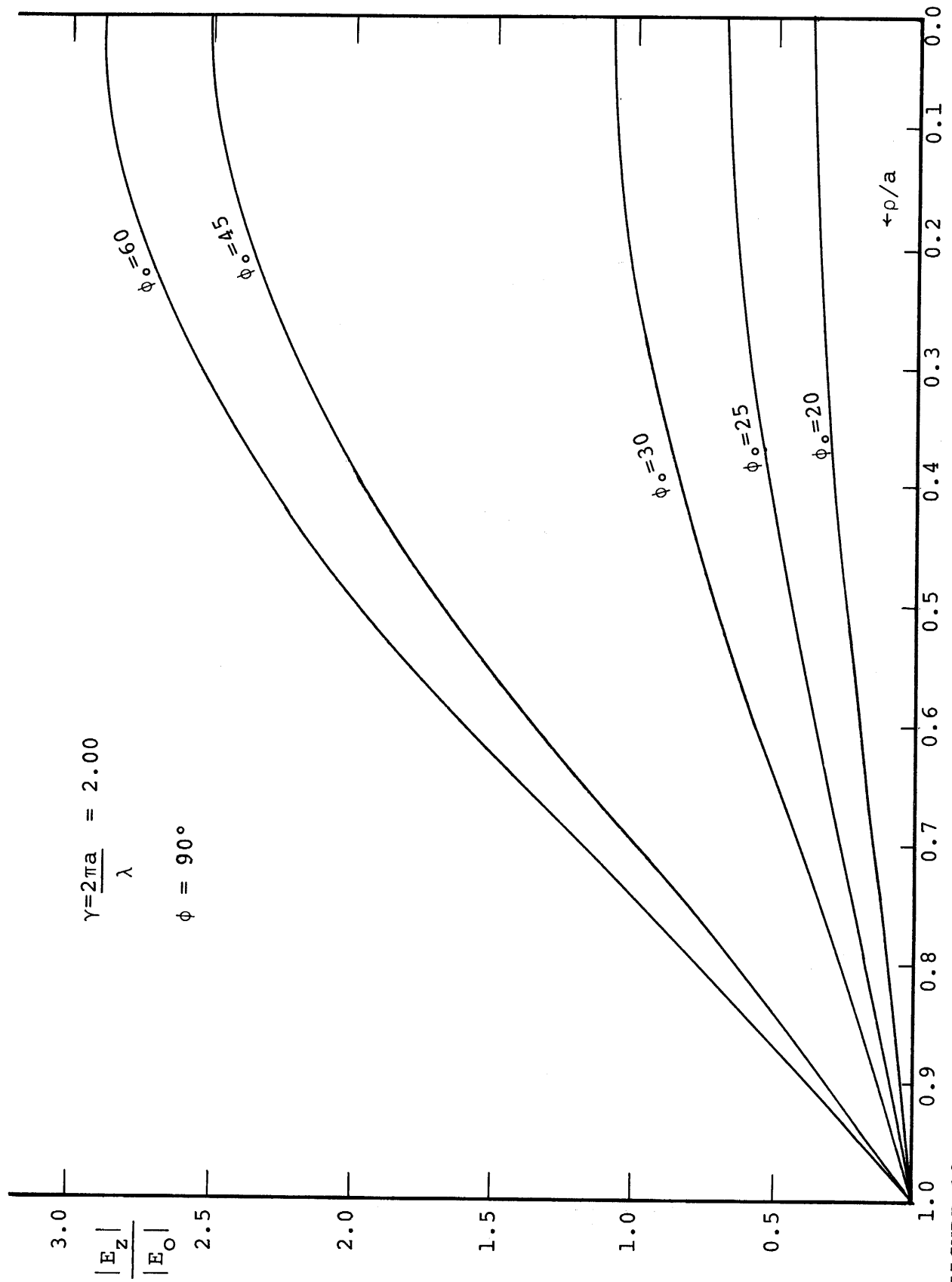


FIGURE 12. RADIAL DISTRIBUTION OF ELECTRIC FIELD ALONG $\phi=90^\circ$ RAY FOR $\gamma=2.00$ AND HALF SLOT ANGLE ϕ_0 .

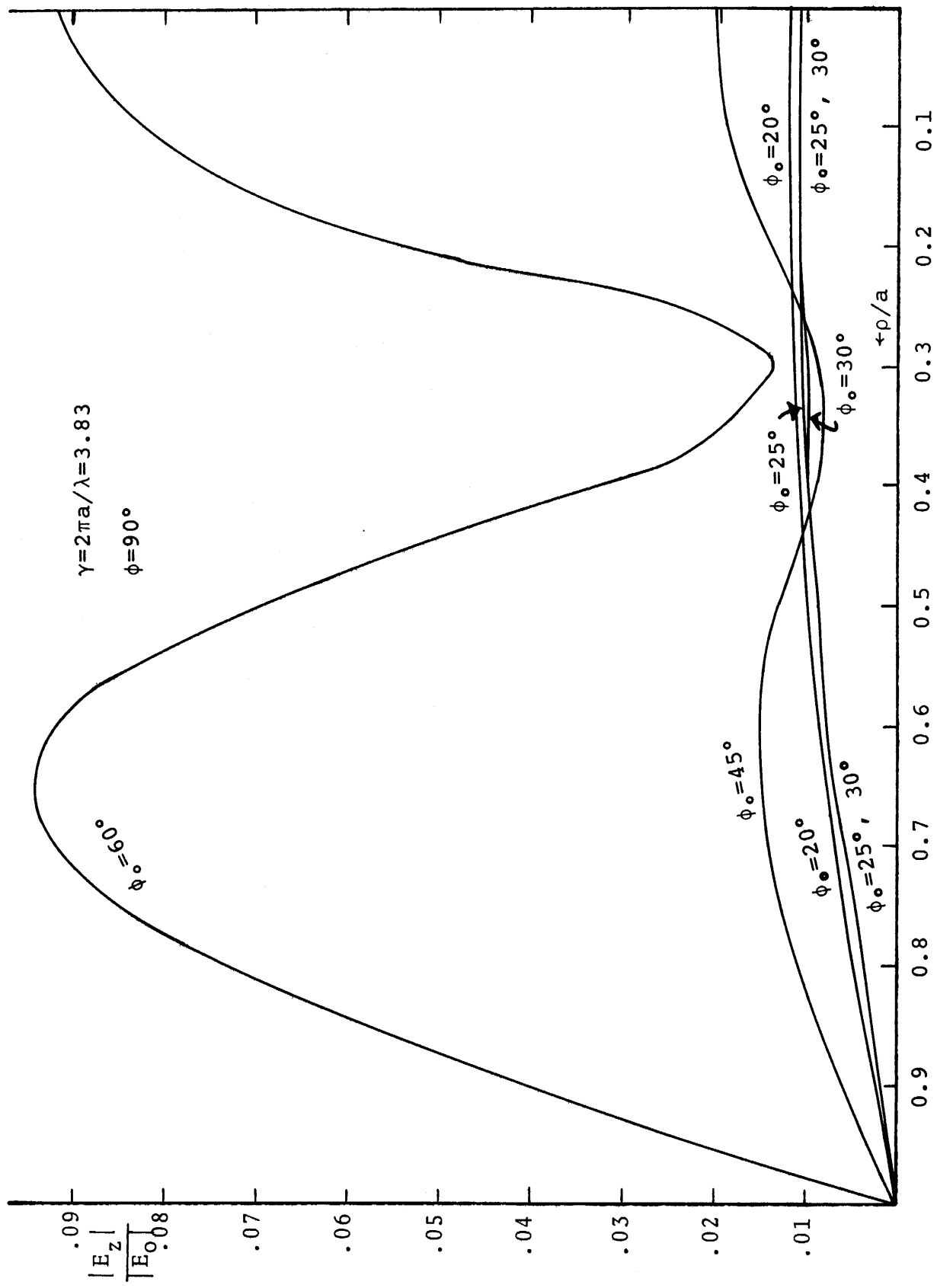


FIGURE 13. RADIAL DISTRIBUTION OF ELECTRIC FIELD ALONG $\phi = 90^\circ$ RAY FOR $\gamma = 3.83$ AND HALF SLOT ANGLE ϕ_0 .

cutoff of a mode the shorter wavelength radiation again penetrates more easily. It is of interest to point out that in Figures 5 and 11 for $\gamma=1.000$ the radial distributions for each ϕ_0 along the $\phi=90^\circ$ ray are concave toward the radial axis whereas along the $\phi=180^\circ$ ray they are convex toward that coordinate axis. Examination of Figures 6 and 12 show that for $\gamma=2.000$ the $\phi=180^\circ$ and $\phi=90^\circ$ radial distributions have the same features for slot angles ϕ_0 up to about 30° . For larger slot angles the distribution normal to the symmetry diameter seems to be almost the same as that along the symmetry diameter from the cylinder axis back to the conducting wall.

At the resonance value of γ a very dramatic change in the amplitude of the electric field along the $\phi=90^\circ$ ray is evident. We find that by comparing Figures 7 and 13 for the $\phi=180^\circ$ and $\phi=90^\circ$ rays a decrease of about two orders of magnitude occurs. It can also be seen that along the $\phi=90^\circ$ ray the larger slot angle roughly speaking has the larger amplitude. This then reverses at some smaller value of ϕ_0 .

We see in Figure 13 that along the $\phi=90^\circ$ ray we do not have a monotonic behavior from $\rho=0$ out to $\rho=a$. Actually for ϕ_0 greater than 20° a minimum in the radial distribution of the field is evident at about $\rho = \frac{a}{3}$. Summarizing we find that the behavior of the field along the ray normal to the symmetry diameter rather closely approximates that along the $\phi=180^\circ$ ray. However, at a resonance the field drops sharply along the $\phi=90^\circ$ ray.

d) Radial Distribution Along A Ray Inside But Just Beyond the Slot Edge, $\phi \geq \phi_0$.

We are now considering the radial distribution of electric field along a ray located entirely within the slotted cylinder and about 10° beyond the edge of the slot. Comparing Figures 14 and 15 we see again that for each slot size the shorter wavelength radiation penetrates more readily. The behavior of the $\phi_0=90^\circ$ distributions in these figures is not too surprising in view of the fact that they lie along rays that are back past the direction normal to the symmetry diameter. If we compare the distributions for $\gamma=1.000$ and $\gamma=2.000$ along the

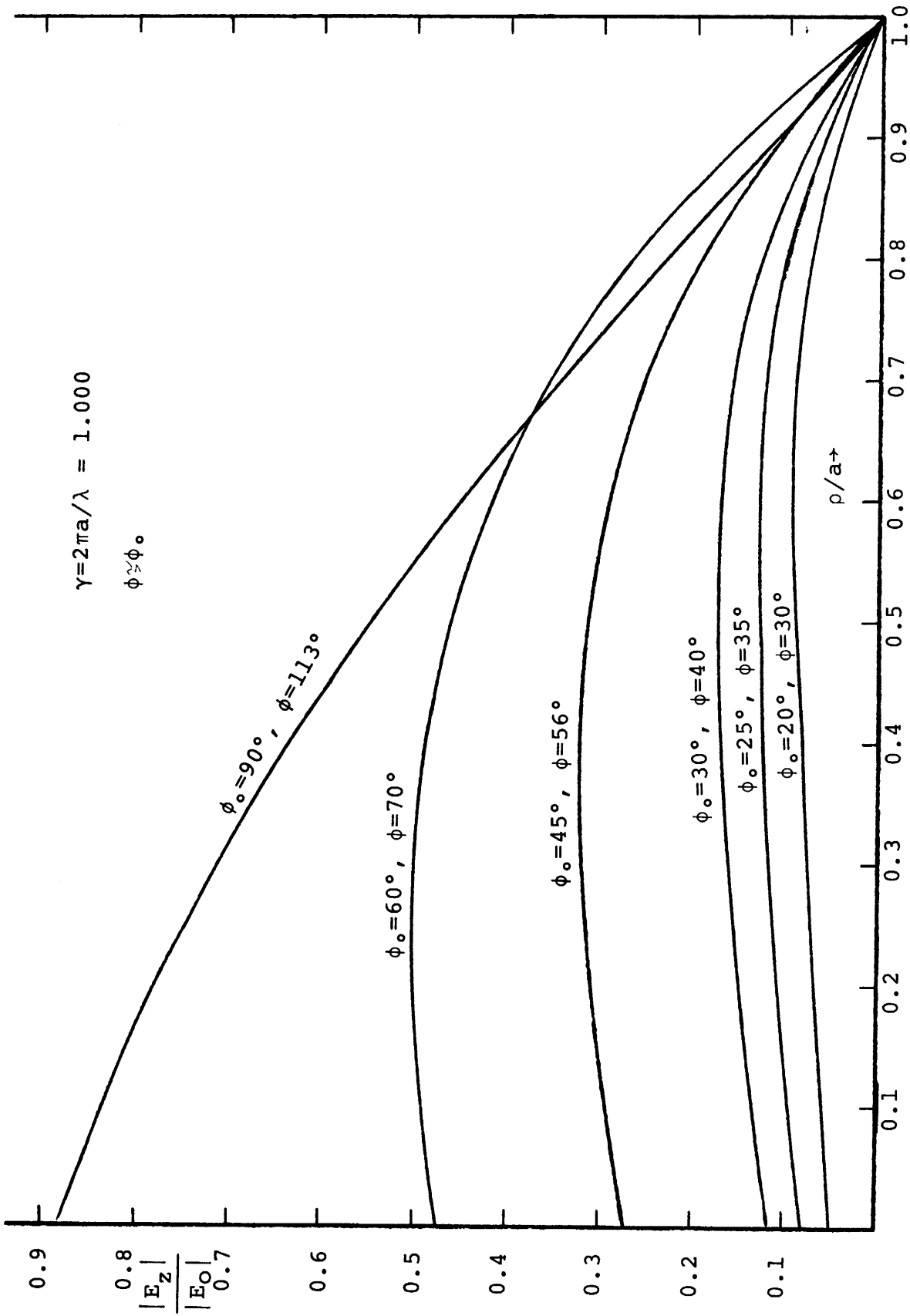


FIGURE 14. RADIAL DISTRIBUTION OF ELECTRIC FIELD ALONG RAY INSIDE CYLINDER, $\phi \neq \phi_0$, FOR $\gamma=1.000$ AND HALF SLOT ANGLE ϕ_0 .

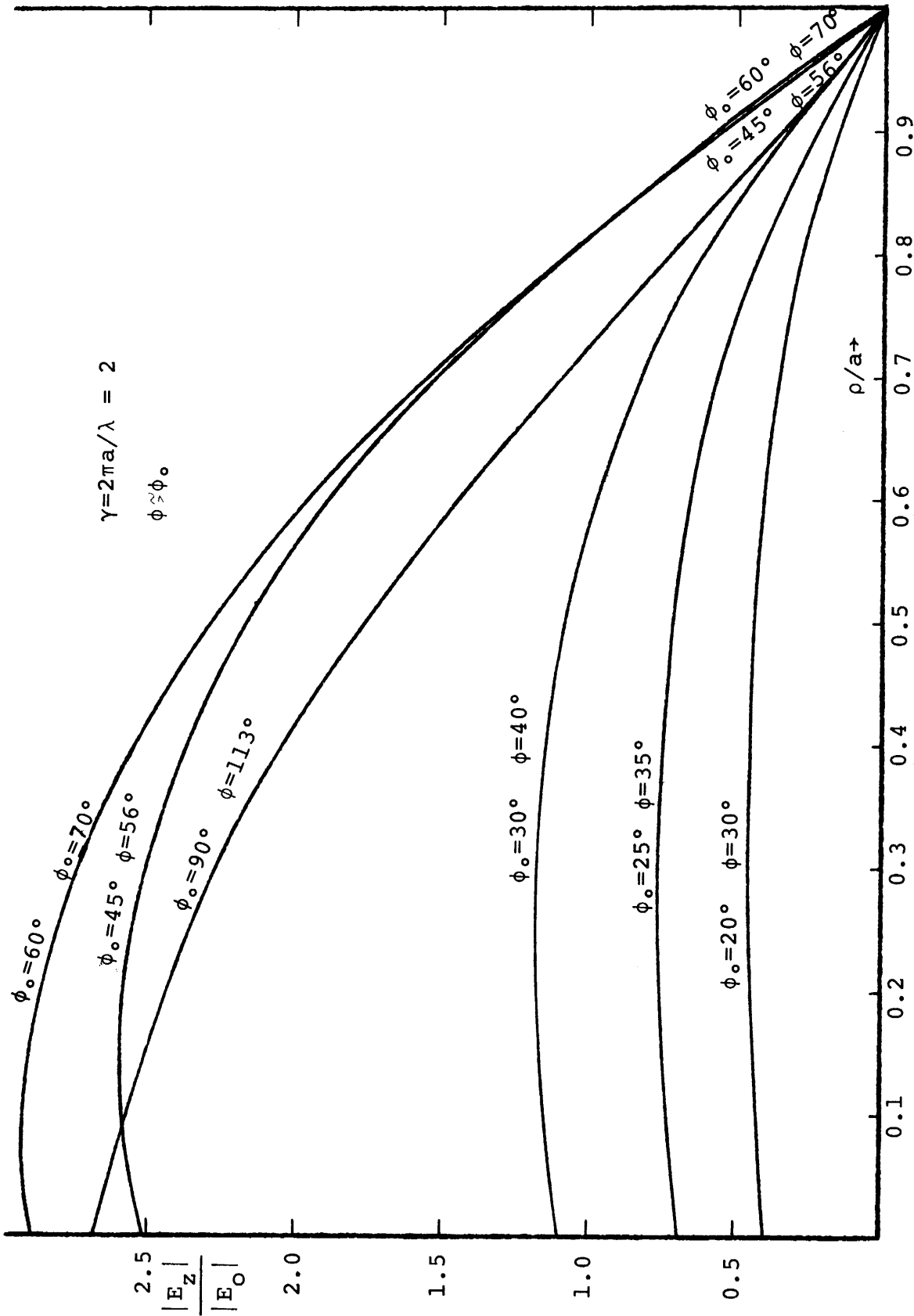


FIGURE 15. RADIAL DISTRIBUTION OF ELECTRIC FIELD ALONG RAY INSIDE CYLINDER $\phi = \phi_0$ FOR $\gamma = 2.00$ AND HALF SLOT ANGLE ϕ_0 .

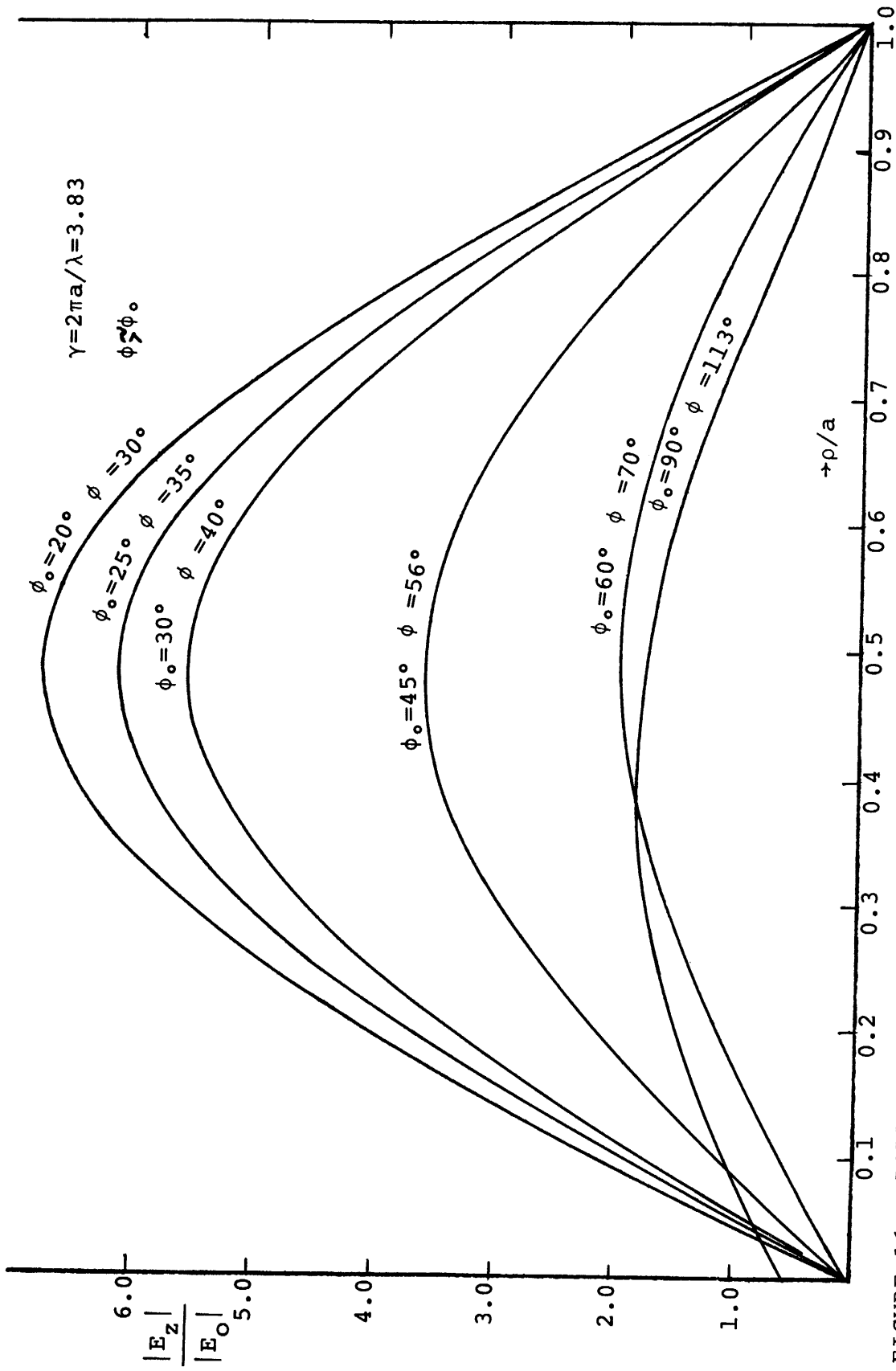


FIGURE 16. RADIAL DISTRIBUTION OF ELECTRIC FIELD ALONG RAY INSIDE CYLINDER $\phi \neq \phi_0$. FOR $\gamma = 3.83$ AND HALF SLOT ANGLE ϕ_0 .

$\phi \geq \phi_0$ and the $\phi=90^\circ$ ray we find that for each γ separately there is not too much difference in the fields. The only evident significant difference is that in the region just behind the slot edge a maximum field occurs, inside, away from the cylinder axis. The larger the slot angle the closer to this axis this maximum is located. Basically this gives the behavior for γ beyond cutoff.

At the second resonance we very readily find by comparing Figure 13 for the $\phi=90^\circ$ ray with Figure 16 for a ray about 10° beyond the slot edge a most striking difference in behavior. For the smaller slot angles up to about $\phi_0=45^\circ$ the same radial distribution with somewhat lower amplitudes are observed along the $\phi \geq \phi_0$ ray as exists along the back half ($\phi=180^\circ$) of the symmetry diameter as shown in Figure 7. The resonance maxima exhibit decreasing amplitude as ϕ_0 increases. The case is somewhat different for the larger slot angles. Thus for $\phi_0=60^\circ$ and $\phi=70^\circ$ the field amplitudes are about half those for the $\phi_0=60^\circ$ $\phi=180^\circ$ distribution and the maxima has shifted toward the conducting wall. Up to slot angles $\phi_0 \sim 60^\circ$ the internal field resembles very strongly the resonance case for no slot. At $\phi_0=90^\circ$, with only half the cylinder intact we find along the $\phi=113^\circ$ ray the amplitude is about the same as that for $\phi_0=60^\circ$ along the 70° ray. Further for $\phi_0=90^\circ$ the peak which is not too pronounced along the $\phi=113^\circ$ ray shifts toward the cylinder axis. In summary the field distribution inside the conductor at the second resonance is pretty much that of the slotless circular waveguide. The larger the aperture the greater the difference from this closed cylinder behavior.

e) Radial Distribution Along An Asymmetric Ray Toward the Back Wall

By finally examining the radial distribution of electric field along the $\phi=135^\circ$ ray we have pretty nearly mapped out the behavior of the electric field inside the slotted cylinder. For $\gamma=1.000$ and $\phi_0=90^\circ$ comparing Figures 17, 14 and 5 we find that the radial distributions of electric field are nearly the same along the $\phi=135^\circ$, 180° and 113° rays respectively. They start at a value of about 0.9 at the axis of the cylinder and monotonically drop to zero at the conducting wall. The radial distributions for the remaining $\gamma=1.000$

fields for slot angles $\phi_0=60^\circ$ and less are nearly the same along the $\phi=135^\circ$ and $\phi=180^\circ$ rays. Although for $\gamma=1.000$ they display nearly the same amplitude characteristics along $\phi=135^\circ$ and $\phi \geq \phi_0$, in the latter case we recall (see Figure 14) a maximum is seen to occur such that the smaller the slot angle the closer to the wall the maximum can be found. For $\gamma=2.000$ the $\phi=135^\circ$ radial distributions are pretty much the same as those along the $\phi=180^\circ$ ray for ϕ_0 up to 45° . The $\phi_0=90^\circ$ distributions are very close to one another also. For $\phi_0=60^\circ$ we find that from $\rho/a \approx 0.6$ on out the electric field amplitude is very nearly coincident with the $\phi_0=90^\circ$ field along the $\phi=135^\circ$ ray. Actually the $\phi_0=60^\circ$ field along the $\phi=135^\circ$ is somewhat lower in amplitude than along the back half of the symmetry diameter.

In the case of the second resonance we find that outside of the fact that the amplitude is smaller along the $\phi=135^\circ$ ray the same behavior is exhibited by the radial distribution of the field as along the $\phi=180^\circ$ ray. Thus over the area on the back side of the $\phi=90^\circ$ ray toward the conducting wall the behavior at resonance is about that of the closed cylindrical waveguide with a shifting of the energy away from the slot itself occurring.

At this point we pause to reflect that we now have a pretty complete idea or picture of the interior fields and exterior fields near the slot from beyond cutoff at $\gamma=1.000$ and 2.000 and at the second effective resonance for cylinders with intermediate as well as large slot angles. With this analytical information in our possession we can proceed to consider some laboratory investigations to determine the limitations inherent in describing finite systems in terms of known infinite systems.

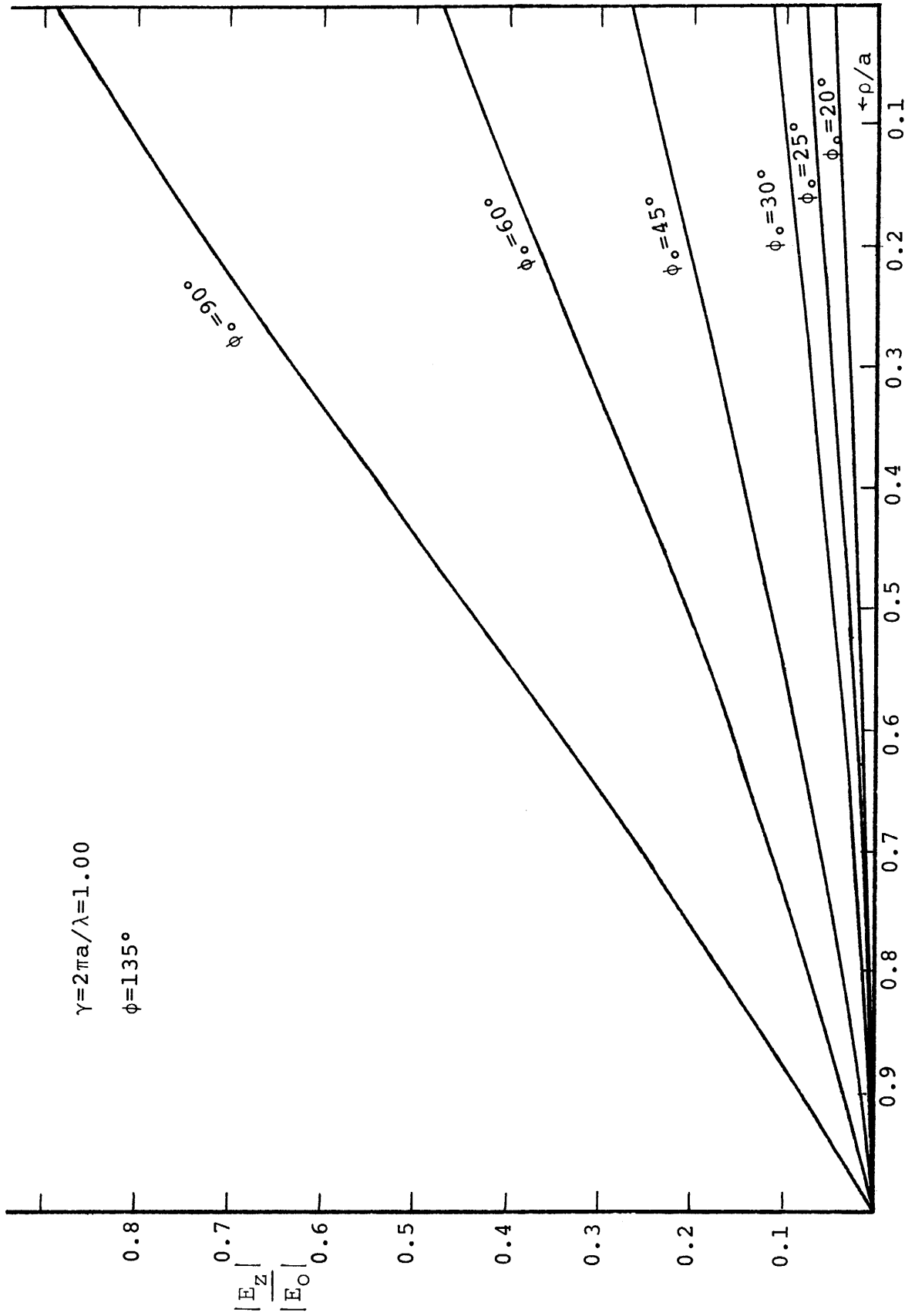


FIGURE 17. RADIAL DISTRIBUTION OF ELECTRIC FIELD ALONG $\phi=135^\circ$ RAY FOR $\gamma=1.00$ AND HALF SLOT ANGLE ϕ_0 .

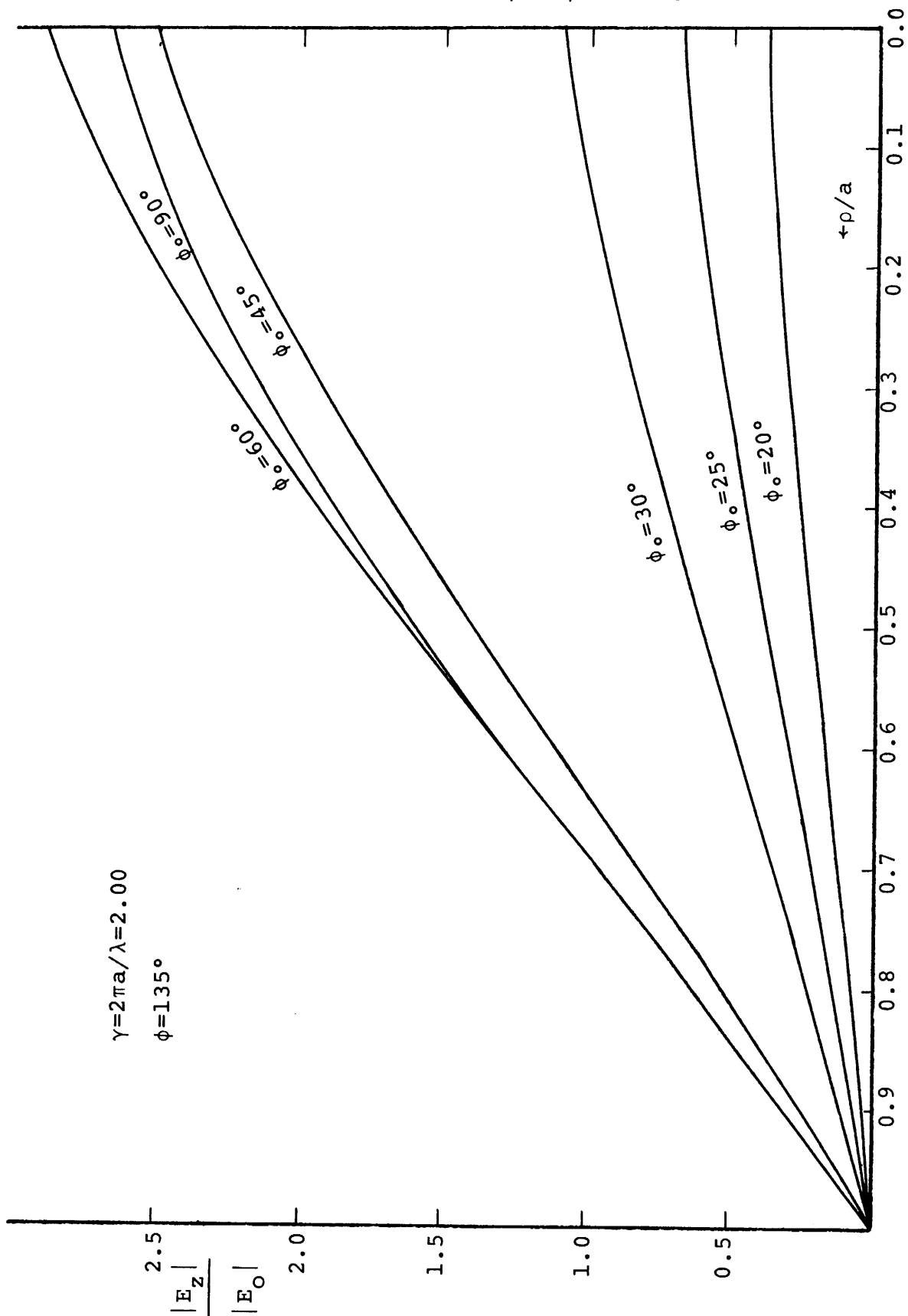


FIGURE 18. RADIAL DISTRIBUTION OF ELECTRIC FIELD ALONG $\phi = 135^\circ$ RAY FOR $\gamma = 2.00$ AND HALF SLOT ANGLE ϕ_0 .

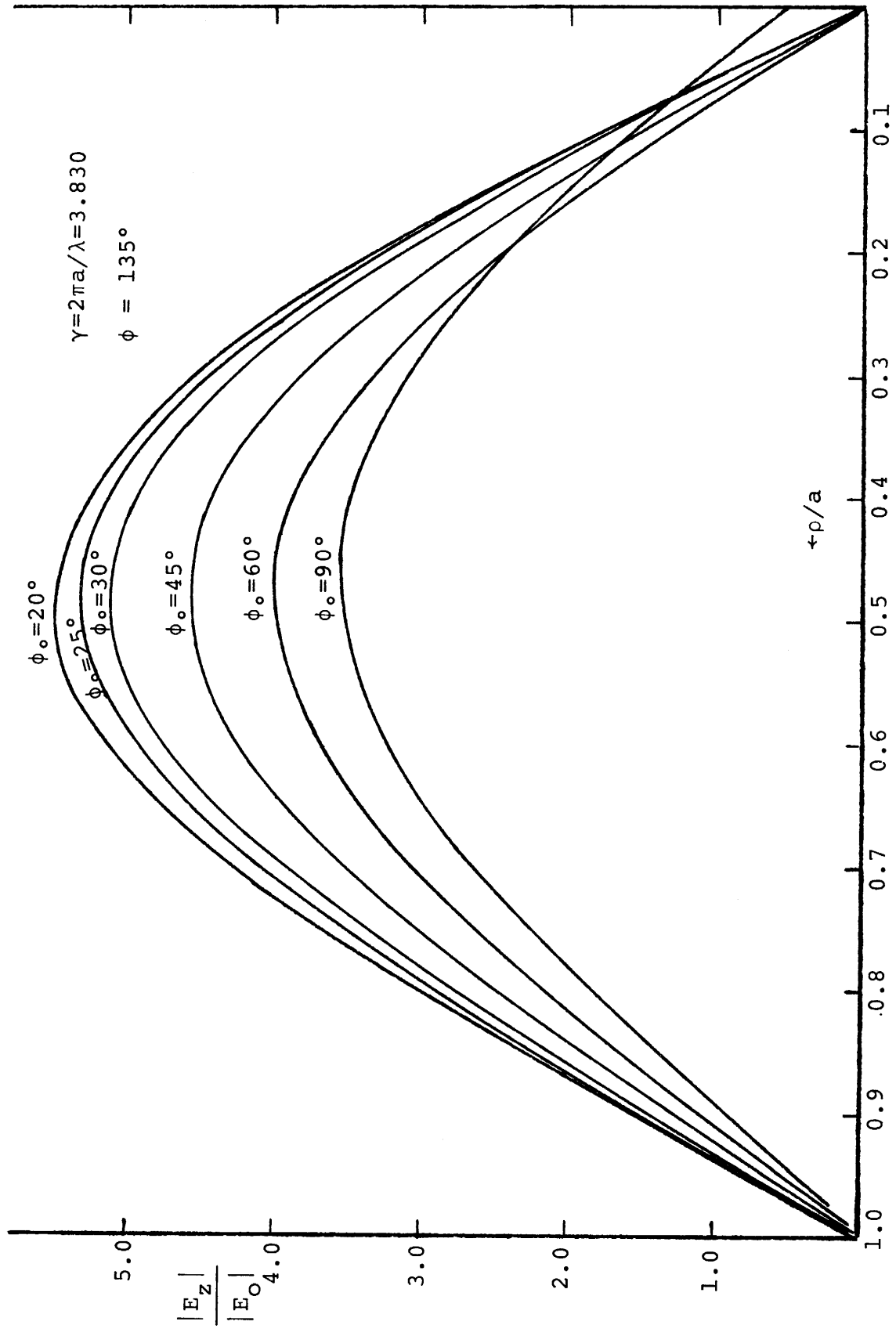


FIGURE 19. RADIAL DISTRIBUTION OF ELECTRIC FIELD ALONG THE $\phi=135^\circ$ RAY FOR $\gamma=3.83$ AND HALF SLOT ANGLE ϕ_o .

TABLE 1. RADIAL DISTRIBUTION OF ELECTRIC FIELD, $|E_z|/|E_0|$, ALONG THE $\phi=0^\circ$ RAY FOR HALF SLOT ANGLE $\phi_0 = 20^\circ$ AND CIRCUM-FERENCE TO WAVELENGTH RATIOS, $\gamma=1.000$, 2.000 AND 3.830

ρ/a	$\gamma=1.000$	$\gamma=2.000$	$\gamma=3.830$
0.000	0.051	0.399	0.012
0.050	0.055	0.413	1.270
0.100	0.060	0.427	2.517
0.150	0.066	0.441	3.695
0.200	0.072	0.454	4.773
0.250	0.078	0.466	5.720
0.300	0.085	0.479	6.514
0.350	0.093	0.491	7.132
0.400	0.103	0.504	7.560
0.450	0.113	0.518	7.789
0.500	0.125	0.534	7.816
0.550	0.139	0.552	7.643
0.600	0.155	0.574	7.278
0.650	0.174	0.600	6.736
0.700	0.197	0.632	6.037
0.750	0.224	0.672	5.203
0.800	0.255	0.720	4.262
0.850	0.293	0.780	3.245
0.900	0.337	0.850	2.182
0.950	0.387	0.932	1.107
1.000	0.444	1.024	0.059
1.050	0.505	1.122	0.332
1.100	0.570	1.224	0.688
1.150	0.637	1.326	1.003
1.200	0.706	1.425	1.270
1.250	0.775	1.519	1.482
1.300	0.844	1.603	1.633
1.350	0.911	1.676	1.721
1.400	0.977	1.737	1.746
1.450	1.040	1.784	1.708
1.500	1.100	1.816	1.611
1.550	1.158	1.833	1.462
1.600	1.212	1.834	1.267
1.650	1.263	1.819	1.039
1.700	1.311	1.789	0.791
1.750	1.355	1.744	0.554
1.800	1.395	1.684	0.396
1.850	1.432	1.610	0.435
1.900	1.465	1.523	0.624
1.950	1.494	1.424	0.849
2.000	1.519	1.314	1.064

TABLE 2. RADIAL DISTRIBUTION OF ELECTRIC FIELD, $|E_z|/|E_0|$, ALONG THE $\phi=0^\circ$ RAY FOR HALF SLOT ANGLE $\phi_0 = 25^\circ$ AND CIRCUMFERENCE TO WAVELENGTH RATIOS, $\gamma=1.000, 2.000$ AND 3.830

ρ/a	$\gamma=1.000$	$\gamma=2.000$	$\gamma=3.830$
0.000	0.081	0.691	0.011
0.050	0.088	0.716	1.222
0.100	0.095	0.741	2.422
0.150	0.104	0.763	3.556
0.200	0.113	0.785	4.593
0.250	0.123	0.806	5.505
0.300	0.134	0.826	6.268
0.350	0.146	0.846	6.863
0.400	0.160	0.867	7.275
0.450	0.175	0.888	7.495
0.500	0.193	0.912	7.521
0.550	0.213	0.937	7.354
0.600	0.235	0.967	7.002
0.650	0.261	1.001	6.481
0.700	0.291	1.041	5.807
0.750	0.325	1.087	5.003
0.800	0.363	1.141	4.097
0.850	0.406	1.203	3.116
0.900	0.455	1.273	2.092
0.950	0.507	1.349	1.055
1.000	0.564	1.430	0.070
1.050	0.624	1.513	0.349
1.100	0.687	1.595	0.702
1.150	0.751	1.675	1.016
1.200	0.815	1.749	1.283
1.250	0.880	1.815	1.494
1.300	0.944	1.870	1.645
1.350	1.006	1.914	1.733
1.400	1.067	1.944	1.757
1.450	1.125	1.960	1.718
1.500	1.181	1.961	1.621
1.550	1.234	1.947	1.470
1.600	1.284	1.918	1.275
1.650	1.330	1.873	1.045
1.700	1.374	1.812	0.796
1.750	1.414	1.738	0.555
1.800	1.450	1.649	0.393
1.850	1.483	1.547	0.429
1.900	1.512	1.434	0.619
1.950	1.537	1.309	0.846
2.000	1.559	1.176	1.062

TABLE 3. RADIAL DISTRIBUTION OF ELECTRIC FIELD, $|E_z|/|E_0|$, ALONG THE $\phi=0^\circ$ RAY FOR HALF SLOT ANGLE $\phi_0=30^\circ$ AND CIRCUM-FERENCE TO WAVELENGTH RATIOS, $\gamma=1.000, 2.000$ AND 3.830

ρ/a	$\gamma=1.000$	$\gamma=2.000$	$\gamma=3.830$
0.000	0.117	1.098	0.011
0.050	0.128	1.138	1.180
0.100	0.139	1.176	2.338
0.150	0.151	1.211	3.432
0.200	0.164	1.244	4.433
0.250	0.178	1.276	5.314
0.300	0.193	1.306	6.050
0.350	0.210	1.335	6.625
0.400	0.229	1.364	7.022
0.450	0.250	1.394	7.235
0.500	0.273	1.424	7.259
0.550	0.299	1.456	7.097
0.600	0.328	1.491	6.758
0.650	0.360	1.529	6.253
0.700	0.396	1.571	5.602
0.750	0.436	1.618	4.825
0.800	0.479	1.670	3.949
0.850	0.527	1.725	3.001
0.900	0.578	1.784	2.011
0.950	0.632	1.845	1.010
1.000	0.689	1.905	0.108
1.050	0.748	1.964	0.374
1.100	0.808	2.018	0.723
1.150	0.869	2.066	1.036
1.200	0.930	2.105	1.303
1.250	0.991	2.134	1.514
1.300	1.050	2.150	1.665
1.350	1.108	2.154	1.753
1.400	1.164	2.144	1.777
1.450	1.218	2.119	1.738
1.500	1.269	2.079	1.640
1.550	1.317	2.024	1.488
1.600	1.362	1.954	1.291
1.650	1.404	1.869	1.058
1.700	1.443	1.770	0.806
1.750	1.478	1.657	0.560
1.800	1.510	1.532	0.388
1.850	1.538	1.396	0.417
1.900	1.562	1.250	0.608
1.950	1.583	1.095	0.838
2.000	1.601	0.933	1.057

TABLE 4. RADIAL DISTRIBUTION OF ELECTRIC FIELD, $|E_z|/|E_0|$, ALONG THE $\phi=0^\circ$ RAY FOR HALF SLOT ANGLE $\phi_0 = 45^\circ$ AND CIRCUM-FERENCE TO WAVELENGTH RATIOS, $\gamma=1.000$, 2.000 AND 3.830

ρ/a	$\gamma=1.000$	$\gamma=2.000$	$\gamma=3.830$
0.000	0.271	2.513	0.020
0.050	0.293	2.600	1.048
0.100	0.317	2.680	2.081
0.150	0.342	2.753	3.057
0.200	0.370	2.819	3.949
0.250	0.398	2.878	4.734
0.300	0.429	2.930	5.389
0.350	0.462	2.976	5.900
0.400	0.497	3.015	6.252
0.450	0.534	3.047	6.439
0.500	0.574	3.074	6.457
0.550	0.616	3.093	6.308
0.600	0.660	3.106	6.000
0.650	0.706	3.113	5.545
0.700	0.755	3.112	4.958
0.750	0.805	3.103	4.259
0.800	0.857	3.085	3.472
0.850	0.910	3.058	2.623
0.900	0.964	3.021	1.744
0.950	1.018	2.973	0.883
1.000	1.072	2.913	0.391
1.050	1.126	2.841	0.630
1.100	1.179	2.756	0.949
1.150	1.231	2.658	1.253
1.200	1.281	2.547	1.517
1.250	1.329	2.422	1.726
1.300	1.376	2.284	1.874
1.350	1.420	2.134	1.957
1.400	1.461	1.973	1.973
1.450	1.500	1.800	1.922
1.500	1.535	1.618	1.809
1.550	1.568	1.428	1.638
1.600	1.597	1.231	1.417
1.650	1.623	1.030	1.155
1.700	1.645	0.827	0.864
1.750	1.664	0.626	0.563
1.800	1.680	0.436	0.298
1.850	1.691	0.285	0.286
1.900	1.699	0.253	0.531
1.950	1.704	0.367	0.806
2.000	1.705	0.536	1.060

TABLE 5. RADIAL DISTRIBUTION OF ELECTRIC FIELD, $|E_z|/|E_0|$, ALONG THE $\phi=0^\circ$ RAY FOR HALF SLOT ANGLE $\phi_0 = 60^\circ$ AND CIRCUMFERENCE TO WAVELENGTH RATIOS, $\gamma=1.000$, 2.000 AND 3.830

ρ/a	$\gamma=1.000$	$\gamma=2.000$	$\gamma=3.830$
0.000	0.472	2.883	0.092
0.050	0.508	2.975	0.862
0.100	0.547	3.057	1.754
0.150	0.586	3.129	2.596
0.200	0.628	3.189	3.363
0.250	0.671	3.238	4.035
0.300	0.716	3.275	4.592
0.350	0.762	3.301	5.021
0.400	0.810	3.313	5.310
0.450	0.859	3.313	5.453
0.500	0.909	3.299	5.447
0.550	0.960	3.272	5.295
0.600	1.011	3.230	5.004
0.650	1.063	3.175	4.584
0.700	1.115	3.105	4.051
0.750	1.167	3.021	3.425
0.800	1.219	2.922	2.730
0.850	1.269	2.809	1.999
0.900	1.318	2.682	1.290
0.950	1.366	2.542	0.782
1.000	1.413	2.389	0.915
1.050	1.457	2.224	1.219
1.100	1.499	2.048	1.534
1.150	1.538	1.862	1.820
1.200	1.575	1.668	2.058
1.250	1.609	1.467	2.233
1.300	1.640	1.262	2.340
1.350	1.663	1.056	2.373
1.400	1.693	0.852	2.332
1.450	1.715	0.660	2.218
1.500	1.733	0.495	2.035
1.550	1.747	0.396	1.790
1.600	1.758	0.409	1.492
1.650	1.765	0.520	1.151
1.700	1.769	0.678	0.781
1.750	1.769	0.851	0.400
1.800	1.765	1.024	0.137
1.850	1.758	1.192	0.433
1.900	1.747	1.350	0.792
1.950	1.733	1.497	1.124
2.000	1.715	1.629	1.414

TABLE 6. RADIAL DISTRIBUTION OF ELECTRIC FIELD, $|E_z|/|E_0|$, ALONG THE $\phi=0^\circ$ RAY FOR HALF SLOT ANGLE $\phi_0 = 90^\circ$ AND CIRCUM-FERENCE TO WAVELENGTH RATIOS, $\gamma=1.000, 2.000$ AND 3.830

ρ/a	$\gamma=1.000$	$\gamma=2.000$	$\gamma=3.830$
0.000	0.883	2.649	0.554
0.050	0.939	2.706	0.269
0.100	0.995	2.748	0.960
0.150	1.051	2.776	1.632
0.200	1.106	2.787	2.237
0.250	1.161	2.782	2.758
0.300	1.215	2.760	3.178
0.350	1.268	2.721	3.486
0.400	1.319	2.665	3.675
0.450	1.369	2.592	3.741
0.500	1.416	2.502	3.685
0.550	1.462	2.396	3.510
0.600	1.505	2.274	3.226
0.650	1.546	2.138	2.844
0.700	1.583	1.988	2.378
0.750	1.618	1.825	1.846
0.800	1.650	1.651	1.268
0.850	1.679	1.467	0.670
0.900	1.705	1.276	0.157
0.950	1.727	1.079	0.578
1.000	1.746	0.879	1.130
1.050	1.761	0.682	1.383
1.100	1.772	0.497	1.586
1.150	1.780	0.349	1.733
1.200	1.785	0.300	1.817
1.250	1.785	0.386	1.836
1.300	1.782	0.542	1.790
1.350	1.776	0.718	1.679
1.400	1.766	0.896	1.509
1.450	1.752	1.070	1.287
1.500	1.734	1.235	1.020
1.550	1.713	1.389	0.722
1.600	1.689	1.529	0.409
1.650	1.661	1.656	0.176
1.700	1.630	1.766	0.357
1.750	1.596	1.859	0.665
1.800	1.559	1.935	0.964
1.850	1.519	1.992	1.231
1.900	1.476	2.030	1.456
1.950	1.430	2.050	1.629
2.000	1.382	2.050	1.744

TABLE 7. RADIAL DISTRIBUTION OF ELECTRIC FIELD, $|E_z|/|E_0|$, ALONG THE $\phi=10^\circ$ RAY FOR HALF SLOT ANGLE $\phi_0 = 20^\circ$ AND CIRCUMFERENCE TO WAVELENGTH RATIOS $\gamma=1.000$, 2.000, AND 3.830

ρ/a	$\gamma=1.000$	$\gamma=2.000$	$\gamma=3.830$
0.000	0.051	0.399	0.012
0.050	0.055	0.413	1.251
0.100	0.066	0.427	2.479
0.150	0.065	0.440	3.639
0.200	0.071	0.452	4.700
0.250	0.077	0.464	5.633
0.300	0.084	0.475	6.414
0.350	0.092	0.486	7.023
0.400	0.100	0.497	7.445
0.450	0.109	0.508	7.670
0.500	0.120	0.520	7.696
0.550	0.132	0.533	7.525
0.600	0.145	0.548	7.166
0.650	0.160	0.565	6.632
0.700	0.178	0.585	5.942
0.750	0.199	0.610	5.120
0.800	0.223	0.640	4.193
0.850	0.252	0.679	3.190
0.900	0.287	0.729	2.144
0.950	0.331	0.796	1.085
1.000	0.384	0.878	0.046
1.050	0.447	0.982	0.336
1.100	0.516	1.093	0.686
1.150	0.589	1.209	0.998
1.200	0.663	1.322	1.263
1.250	0.738	1.427	1.473
1.300	0.811	1.523	1.625
1.350	0.881	1.607	1.716
1.400	0.950	1.676	1.745
1.450	1.015	1.731	1.712
1.000	1.077	1.771	1.621
1.550	1.137	1.795	1.478
1.600	1.192	1.802	1.291
1.650	1.244	1.794	1.068
1.700	1.293	1.770	0.825
1.750	1.338	1.731	0.586
1.800	1.379	1.677	0.411
1.850	1.417	1.609	0.416
1.900	1.451	1.528	0.587
1.950	1.481	1.435	0.808
2.000	1.508	1.331	1.024

TABLE 8. RADIAL DISTRIBUTION OF ELECTRIC FIELD, $|E_z|/|E_0|$, ALONG THE $\phi=10^\circ$ RAY FOR HALF SLOT ANGLE $\phi_0 = 25^\circ$ AND CIRCUMFERENCE TO WAVELENGTH RATIOS, $\gamma=1.000, 2.000$ AND 3.830

ρ/a	$\gamma=1.000$	$\gamma=2.000$	$\gamma=3.830$
0.000	0.081	0.691	0.011
0.050	0.087	0.716	1.203
0.100	0.095	0.739	2.385
0.150	0.103	0.761	3.502
0.200	0.112	0.782	4.523
0.250	0.121	0.802	5.421
0.300	0.132	0.820	6.172
0.350	0.143	0.838	6.758
0.400	0.156	0.855	7.164
0.450	0.170	0.873	7.381
0.500	0.186	0.891	7.406
0.550	0.203	0.910	7.241
0.600	0.223	0.931	6.895
0.650	0.245	0.954	6.381
0.700	0.270	0.982	5.717
0.750	0.298	1.014	4.926
0.800	0.331	1.052	4.033
0.850	0.368	1.099	3.067
0.900	0.411	1.156	2.058
0.950	0.461	1.223	1.038
1.000	0.516	1.300	0.039
1.050	0.576	1.383	0.343
1.100	0.640	1.471	0.693
1.150	0.707	1.558	1.005
1.200	0.775	1.642	1.270
1.250	0.843	1.717	1.480
1.300	0.909	1.782	1.633
1.350	0.974	1.836	1.723
1.400	1.037	1.875	1.752
1.450	1.098	1.900	1.719
1.500	1.155	1.910	1.628
1.550	1.210	1.904	1.484
1.600	1.261	1.882	1.296
1.650	1.309	1.845	1.072
1.700	1.354	1.792	0.828
1.750	1.395	1.725	0.587
1.800	1.433	1.644	0.409
1.850	1.467	1.549	0.411
1.900	1.497	1.443	0.583
1.950	1.523	1.326	0.806
2.000	1.546	1.199	

TABLE 9. RADIAL DISTRIBUTION OF ELECTRIC FIELD, $|E_z|/|E_0|$, ALONG THE $\phi=15^\circ$ RAY FOR HALF SLOT ANGLE $\phi_0 = 30^\circ$ AND CIRCUMFERENCE TO WAVELENGTH RATIOS, $\gamma=1.000, 2.000$ AND 3.830

ρ/a	$\gamma=1.000$	$\gamma=2.000$	$\gamma=3.830$
0.000	0.117	1.098	0.011
0.050	0.127	1.137	1.139
0.100	0.138	1.172	2.258
0.150	0.149	1.205	3.315
0.200	0.161	1.234	4.282
0.250	0.174	1.261	5.132
0.300	0.188	1.286	5.844
0.350	0.202	1.308	6.398
0.400	0.218	1.327	6.782
0.450	0.236	1.345	6.987
0.500	0.254	1.361	7.010
0.550	0.275	1.376	6.854
0.600	0.297	1.390	6.526
0.650	0.321	1.404	6.039
0.700	0.347	1.420	5.410
0.750	0.377	1.437	4.660
0.800	0.410	1.458	3.814
0.850	0.447	1.486	2.899
0.900	0.490	1.521	1.944
0.950	0.538	1.566	0.977
1.000	0.593	1.621	0.028
1.050	0.651	1.681	0.347
1.100	0.714	1.745	0.692
1.150	0.779	1.807	1.000
1.200	0.845	1.864	1.262
1.250	0.910	1.913	1.473
1.300	0.975	1.951	1.627
1.350	1.037	1.976	1.721
1.400	1.097	1.986	1.754
1.450	1.155	1.982	1.728
1.500	1.210	1.963	1.644
1.550	1.261	1.928	1.509
1.600	1.310	1.877	1.328
1.650	1.355	1.812	1.110
1.700	1.396	1.732	0.870
1.750	1.434	1.639	0.627
1.800	1.469	1.533	0.430
1.850	1.500	1.415	0.388
1.900	1.527	1.287	0.536
1.950	1.551	1.150	0.753
2.000	1.570	1.005	0.973

TABLE 10. RADIAL DISTRIBUTION OF ELECTRIC FIELD, $|E_z|/|E_0|$, ALONG THE $\phi=22^\circ$ RAY FOR HALF SLOT ANGLE $\phi_0 = 45^\circ$ AND CIRCUMFERENCE TO WAVELENGTH RATIOS, $\gamma=1.000, 2.000$ AND 3.830

ρ/a	$\gamma=1.000$	$\gamma=2.000$	$\gamma=3.830$
0.000	0.271	2.513	0.020
0.050	0.291	2.592	0.970
0.100	0.313	2.663	1.928
0.150	0.335	2.725	2.834
0.200	0.359	2.777	3.661
0.250	0.383	2.819	4.389
0.300	0.408	2.852	4.997
0.350	0.434	2.875	5.472
0.400	0.461	2.888	5.800
0.450	0.489	2.892	5.975
0.500	0.519	2.886	5.994
0.550	0.549	2.872	5.860
0.600	0.582	2.850	5.578
0.650	0.615	2.821	5.161
0.700	0.651	2.785	4.623
0.750	0.689	2.745	3.981
0.800	0.730	2.700	3.257
0.850	0.773	2.653	2.474
0.900	0.819	2.604	1.657
0.950	0.868	2.553	0.829
1.000	0.919	2.497	0.051
1.050	0.972	2.439	0.354
1.100	1.025	2.375	0.687
1.150	1.079	2.304	0.987
1.200	1.133	2.224	1.245
1.250	1.185	2.135	1.454
1.300	1.236	2.036	1.610
1.350	1.285	1.926	1.710
1.400	1.332	1.806	1.751
1.450	1.376	1.676	1.735
1.500	1.417	1.536	1.663
1.550	1.455	1.387	1.539
1.600	1.490	1.230	1.370
1.650	1.522	1.065	1.163
1.700	1.550	0.895	0.929
1.750	1.575	0.720	0.684
1.800	1.597	0.542	0.462
1.850	1.615	0.364	0.355
1.900	1.630	0.189	0.458
1.950	1.641	0.073	0.669
2.000	1.649	0.199	0.895

TABLE 11. RADIAL DISTRIBUTION OF ELECTRIC FIELD, $|E_z|/|E_0|$, ALONG THE $\phi=30^\circ$ RAY FOR HALF SLOT ANGLE $\phi_0 = 60^\circ$ AND CIRCUMFERENCE TO WAVELENGTH RATIOS, $\gamma=1.000, 2.000$ AND 3.830

ρ/a	$\gamma=1.000$	$\gamma=2.000$	$\gamma=3.830$
0.000	0.472	2.883	0.092
0.050	0.503	2.961	0.740
0.100	0.535	3.026	1.513
0.150	0.567	3.078	2.246
0.200	0.599	3.117	2.915
0.250	0.632	3.143	3.505
0.300	0.665	3.154	3.998
0.350	0.698	3.152	4.384
0.400	0.732	3.137	4.652
0.450	0.766	3.108	4.798
0.500	0.800	3.067	4.820
0.550	0.835	3.014	4.719
0.600	0.871	2.951	4.501
0.650	0.908	2.877	4.175
0.700	0.946	2.794	3.753
0.750	0.985	2.703	3.250
0.800	1.025	2.604	2.682
0.850	1.066	2.499	2.068
0.900	1.108	2.387	1.429
0.950	1.151	2.270	0.790
1.000	1.194	2.146	0.260
1.050	1.238	2.017	0.322
1.100	1.280	1.882	0.571
1.150	1.322	1.741	0.828
1.200	1.363	1.595	1.057
1.250	1.402	1.443	1.250
1.300	1.439	1.286	1.398
1.350	1.474	1.126	1.500
1.400	1.507	0.962	1.552
1.450	1.537	0.795	1.555
1.500	1.564	0.628	1.510
1.550	1.588	0.463	1.421
1.600	1.609	0.304	1.293
1.650	1.627	0.176	1.132
1.700	1.642	0.165	0.950
1.750	1.654	0.281	0.761
1.800	1.662	0.426	0.593
1.850	1.668	0.575	0.497
1.900	1.670	0.720	0.523
1.950	1.669	0.859	0.652
2.000	1.665	0.990	0.825

TABLE 12. RADIAL DISTRIBUTION OF ELECTRIC FIELD, $|E_z|/|E_0|$, ALONG THE $\phi=45^\circ$ RAY FOR HALF SLOT ANGLE $\phi_0 = 90^\circ$ AND CIRCUMFERENCE TO WAVELENGTH RATIOS, $\gamma=1.000, 2.000$ AND 3.830

ρ/a	$\gamma=1.000$	$\gamma=2.000$	$\gamma=3.830$
0.000	0.883	2.649	0.554
0.050	0.922	2.687	0.150
0.100	0.959	2.713	0.564
0.150	0.996	2.725	1.073
0.200	1.032	2.725	1.558
0.250	1.067	2.712	2.003
0.300	1.101	2.687	2.395
0.350	1.134	2.650	2.725
0.400	1.167	2.602	2.986
0.450	1.199	2.544	3.172
0.500	1.230	2.477	3.279
0.550	1.261	2.400	3.307
0.600	1.291	2.314	3.255
0.650	1.321	2.222	3.128
0.700	1.350	2.122	2.929
0.750	1.378	2.015	2.665
0.800	1.406	1.903	2.345
0.850	1.433	1.786	1.978
0.900	1.459	1.663	1.574
0.950	1.484	1.537	1.145
1.000	1.508	1.407	0.703
1.050	1.530	1.275	0.441
1.100	1.551	1.141	0.198
1.150	1.569	1.005	0.189
1.200	1.586	0.870	0.421
1.250	1.601	0.737	0.667
1.300	1.614	0.609	0.900
1.350	1.625	0.490	1.109
1.400	1.634	0.390	1.291
1.450	1.640	0.324	1.441
1.500	1.644	0.314	1.556
1.550	1.646	0.360	1.632
1.600	1.645	0.442	1.670
1.650	1.642	0.541	1.669
1.700	1.636	0.646	1.630
1.750	1.628	0.751	1.554
1.800	1.618	0.853	1.445
1.850	1.606	0.950	1.306
1.900	1.591	1.041	1.143
1.950	1.574	1.125	0.963
2.000	1.554	1.202	0.778

TABLE 13. RADIAL DISTRIBUTION OF ELECTRIC FIELD, $|E_z|/|E_0|$, ALONG THE $\phi=30^\circ$ RAY FOR HALF SLOT ANGLE $\phi_0 = 20^\circ$ AND CIRCUMFERENCE TO WAVELENGTH RATIOS, $\gamma=1.000$, 2.000 AND 3.830

ρ/a	$\gamma=1.000$	$\gamma=2.000$	$\gamma=3.830$
0.000	0.051	0.399	0.012
0.100	0.059	0.422	2.178
0.200	0.067	0.439	4.131
0.300	0.075	0.448	5.638
0.400	0.083	0.449	6.543
0.500	0.090	0.437	6.762
0.600	0.093	0.410	6.292
0.700	0.090	0.361	5.212
0.800	0.076	0.281	3.668
0.900	0.046	0.158	1.856
1.000	0.000	0.000	0.000

TABLE 14. RADIAL DISTRIBUTION OF ELECTRIC FIELD, $|E_z|/|E_0|$, ALONG THE $\phi=35^\circ$ RAY FOR HALF SLOT ANGLE $\phi_0 = 25^\circ$ AND CIRCUMFERENCE TO WAVELENGTH RATIOS, $\gamma=1.000$, 2.000 AND 3.830

ρ/a	$\gamma=1.000$	$\gamma=2.000$	$\gamma=3.830$
0.000	0.081	0.691	0.011
0.100	0.092	0.728	1.982
0.200	0.103	0.752	3.759
0.300	0.114	0.761	5.131
0.400	0.124	0.751	5.954
0.500	0.130	0.270	6.153
0.600	0.131	0.662	5.726
0.700	0.123	0.569	4.742
0.800	0.101	0.431	3.337
0.900	0.059	0.237	1.689
1.000	0.000	0.000	0.000

TABLE 15. RADIAL DISTRIBUTION OF ELECTRIC FIELD, $|E_z|/|E_0|$, ALONG THE $\phi=40^\circ$ RAY FOR HALF SLOT ANGLE $\phi_0 = 30^\circ$ AND CIRCUMFERENCE TO WAVELENGTH RATIOS, $\gamma=1.000$, 2.000 AND 3.830

ρ/a	$\gamma=1.000$	$\gamma=2.000$	$\gamma=3.830$
0.000	0.117	1.098	0.011
0.050	0.125		
0.100	0.133	1.151	1.788
0.150	0.140		
0.200	0.147	1.180	3.393
0.250	0.153		
0.300	0.160	1.183	4.631
0.350	0.165		
0.400	0.169	1.154	5.374
0.450	0.172		
0.500	0.174	1.090	5.554
0.550	0.174		
0.600	0.171	0.984	5.168
0.650	0.166		
0.700	0.157	0.830	4.280
0.750	0.144		
0.800	0.124	0.616	3.012
0.850	0.103		
0.900	0.073	0.334	1.524
0.950	0.038		
1.000	0.000	0.000	0.000

TABLE 16. RADIAL DISTRIBUTION OF ELECTRIC FIELD, $|E_z|/|E_0|$, ALONG THE $\phi=56^\circ$ RAY FOR HALF SLOT ANGLE $\phi_0 = 45^\circ$ AND CIRCUMFERENCE TO WAVELENGTH RATIOS, $\gamma=1.000$, 2.000 AND 3.830

ρ/a	$\gamma=1.000$	$\gamma=2.000$	$\gamma=3.830$
0.000	0.271	2.513	0.020
0.100	0.293	2.583	1.158
0.200	0.310	2.589	2.204
0.300	0.320	2.525	3.012
0.400	0.322	2.388	3.500
0.500	0.313	2.177	3.621
0.600	0.291	1.891	3.375
0.700	0.253	1.528	2.801
0.800	0.192	1.085	1.976
0.900	0.106	0.564	1.003
1.000	0.000	0.000	0.000

TABLE 17. RADIAL DISTRIBUTION OF ELECTRIC FIELD, $|E_z|/|E_0|$, ALONG THE $\phi=70^\circ$ RAY FOR HALF SLOT ANGLE $\phi_0 = 60^\circ$ AND CIRCUMFERENCE TO WAVELENGTH RATIOS, $\gamma=1.000$, 2.000 AND 3.830

ρ/a	$\gamma=1.000$	$\gamma=2.000$	$\gamma=3.830$
0.000	0.472	2.883	0.092
0.100	0.492	2.913	0.569
0.200	0.501	2.868	1.138
0.300	0.500	2.747	1.594
0.400	0.487	2.554	1.888
0.500	0.460	2.290	1.992
0.600	0.417	1.958	1.898
0.700	0.354	1.561	1.616
0.800	0.265	1.098	1.174
0.900	0.145	0.568	0.613
1.000	0.000	0.000	0.000

TABLE 18. RADIAL DISTRIBUTION OF ELECTRIC FIELD, $|E_z|/|E_0|$, ALONG THE $\phi=113^\circ$ RAY FOR HALF SLOT ANGLE $\phi_0 = 90^\circ$ AND CIRCUMFERENCE TO WAVELENGTH RATIOS, $\gamma=1.000$, 2.000 AND 3.830

ρ/a	$\gamma=1.000$	$\gamma=2.000$	$\gamma=3.830$
0.000	0.838	2.649	0.554
0.100	0.835	2.572	1.086
0.200	0.778	2.444	1.497
0.300	0.712	2.265	1.751
0.400	0.635	2.036	1.834
0.500	0.549	1.762	1.754
0.600	0.452	1.448	1.534
0.700	0.345	1.101	1.210
0.800	0.231	0.733	0.821
0.900	0.113	0.359	0.407
1.000	0.000	0.000	0.000

TABLE 19. RADIAL DISTRIBUTION OF ELECTRIC FIELD, $|E_z|/|E_0|$, ALONG THE $\phi=90^\circ$ RAY FOR HALF SLOT ANGLE $\phi_0 = 20^\circ$ AND CIRCUMFERENCE TO WAVELENGTH RATIOS, $\gamma=1.000$, 2.000 AND 3.830

ρ/a	$\gamma=1.000$	$\gamma=2.000$	$\gamma=3.830$
0.000	0.051	0.399	0.012
0.100	0.050	0.392	0.012
0.200	0.047	0.374	0.012
0.300	0.043	0.344	0.011
0.400	0.038	0.305	0.011
0.500	0.032	0.259	0.010
0.600	0.025	0.208	0.008
0.700	0.018	0.155	0.007
0.800	0.012	0.101	0.005
0.900	0.006	0.049	0.002
1.000	0.000	0.000	0.000

TABLE 20. RADIAL DISTRIBUTION OF ELECTRIC FIELD, $|E_z|/|E_0|$, ALONG THE $\phi=90^\circ$ RAY FOR HALF SLOT ANGLE $\phi_0 = 25^\circ$ AND CIRCUMFERENCE TO WAVELENGTH RATIOS, $\gamma=1.000$, 2.000 AND 3.830

ρ/a	$\gamma=1.000$	$\gamma=2.000$	$\gamma=3.830$
0.000	0.081	0.691	0.011
0.100	0.079	0.680	0.011
0.200	0.075	0.648	0.011
0.300	0.069	0.597	0.011
0.400	0.060	0.530	0.010
0.500	0.050	0.450	0.009
0.600	0.040	0.362	0.008
0.700	0.029	0.269	0.006
0.800	0.019	0.176	0.004
0.900	0.009	0.085	0.002
1.000	0.000	0.000	0.000

TABLE 21. RADIAL DISTRIBUTION OF ELECTRIC FIELD, $|E_z|/|E_0|$, ALONG THE $\phi=90^\circ$ RAY FOR HALF SLOT ANGLE $\phi_0 = 30^\circ$ AND CIRCUMFERENCE TO WAVELENGTH RATIOS, $\gamma=1.000, 2.000$ AND 3.830

ρ/a	$\gamma=1.000$	$\gamma=2.000$	$\gamma=3.830$
0.000	0.117	1.098	0.011
0.100	0.116	1.081	0.011
0.200	0.110	1.031	0.011
0.300	0.100	0.951	0.010
0.400	0.088	0.845	0.010
0.500	0.074	0.719	0.009
0.600	0.059	0.579	0.008
0.700	0.044	0.431	0.006
0.800	0.028	0.281	0.004
0.900	0.014	0.136	0.002
1.000	0.000	0.000	0.000

TABLE 22. RADIAL DISTRIBUTION OF ELECTRIC FIELD, $|E_z|/|E_0|$, ALONG THE $\phi=90^\circ$ RAY FOR HALF SLOT ANGLE $\phi_0 = 45^\circ$ AND CIRCUMFERENCE TO WAVELENGTH RATIOS, $\gamma=1.000, 2.000$ AND 3.830

ρ/a	$\gamma=1.000$	$\gamma=2.000$	$\gamma=3.830$
0.000	0.271	2.513	0.020
0.100	0.267	2.476	0.019
0.200	0.255	2.368	0.014
0.300	0.236	2.193	0.009
0.400	0.211	1.958	0.009
0.500	0.180	1.674	0.013
0.600	0.145	1.354	0.015
0.700	0.108	1.012	0.014
0.800	0.070	0.663	0.011
0.900	0.034	0.322	0.006
1.000	0.000	0.000	0.000

TABLE 23. RADIAL DISTRIBUTION OF ELECTRIC FIELD, $|E_z|/|E_0|$, ALONG THE $\phi=90^\circ$ RAY FOR HALF SLOT ANGLE $\phi_0 = 60^\circ$ AND CIRCUMFERENCE TO WAVELENGTH RATIOS, $\gamma=1.000$, 2.000 AND 3.830

ρ/a	$\gamma=1.000$	$\gamma=2.000$	$\gamma=3.830$
0.000	0.472	2.883	0.092
0.100	0.466	2.845	0.082
0.200	0.450	2.730	0.053
0.300	0.422	2.544	0.013
0.400	0.384	2.290	0.033
0.500	0.335	1.977	0.070
0.600	0.277	1.616	0.092
0.700	0.211	1.219	0.093
0.800	0.140	0.805	0.074
0.900	0.068	0.392	0.040
1.000	0.000	0.000	0.000

TABLE 24. RADIAL DISTRIBUTION OF ELECTRIC FIELD, $|E_z|/|E_0|$, ALONG THE $\phi=135^\circ$ RAY FOR HALF SLOT ANGLE $\phi_0 = 20^\circ$ AND CIRCUMFERENCE TO WAVELENGTH RATIOS, $\gamma=1.000$, 2.000 AND 3.830

ρ/a	$\gamma=1.000$	$\gamma=2.000$	$\gamma=3.830$
0.000	0.051	0.399	0.012
0.100	0.045	0.373	1.799
0.200	0.038	0.341	3.391
0.300	0.032	0.304	4.617
0.400	0.027	0.263	5.350
0.500	0.021	0.219	5.523
0.600	0.016	0.174	5.135
0.700	0.012	0.128	4.250
0.800	0.007	0.083	2.988
0.900	0.004	0.040	1.511
1.000	0.000	0.000	0.000

TABLE 25. RADIAL DISTRIBUTION OF ELECTRIC FIELD, $|E_z|/|E_0|$, ALONG THE $\phi=135^\circ$ RAY FOR HALF SLOT ANGLE $\phi_0 = 25^\circ$ AND CIRCUMFERENCE TO WAVELENGTH RATIOS, $\gamma=1.000, 2.000$ AND 3.830

ρ/a	$\gamma=1.000$	$\gamma=2.000$	$\gamma=3.830$
0.000	0.081	0.691	0.011
0.100	0.071	0.647	1.731
0.200	0.061	0.592	3.263
0.300	0.051	0.528	4.443
0.400	0.042	0.457	5.149
0.500	0.034	0.381	5.316
0.600	0.026	0.302	4.942
0.700	0.019	0.223	4.090
0.800	0.012	0.145	2.876
0.900	0.006	0.070	1.454
1.000	0.000	0.000	0.000

TABLE 26. RADIAL DISTRIBUTION OF ELECTRIC FIELD, $|E_z|/|E_0|$, ALONG THE $\phi=135^\circ$ RAY FOR HALF SLOT ANGLE $\phi_0 = 30^\circ$ AND CIRCUMFERENCE TO WAVELENGTH RATIOS, $\gamma=1.000, 2.000$ AND 3.830

ρ/a	$\gamma=1.000$	$\gamma=2.000$	$\gamma=3.830$
0.000	0.117	1.098	0.011
0.100	0.116	1.081	0.011
0.200	0.110	1.031	0.011
0.300	0.100	0.951	0.010
0.400	0.088	0.845	0.010
0.500	0.074	0.719	0.009
0.600	0.059	0.579	0.008
0.700	0.044	0.431	0.006
0.800	0.028	0.281	0.004
0.900	0.014	0.136	0.502
1.000	0.000	0.000	0.000

TABLE 27. RADIAL DISTRIBUTION OF ELECTRIC FIELD, $|E_z|/|E_0|$, ALONG THE $\phi=135^\circ$ RAY FOR HALF SLOT ANGLE $\phi_0 = 45^\circ$ AND CIRCUMFERENCE TO WAVELENGTH RATIOS, $\gamma=1.000$, 2.000 AND 3.830

ρ/a	$\gamma=1.000$	$\gamma=2.000$	$\gamma=3.830$
0.000	0.271	2.513	0.020
0.100	0.239	2.361	1.496
0.200	0.208	2.166	2.815
0.300	0.176	1.936	3.830
0.400	0.146	1.678	4.438
0.500	0.117	1.400	4.581
0.600	0.090	1.112	4.259
0.700	0.065	0.820	3.525
0.800	0.041	0.533	2.478
0.900	0.020	0.257	1.253
1.000	0.000	0.000	0.000

TABLE 28. RADIAL DISTRIBUTION OF ELECTRIC FIELD, $|E_z|/|E_0|$, ALONG THE $\phi=135^\circ$ RAY FOR HALF SLOT ANGLE $\phi_0 = 60^\circ$ AND CIRCUMFERENCE TO WAVELENGTH RATIOS, $\gamma=1.000$, 2.000 AND 3.830

ρ/a	$\gamma=1.000$	$\gamma=2.000$	$\gamma=3.830$
0.000	0.472	2.883	0.092
0.100	0.420	2.718	1.345
0.200	0.367	2.502	2.483
0.300	0.314	2.242	3.359
0.400	0.262	1.948	3.881
0.500	0.211	1.629	4.000
0.600	0.163	1.295	3.715
0.700	0.117	0.956	3.073
0.800	0.075	0.621	2.160
0.900	0.036	0.300	1.092
1.000	0.000	0.000	0.000

TABLE 29. RADIAL DISTRIBUTION OF ELECTRIC FIELD, $|E_z|/|E_0|$, ALONG THE $\phi=135^\circ$ RAY FOR HALF SLOT ANGLE $\phi_0 = 90^\circ$ AND CIRCUMFERENCE TO WAVELENGTH RATIOS, $\gamma=1.000$, 2.000 AND 3.830

ρ/a	$\gamma=1.000$	$\gamma=2.000$	$\gamma=3.830$
0.000	0.883	2.649	0.554
0.100	0.835	2.572	1.086
0.200	0.778	2.444	1.497
0.300	0.712	2.265	1.751
0.400	0.635	2.036	1.834
0.500	0.549	1.762	1.754
0.600	0.452	1.448	1.534
0.700	0.345	1.101	1.210
0.800	0.231	0.733	0.821
0.900	0.113	0.359	0.407
1.000	0.000	0.000	0.000

TABLE 30. RADIAL DISTRIBUTION OF ELECTRIC FIELD, $|E_z|/|E_0|$, ALONG THE $\phi=180^\circ$ RAY FOR HALF SLOT ANGLE $\phi_0 = 20^\circ$ AND CIRCUMFERENCE TO WAVELENGTH RATIOS, $\gamma=1.000$, 2.000 AND 3.830

ρ/a	$\gamma=1.000$	$\gamma=2.000$	$\gamma=3.830$
0.000	0.051	0.399	0.012
0.100	0.043	0.366	2.539
0.200	0.036	0.331	4.790
0.300	0.029	0.293	6.523
0.400	0.024	0.252	7.560
0.500	0.019	0.209	7.806
0.600	0.014	0.165	7.257
0.700	0.010	0.122	6.006
0.800	0.007	0.079	4.223
0.900	0.003	0.038	2.135
1.000	0.000	0.000	0.000

TABLE 31. RADIAL DISTRIBUTION OF ELECTRIC FIELD, $|E_z|/|E_0|$, ALONG THE $\phi=180^\circ$ RAY FOR HALF SLOT ANGLE $\phi_0 = 25^\circ$ AND CIRCUMFERENCE TO WAVELENGTH RATIOS, $\gamma=1.000$, 2.000 AND 3.830

ρ/a	$\gamma=1.000$	$\gamma=2.000$	$\gamma=3.830$
0.000	0.081	0.691	0.011
0.100	0.068	0.636	2.443
0.200	0.057	0.574	4.609
0.300	0.047	0.508	6.278
0.400	0.038	0.437	7.276
0.500	0.030	0.363	7.512
0.600	0.023	0.287	6.984
0.700	0.016	0.211	5.780
0.800	0.010	0.137	4.064
0.900	0.005	0.066	2.055
1.000	0.000	0.000	0.000

TABLE 32. RADIAL DISTRIBUTION OF ELECTRIC FIELD, $|E_z|/|E_0|$, ALONG THE $\phi=180^\circ$ RAY FOR HALF SLOT ANGLE $\phi_0 = 30^\circ$ AND CIRCUMFERENCE TO WAVELENGTH RATIOS, $\gamma=1.000$, 2.000 AND 3.830

ρ/a	$\gamma=1.000$	$\gamma=2.000$	$\gamma=3.830$
0.000	0.117	1.098	0.011
0.100	0.099	1.011	2.359
0.200	0.083	0.914	4.450
0.300	0.068	0.808	6.061
0.400	0.056	0.696	7.024
0.500	0.044	0.578	7.252
0.600	0.033	0.457	6.743
0.700	0.024	0.336	5.580
0.800	0.015	0.218	3.923
0.900	0.007	0.105	1.984
1.000	0.000	0.000	0.000

TABLE 33. RADIAL DISTRIBUTION OF ELECTRIC FIELD, $|E_z|/|E_0|$, ALONG THE $\phi=180^\circ$ RAY FOR HALF SLOT ANGLE $\phi_0 = 45^\circ$ AND CIRCUMFERENCE TO WAVELENGTH RATIOS, $\gamma=1.000$, 2.000 AND 3.830

ρ/a	$\gamma=1.000$	$\gamma=2.000$	$\gamma=3.830$
0.000	0.271	2.513	0.020
0.100	0.230	2.319	2.109
0.200	0.193	2.100	3.975
0.300	0.160	1.859	5.412
0.400	0.130	1.601	6.272
0.500	0.103	1.331	6.476
0.600	0.078	1.053	6.020
0.700	0.056	0.775	4.982
0.800	0.036	0.503	3.503
0.900	0.017	0.243	1.771
1.000	0.000	0.000	0.000

TABLE 34. RADIAL DISTRIBUTION OF ELECTRIC FIELD, $|E_z|/|E_0|$, ALONG THE $\phi=180^\circ$ RAY FOR HALF SLOT ANGLE $\phi_0 = 60^\circ$ AND CIRCUMFERENCE TO WAVELENGTH RATIOS, $\gamma=1.000$, 2.000 AND 3.830

ρ/a	$\gamma=1.000$	$\gamma=2.000$	$\gamma=3.830$
0.000	0.472	2.883	0.092
0.100	0.403	2.671	1.879
0.200	0.341	2.425	3.500
0.300	0.284	2.151	4.749
0.400	0.231	1.855	5.495
0.500	0.184	1.542	5.669
0.600	0.140	1.222	5.268
0.700	0.100	0.899	4.359
0.800	0.064	0.584	3.064
0.900	0.030	0.282	1.549
1.000	0.000	0.000	0.000

TABLE 35. RADIAL DISTRIBUTION OF ELECTRIC FIELD, $|E_z|/|E_0|$, ALONG THE $\phi=180^\circ$ RAY FOR HALF SLOT ANGLE $\phi_0 = 90^\circ$ AND CIRCUMFERENCE TO WAVELENGTH RATIOS, $\gamma=1.000, 2.000$ AND 3.830

ρ/a	$\gamma=1.000$	$\gamma=2.000$	$\gamma=3.830$
0.000	0.883	2.649	0.554
0.050			1.301
0.100	0.772	2.494	2.042
0.150			2.745
0.200	0.664	2.291	3.390
0.250			3.958
0.300	0.560	2.050	4.430
0.350			4.795
0.400	0.462	1.778	5.041
0.450			5.162
0.500	0.370	1.485	5.155
0.550			5.023
0.600	0.283	1.180	4.769
0.650			4.402
0.700	0.203	0.870	3.935
0.750			3.383
0.800	0.129	0.565	2.762
0.850			2.093
0.900	0.062	0.273	1.396
0.950			0.691
1.000	0.000	0.000	0.000

IV. APERTURE ELECTRIC FIELD, SURFACE CURRENTS AND BACK-SCATTERING CROSS-SECTION

a) Aperture Electric Field and Surface Currents

The results in the aperture and on the conductor reported on here are merely an extension to smaller slot angles of the study published earlier in S.E.R.A.V.¹ In Figures 20, 21 and 22 we present in graphical form the distribution of the tangential component of electric field over the aperture and the distribution of surface current on the conductor for a slotted cylinder with half slot angle $\phi_0 = 20^\circ$. These figures correspond to the results calculated for the circumference to wavelength ratios $\gamma = 1.000, 2.000$ and 3.830 . Tables 36 and 40 give the corresponding numerical values for the amplitudes and phases (in degrees) of the electric field and surface currents. Figures 24, 25 and 26 and Tables 37 and 41 contain the same information for the case of a half slot angle $\phi_0 = 25^\circ$. In both cases we have approximated the conducting portion of the cylinder by $L = 124$ zones each carrying a current of constant amplitude. Then the increment for the 62 equally spaced points over half the conductor implies for $\phi_0 = 20^\circ$

$$\frac{\Delta\phi}{\phi_0} = \frac{(180^\circ - 20^\circ) / 62}{20^\circ} = \frac{4}{31} \sim .125$$

i.e. the angular width of a zone is about 1/8 the value of ϕ_0 . For the largest γ considered we find the ratio of arc length of these zones to the incident wavelength is

$$\frac{a\Delta\phi}{\lambda} = \frac{2\pi a}{\lambda} \frac{\Delta\phi}{360} = \gamma \frac{\Delta\phi}{360} = 3.830 \times \frac{160/62}{360} = 0.028$$

This is the largest ratio of arclength per zone to incident wavelength that we consider for $\phi_0 = 20^\circ$. Consequently we should be able to generate good numerical results for the quantities we are evaluating. Similarly for the ϕ_0 half-slot angle we assumed $L = 124$.

1. J. Bombardt, L. Libelo, S.E.R.A.V op.cit.

Hence we have for this case

$$\frac{\Delta\phi}{\phi_0} = \frac{(180-25)/62}{25} = \frac{1}{10}$$

The corresponding maximum ratio of zone arclength to incident wavelength is

$$\frac{a\Delta\phi}{\lambda} = \frac{2\pi a}{\lambda} \frac{\Delta\phi}{360} = \gamma \frac{\Delta\phi}{360} = 3.830 \times \frac{5/2}{360} = 0.0266$$

Again the numerical results should be reliable and about as precise as for the $\phi_0 = 20^\circ$ case.

Now consider the results shown for $\gamma = 1.000$ the half-slot angle ϕ_0 in Figure 20. At the slot center the electric field assumes its maximum value at about 0.45 and as we move around the slot it decreases continuously to zero at the slot edge. The distribution of the amplitude of the slot electric field is roughly parabolic in form as we show below. If we keep γ fixed and increase ϕ_0 to 25° we observe in Figure 23 precisely the same qualitative behavior for the aperture electric field. In this case however the maximum at the center increased to the value 0.560. If we examine the results for $\gamma = 1.000$ and $\phi_0 = 30^\circ$ in Figure 4 in S.E.R.A.V.¹ we observe that the same qualitative behavior exists over the slot. For $\phi_0 = 30^\circ$ the peak value at the slot center is 0.7. What we are seeing is the relative buildup of electric field in the slot, for fixed γ , as the slot gradually widens. The slot electric field behavior for fixed slot angle ϕ_0 and $\gamma = 2.000$ or half the wavelength is also interesting. for $\phi_0 = 20^\circ$ the peak at the slot center is a little more than doubled and the distribution over the slot is again essentially parabolic. This is displayed in Figure 21. For $\phi_0 = 25^\circ$ we observe in Figure 24 almost precisely the same behavior for $\gamma = 2.000$ relative to the slot field distribution for $\gamma = 1.000$. Just the same thing is found to result for the $\phi_0 = 30^\circ$ distribution reported in Figure 5 in S.E.R.A.V.¹ We conclude that beyond cut off at least halving the

1. J. Bombardt, L. Libelo, S.E.R.A.V op.cit.

incident wavelength roughly doubles the electric field in the slot. Figures 22 and 25 show the effect of increasing γ to the second resonance value. For $\phi_0 = 20^\circ$ the field at the slot center is a maximum with height of about 0.06. As we move toward the slot edge a decrease to a minimum of about 0.045 is seen followed by a slight rise to another maximum and then a rapid drop toward zero at the slot follows. Increasing ϕ_0 to 25° we note that at $\gamma = 3.830$ a maximum occurs at the center of height about 0.07 slightly higher than for $\phi_0 = 20^\circ$. As we move away from center we see a rapid drop off to a minimum of about 0.035 followed by a rapid climb to a maximum almost of the same height as the slot-center value. A sharp drop to zero at the slot edge then follows. This behavior is very much like that for $\phi_0 = 30^\circ$ and $\gamma = 3.832$ (which is slightly above the effective resonance) shown in Figure 41 in S.E.R.A.V.¹ For $\phi_0 = 30^\circ$ the peak at center is at about 0.1 in height. Note that as γ increases for fixed ϕ_0 from beyond cutoff the slot-center field increases until a resonance is reached whereupon a sharp drop occurs in the field over the slot as the energy moves into the interior. This is certainly true for $\phi_0 = 20^\circ$ and $\phi_0 = 25^\circ$, the slot angles studied in this report. In Figure 39 of S.E.R.A.V.¹ we showed this explicitly for the $\phi_0 = 30^\circ$ slot. We shall return to the electric fields in the slot for some further discussion later. We now turn our attention to the calculated current distributions. Comparing the current distributions for $\gamma = 1.000$ for the $\phi_0 = 20^\circ$ and $\phi_0 = 25^\circ$ slots we find both have a low lying maximum at the extreme back azimuthal position. These both then decrease very slightly to a minimum at nearly the same azimuth, at about 157° and then slowly increase as we move further around toward the front and about 10° from the slot edge they increase rapidly to become singular at the edge itself. This is the same result found earlier in Figure 4 for $\gamma = 1.000$ and $\phi_0 = 30^\circ$ in S.E.R.A.V.¹ For all three slot angles we note the occurrence, although at lower amplitude, of the same behavior of the current distribution in the shadow region as exhibited by the cylinder without a slot. The difference in character from the

1. J. Bombardt, L. Libelo S.E.R.A.V. op.cit. page 73

entire cylinder is due to the necessity for the singular behavior at the slot edge in the ideal case. At $\gamma = 2.000$ we again find the same behavior in the ϕ -dependence of the current for the slot angles $\phi_0 = 20^\circ$ and $\phi_0 = 25^\circ$. The amplitude in the latter case is slightly larger than that of the former. Further the $\phi_0 = 25^\circ$ distribution is remarkably close to that obtained earlier for $\phi_0 = 30^\circ$. What we are observing is the same qualitative distribution for all three values of ϕ_0 spread over different ranges of ϕ . In Figures 22 and 25 for $\phi_0 = 20^\circ$ and 25° we see the current distribution at $\gamma = 3.83$ the second resonance. From $\phi = 180^\circ$ back to about $\phi = 35^\circ$ the curves are very nearly coincident with one another. Further as we move toward the edge the $\phi_0 = 20^\circ$ current drops lower than the $\phi_0 = 25^\circ$ current and then they both rapidly rise to become singular at the edges. We note they exhibit a maximum at $\phi = 180^\circ$ much larger than found for the γ 's beyond cutoff. They display an inflexion point at about $\phi = 135^\circ$, a minimum at about $\phi = 94^\circ$ and another high maximum at about $\phi = 60^\circ$. This behavior is similar to that at $\gamma = 4$ for $\phi_0 = 30^\circ$ shown in Figure 7 of S.E.R.A.V.¹ What we conclude occurs is that prior to attaining the resonance value of γ the current away from the edges is quite small. It rises as γ increases. This increase reaches its peak at the resonance and then drops off after the resonance is passed. Having thus completed the discussion of the current on the slotted cylinder for the smaller slot angles $\phi_0 = 20^\circ$ and 25° let us now return to further examine the slot electric field distributions.

Morse and Feshbach³ showed that for wavelengths large compared to the slot width the field over the slot in the cylinder could be approximated by assuming it is proportional to the electrostatic field distribution over the slot in an infinite plane. The form they obtained is

$$(18) \quad \mathcal{E}(\phi) = A(\gamma, \phi_0) \sqrt{1 - (\phi/\phi_0)^2} \quad \text{for } a\phi_0 \ll \lambda$$

1. J. Bomhardt, L. Libelo S.E.R.A.V. op.cit.
 3. P. M. Morse and H. Feshbach, Ibid

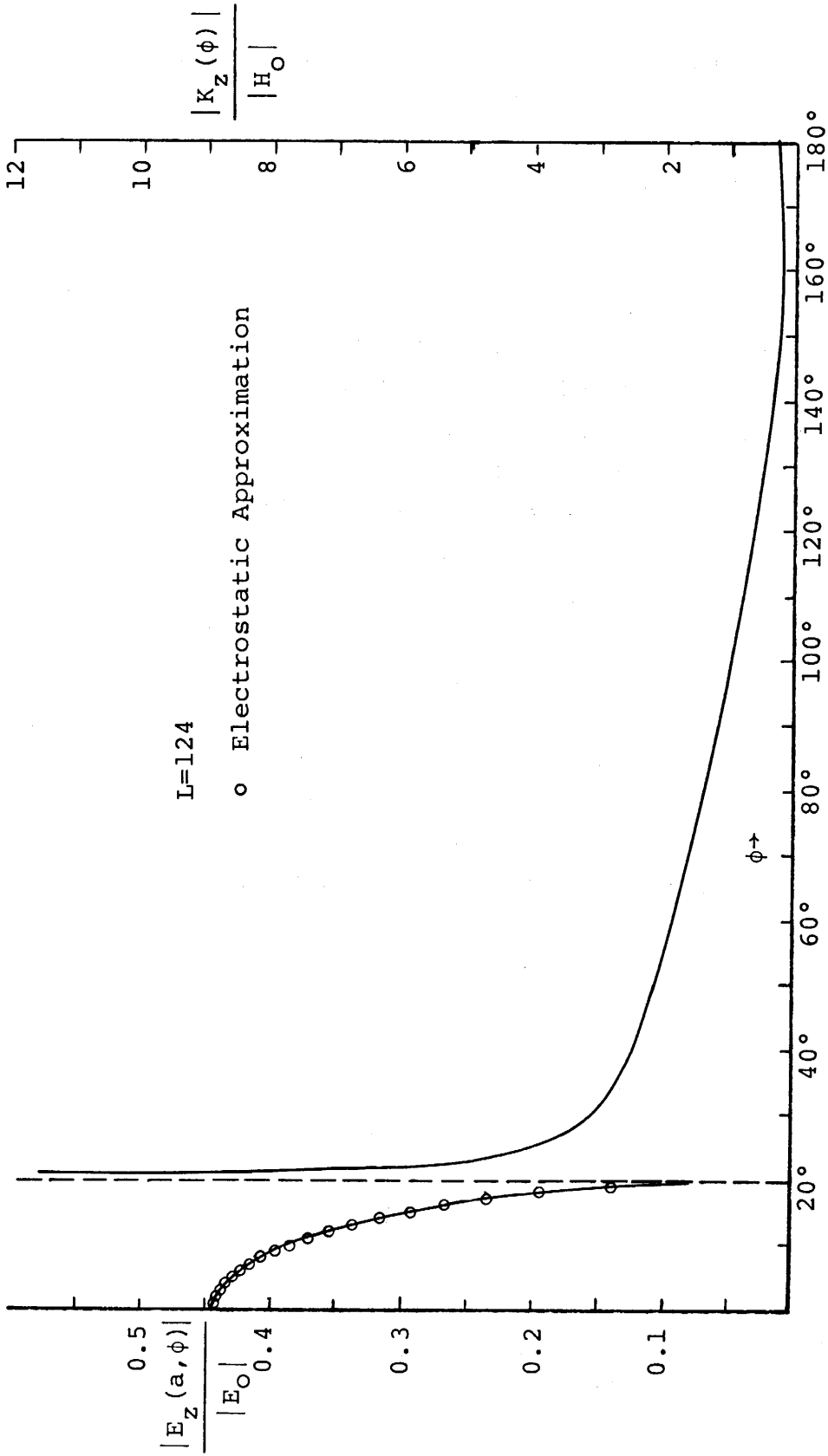


FIGURE 20. ELECTRIC FIELD IN THE SLOT, SURFACE CURRENT ON THE CONDUCTOR;
 $\gamma=1.00, \phi_0=20^\circ$

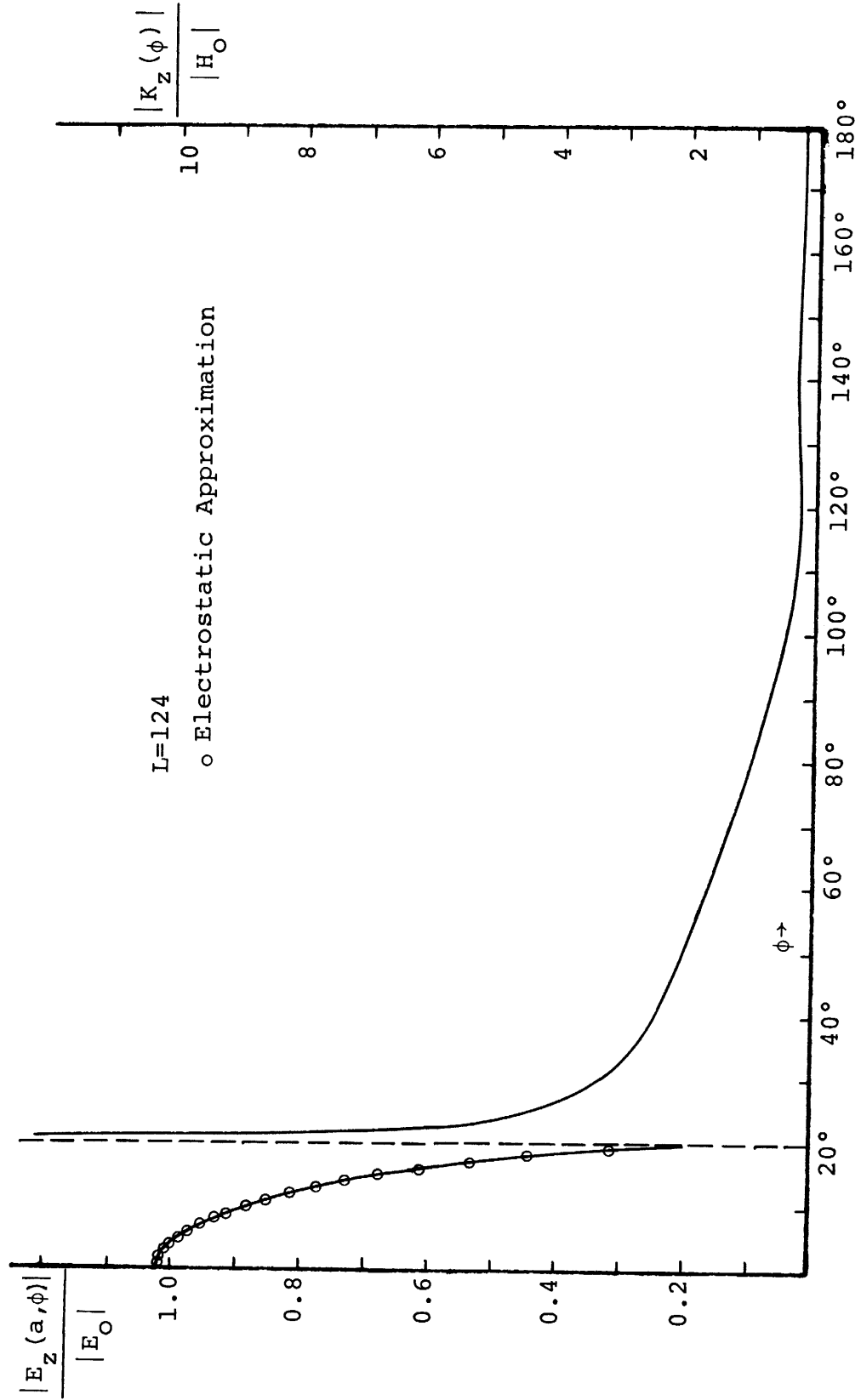
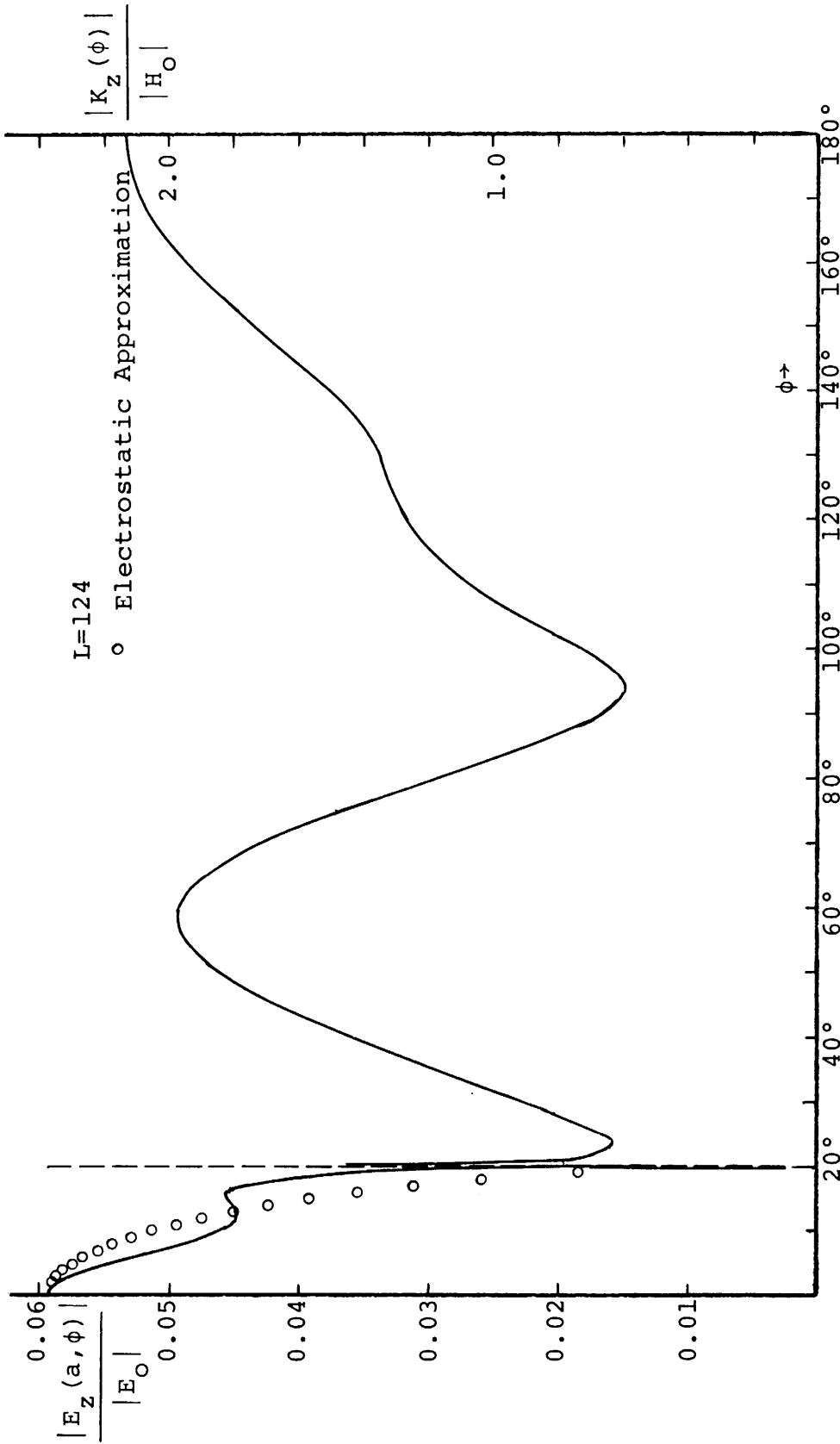


FIGURE 21. ELECTRIC FIELD IN THE SLOT, SURFACE CURRENT ON THE CONDUCTOR;
 $\gamma=2.00, \phi_0=20^\circ$



L=124
 o Electrostatic Approximation

FIGURE 22. ELECTRIC FIELD IN THE SLOT, SURFACE CURRENT ON THE CONDUCTOR;
 $\gamma=3.83, \phi_0=20^\circ$

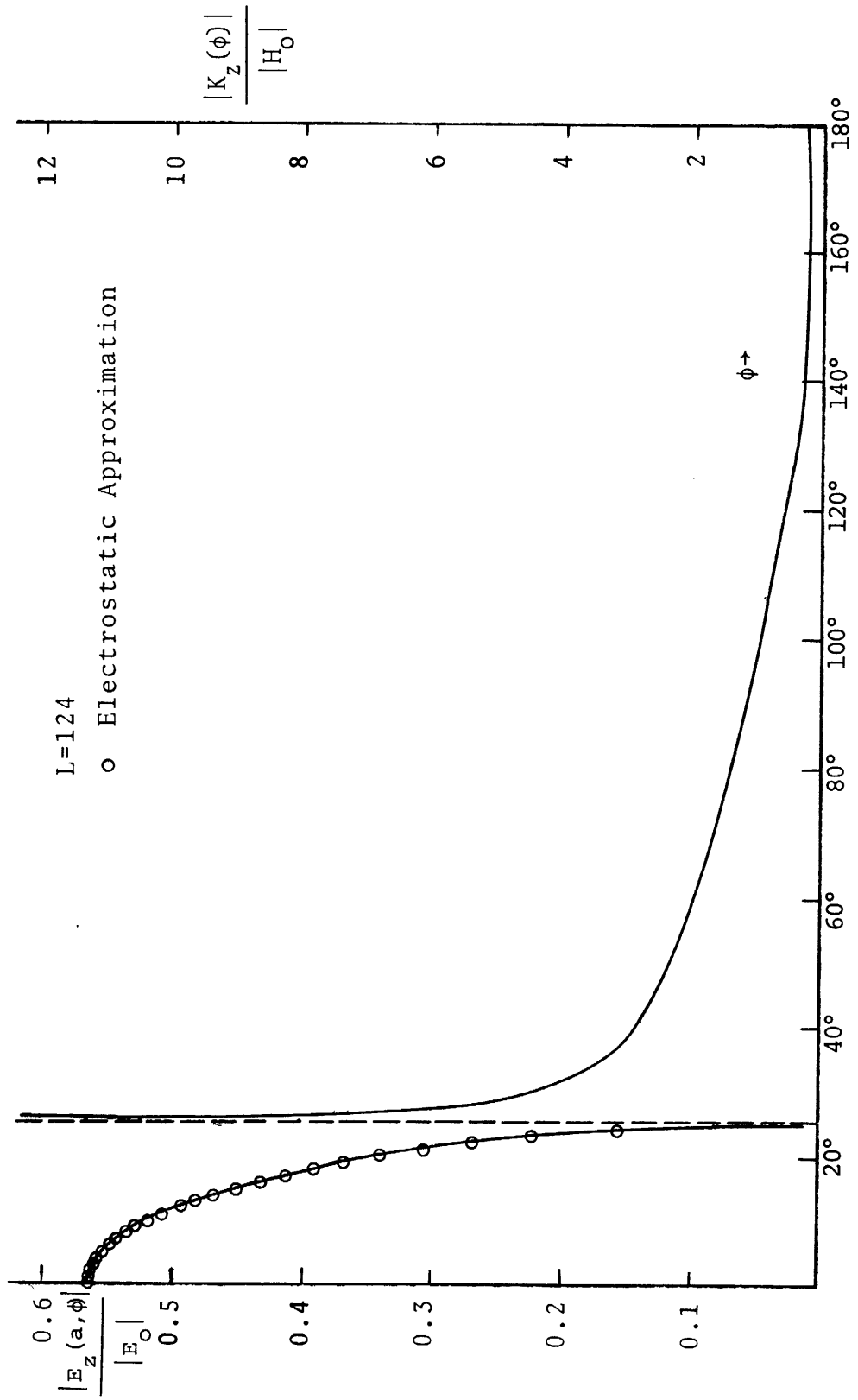


FIGURE 23. ELECTRIC FIELD IN THE SLOT, SURFACE CURRENT ON THE CONDUCTOR, $\gamma=1.000, \phi_0=25^\circ$

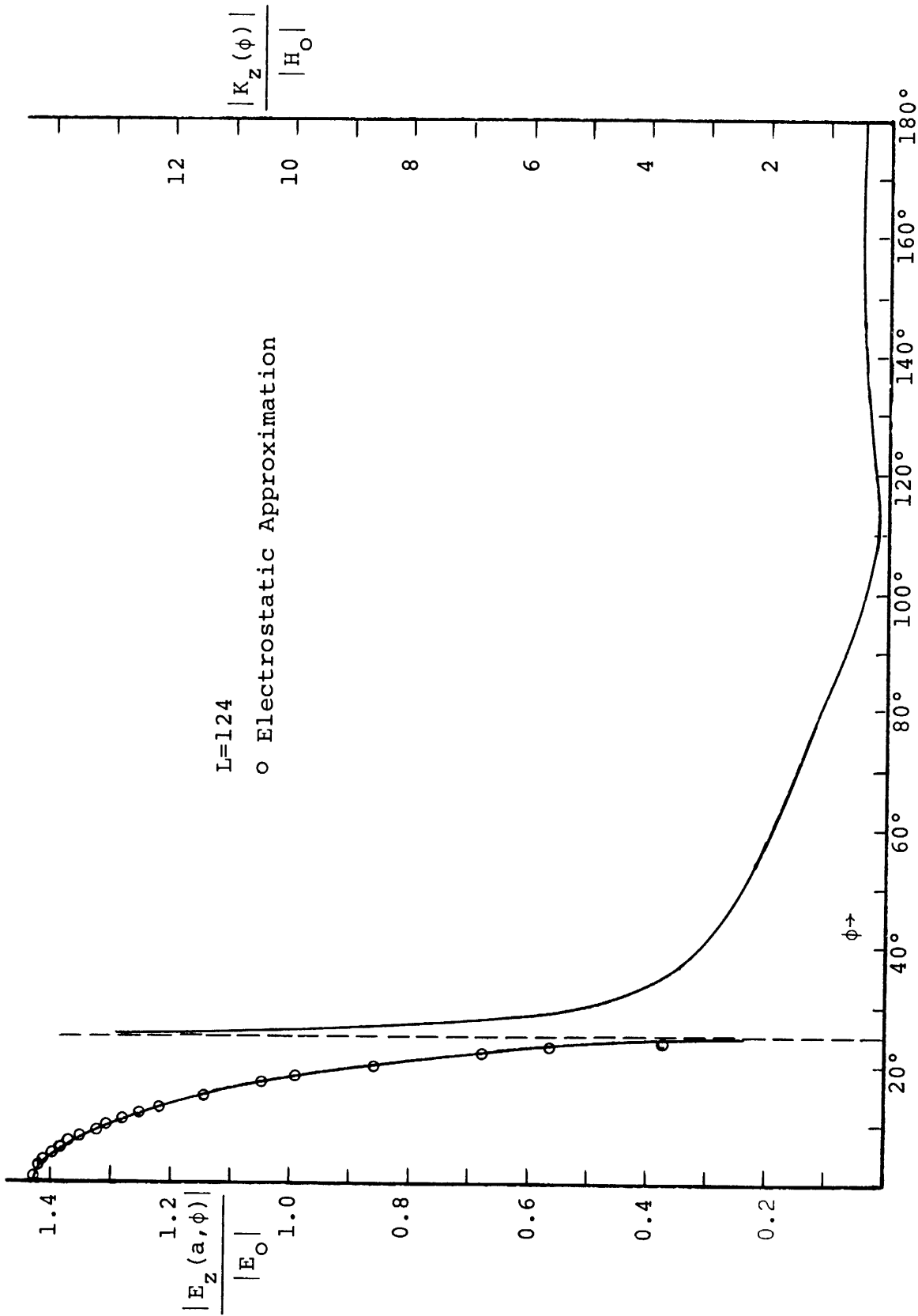


FIGURE 24. ELECTRIC FIELD IN THE SLOT, SURFACE CURRENT ON THE CONDUCTOR;
 $\gamma=2.00$ $\phi_0=25^\circ$

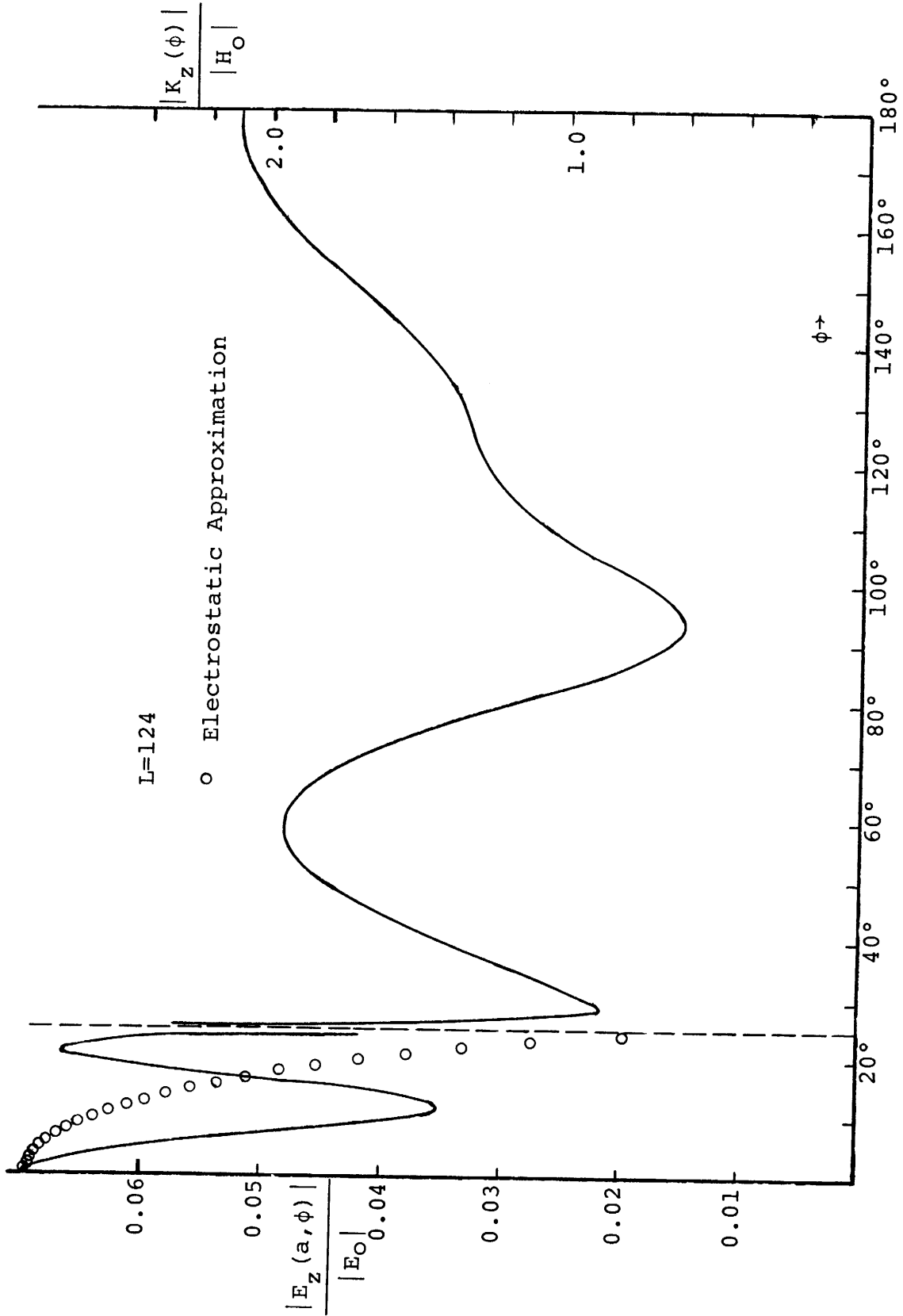


FIGURE 25. ELECTRIC FIELD IN THE SLOT, SURFACE CURRENT ON THE CONDUCTOR;
 $\gamma=3.830$, $\phi_0=25^\circ$

TABLE 36. THE DISTRIBUTION OF THE ELECTRIC FIELD OVER THE APERTURE FOR HALF SLOT ANGLE $\phi_0=20^\circ$

ϕ	$\gamma=1.00$		$\gamma=2.00$		$\gamma=3.83$	
	$ E_z / E_0 $	Phase	$ E_z / E_0 $	Phase	$ E_z / E_0 $	Phase
0°	0.444	-126.7°	1.020	-178.3°	0.0594	-99.1°
1.0	0.443	-126.7	1.020	-178.3	0.0592	-99.3
2.0	0.441	-126.7	1.020	-178.3	0.0585	-100.2
3.0	0.439	-126.7	1.010	-178.3	0.0575	-101.5
4.0	0.435	-126.6	1.000	-178.4	0.0561	-103.5
5.0	0.430	-126.6	0.990	-178.4	0.0544	-106.2
6.0	0.423	-126.6	0.974	-178.4	0.0526	-109.5
7.0	0.416	-126.5	0.956	-178.5	0.0507	-113.6
8.0	0.407	-126.5	0.935	-178.5	0.0488	-118.5
9.0	0.397	-126.4	0.910	-178.6	0.0473	-124.1
10	0.385	-126.4	0.882	-178.7	0.0460	-130.4
11	0.371	-126.3	0.850	-178.8	0.0452	-137.2
12	0.356	-126.2	0.814	-178.9	0.0449	-144.1
13	0.339	-126.1	0.774	-179.0	0.0450	-150.9
14	0.320	-126.1	0.728	-179.1	0.0454	-157.3
15	0.298	-126.0	0.677	-179.2	0.0457	-163.2
16	0.273	-125.9	0.618	-179.3	0.0455	-168.4
17	0.243	-125.8	0.550	-179.5	0.0444	-176.8
18	0.208	-125.6	0.469	-179.6	0.0416	
19	0.164	-125.5	0.369	-179.7	0.0358	-180.0

TABLE 37. THE DISTRIBUTION OF THE ELECTRIC FIELD OVER THE APERTURE FOR HALF SLOT ANGLE $\phi_0=25^\circ$

ϕ	$\gamma=1.00$		$\gamma=2.00$		$\gamma=3.83$	
	$ E_z / E_0 $	Phase	$ E_z / E_0 $	Phase	$ E_z / E_0 $	Phase
0°	0.564	-124.6	1.430	-173.4	0.0699	-67.4
1	0.564	-124.6	1.430	-173.4	0.0695	-67.6
2	0.562	-124.6	1.430	-173.4	0.0683	-68.1
3	0.560	-124.6	1.420	-173.4	0.0663	-69.1
4	0.557	-124.6	1.410	-173.4	0.0636	-70.7
5	0.553	-124.5	1.400	-173.3	0.0603	-72.8
6	0.547	-124.5	1.380	-173.3	0.0564	-75.6
7	0.541	-124.5	1.370	-173.3	0.0521	-79.4
8	0.534	-124.4	1.350	-173.2	0.0477	-84.5
9	0.525	-124.4	1.330	-173.2	0.0433	-91.2
10	0.516	-124.3	1.300	-173.1	0.0394	-100.0
11	0.505	-124.2	1.270	-173.0	0.0365	-111.1
12	0.494	-124.2	1.240	-173.0	0.0351	-124.0
13	0.481	-124.1	1.210	-172.9	0.0357	-137.6
14	0.466	-124.0	1.170	-172.8	0.0381	-150.2
15	0.450	-123.9	1.130	-172.7	0.0420	-160.7
16	0.433	-123.8	1.080	-172.6	0.0469	-169.1
17	0.413	-123.7	1.030	-172.5	0.0521	-175.5
18	0.392	-123.6	0.973	-172.4	0.0572	-179.6
19	0.368	-123.5	0.912	-172.3	0.0617	-175.9
20	0.341	-123.3	0.844	-172.1	0.0652	-173.0
21	0.311	-123.2	0.767	-172.0	0.0671	-170.8
22	0.276	-123.1	0.680	-171.9	0.0666	-169.1
23	0.235	-123.0	0.578	-171.7	0.0629	-167.8
24	0.185	-122.8	0.452	-171.6	0.0542	-166.7

TABLE 38. MORSE-FESHBACH ELECTROSTATIC APPROXIMATION TO THE AMPLITUDE OF THE APERTURE ELECTRIC FIELD NORMALIZED TO THE THEORETICAL VALUE AT THE SLOT CENTER FOR HALF SLOT ANGLES $\phi_0=20^\circ$ AND $\phi_0=25^\circ$

ϕ	$\phi_0=20^\circ$			$\phi_0=25^\circ$		
	$\gamma=1.00$	$\gamma=2.00$	$\gamma=3.830$	$\gamma=1.00$	$\gamma=2.00$	$\gamma=3.830$
0°	0.4440	1.0200	0.0594	0.5640	1.4300	0.0699
1°	0.4436	1.0190	0.0593	0.5635	1.4288	0.0698
2°	0.4418	1.0148	0.0591	0.5622	1.4254	0.0696
3°	0.4390	1.0085	0.0587	0.5599	1.4197	0.0694
4°	0.4350	0.9994	0.0582	0.5567	1.4116	0.0690
5°	0.4299	0.9876	0.0575	0.5526	1.4011	0.0685
6°	0.4235	0.9730	0.0567	0.5475	1.3882	0.0679
7°	0.4159	0.9555	0.0556	0.5414	1.3728	0.0671
8°	0.4069	0.9348	0.0544	0.5343	1.3548	0.0662
9°	0.3965	0.9109	0.0530	0.5262	1.3341	0.0652
10°	0.3845	0.8833	0.0514	0.5169	1.3106	0.0641
11°	0.3708	0.8519	0.0496	0.5065	1.2841	0.0628
12°	0.3552	0.8160	0.0475	0.4948	1.2545	0.0613
13°	0.3374	0.7751	0.0451	0.4817	1.2214	0.0597
14°	0.3171	0.7284	0.0424	0.4673	1.1847	0.0579
15°	0.2937	0.6747	0.0393	0.4512	1.1440	0.0559
16°	0.2664	0.6120	0.0356	0.4334	1.0988	0.0537
17°	0.2339	0.5373	0.0313	0.4135	1.0485	0.0513
18°	0.1935	0.4446	0.0259	0.3914	0.9924	0.0485
19°	0.1386	0.3185	0.0185	0.3666	0.9294	0.0454
20°	0.0000	0.0000	0.0000	0.3384	0.8580	0.0419
21°				0.3060	0.7759	0.0379
22°				0.2679	0.6792	0.0332
23°				0.2210	0.5604	0.0274
24°				0.1579	0.3718	0.0196
25°				0.0000	0.0000	0.0000

TABLE 39. NORMALIZATION CONSTANTS $A(\gamma, \phi_0)$ FOR THE MORSE-FESHBACH ELECTROSTATIC APPROXIMATION TO THE SLOT ELECTRIC FIELD

γ	$\phi_0=20^\circ$	$\phi_0=25^\circ$
	1.00	0.4440
2.00	1.0220	1.4300
3.83	0.0594	0.0699

TABLE 40. SURFACE CURRENT DISTRIBUTION AROUND CONDUCTOR FOR HALF SLOT ANGLE $\phi_0=20^\circ$

ϕ	$\gamma=1.00$		$\gamma=2.00$		$\gamma=3.83$	
	$ K_z / H_0 $	Phase	$ K_z / H_0 $	Phase	$ K_z / H_0 $	Phase
21.3°	9.370	-35.0	10.400	-89.6°	0.740	-98.3
23.9°	4.500	-33.8	4.890	-87.9	0.627	-105.7
26.5°	3.680	-32.5	3.940	-86.2	0.735	-107.0
29.0°	3.240	-31.0	3.410	-84.2	0.863	-106.4
31.6°	2.960	-29.5	3.080	-82.0	1.000	-104.9
34.2°	2.770	-27.7	2.840	-79.5	1.140	-102.8
36.8°	2.620	-25.9	2.650	-76.8	1.280	-100.3
39.4°	2.500	-23.9	2.500	-73.9	1.410	-97.5
41.9°	2.390	-21.8	2.370	-70.8	1.540	-94.3
44.5°	2.300	-19.6	2.250	-67.5	1.650	-91.0
49.7°	2.130	-14.7	2.040	-60.3	1.840	-83.5
54.8°	1.990	-9.4	1.850	-52.2	1.950	-75.2
60.0°	1.850	-3.7	1.670	-43.5	1.970	-66.0
65.2°	1.720	2.5	1.490	-33.9	1.890	-55.9
70.3°	1.600	9.1	1.320	-23.7	1.710	-44.5
75.5°	1.480	16.0	1.160	-12.6	1.460	-31.4
80.6°	1.370	23.3	0.995	-0.7	1.150	-15.1
85.8°	1.250	30.9	0.841	12.3	0.845	7.7
91.0°	1.150	38.7	0.697	26.6	0.630	42.8
96.1°	1.040	46.7	0.567	42.9	0.621	85.9
101.3°	0.941	55.0	0.456	61.7	0.778	117.3
106.5°	0.843	63.4	0.370	84.0	0.966	135.9
111.6°	0.750	72.1	0.314	109.6	1.120	147.2
116.8°	0.660	81.1	0.289	136.5	1.220	153.9
121.9°	0.575	90.6	0.286	161.4	1.290	157.1
127.1°	0.496	100.7	0.295	-177.4	1.330	157.5
132.3°	0.424	111.8	0.305	-159.5	1.380	155.8
137.4°	0.362	124.3	0.310	-144.2	1.460	153.3
142.6°	0.312	138.4	0.310	-130.5	1.560	150.8
147.7°	0.277	154.0	0.304	-118.1	1.680	149.1
152.9°	0.259	170.0	0.296	-106.6	1.800	148.2
158.1°	0.254	-175.4	0.288	-96.1	1.910	148.0
160.6°	0.256	-169.0	0.284	-91.4	1.960	148.1
163.2°	0.259	-163.5	0.281	-87.0	2.000	148.3
165.8°	0.263	-158.8	0.278	-83.1	2.040	148.5
168.4°	0.267	-155.0	0.276	-79.7	2.070	148.7
171.0°	0.271	-152.0	0.274	-76.9	2.090	148.9
173.5°	0.274	-149.7	0.273	-74.8	2.110	149.1
176.1°	0.277	-148.3	0.273	-73.3	2.130	149.2
178.7°	0.278	-147.5	0.272	-72.6	2.130	149.2

TABLE 41. THE SURFACE CURRENT DISTRIBUTION AROUND THE CONDUCTOR FOR HALF SLOT ANGLE $\phi_0=25^\circ$

ϕ	$\gamma=1.00$		$\gamma=2.00$		$\gamma=3.83$	
	$ K_z / H_0 $	Phase	$ K_z / H_0 $	Phase	$ K_z / H_0 $	Phase
26.3°	10.700	-32.2°	12.900	-81.0	11.100	-105.3
28.8°	5.000	-30.8	5.900	-79.4	8.690	-106.2
31.3°	4.030	-29.4	4.660	-77.8	9.640	-105.0
33.8°	3.500	-27.8	3.980	-75.9	1.080	-103.0
36.3°	3.160	-26.1	3.540	-73.9	1.210	-100.6
38.8°	2.920	-24.3	3.230	-71.6	1.340	-97.8
43.8°	2.590	-20.3	2.780	-66.6	1.580	-91.5
48.7°	2.350	-15.8	2.460	-60.8	1.770	-84.3
53.8°	2.160	-10.8	2.200	-54.3	1.900	-76.4
58.7°	2.000	-5.5	1.970	-47.2	1.940	-67.6
63.7°	1.850	0.3	1.750	-39.4	1.900	-58.0
68.7°	1.710	6.4	1.540	-31.2	1.760	-47.4
73.7°	1.580	12.9	1.340	-22.3	1.540	-35.4
78.7°	1.450	19.7	1.140	-12.9	1.270	-21.0
83.7°	1.330	26.8	0.952	-2.9	0.964	-2.1
88.7°	1.220	34.2	0.768	8.0	0.704	26.0
93.7°	1.110	41.8	0.593	20.2	0.591	66.4
98.7°	1.000	49.6	0.433	34.9	0.679	104.3
103.8°	0.903	57.5	0.293	54.6	0.859	128.3
108.8°	0.805	65.7	0.188	86.6	1.030	142.8
113.8°	0.712	74.2	0.155	136.1	1.160	151.8
118.8°	0.623	83.0	0.196	177.1	1.250	157.1
123.8°	0.539	92.4	0.258	-159.0	1.300	159.3
128.8°	0.461	102.5	0.315	-143.0	1.340	159.0
133.8°	0.392	113.8	0.359	-130.6	1.390	157.1
138.8°	0.332	126.7	0.390	-120.0	1.470	154.6
143.8°	0.286	141.5	0.409	-110.6	1.570	152.4
148.8°	0.256	157.8	0.418	-102.0	1.680	150.8
153.8°	0.242	174.3	0.421	-94.2	1.800	150.1
158.8°	0.242	-171.0	0.420	-87.3	1.900	150.0
161.3°	0.245	-164.7	0.418	-84.2	1.950	150.1
163.8°	0.250	-159.4	0.417	-81.3	1.990	150.2
166.3°	0.255	-154.9	0.415	-78.8	2.020	150.4
168.8°	0.260	-151.2	0.414	-76.7	2.050	150.6
171.3°	0.265	-148.4	0.412	-74.9	2.080	150.8
173.8°	0.268	-146.3	0.411	-73.6	2.100	150.9
176.3°	0.271	-144.9	0.411	-72.7	2.110	151.0
178.8°	0.272	-144.2	0.410	-72.2	2.110	151.1

where $A(\gamma)$ is a constant of proportionality. We have normalized the Morse-Feshbach approximation formula in eq. (18) so that it coincides at $\phi = 0^\circ$ with our calculated values. Table 39 contains the corresponding values found for the proportionality constants $A(\gamma, \phi_0)$ and Table 38 gives the values obtained for the amplitude of the slot electric field over the slot using eq. (18). Now for the half slot angle we find for the slot width to wavelength ratio

$$\frac{2a\phi_0}{\lambda} = \gamma \frac{\phi_0}{180}$$

This ratio is about 0.1 for $\gamma = 1.000$, 0.2 for $\gamma = 2.000$ when $\phi_0 = 20^\circ$ and about 0.14 for $\gamma = 1$ and about 0.27 for $\gamma = 2$ when $\phi_0 = 25^\circ$. These ratios are hardly very small compared with unity. Nevertheless if we compare Tables 38 with 36 and 37 we find as shown by the small circles in Figures 20, 21 and 23, 24 that eq. (18) is a quite adequate analytic representation of the slot electric field distribution. For $\gamma = 3.830$ the slot width to wavelength ratios are approximately 0.5 for $\phi_0 = 20^\circ$ and 0.6 for $\phi_0 = 25^\circ$ which are definitely not much smaller than unity. The results using eq. (18) are the small circles superimposed on the more accurate values in Figures 22 and 25. The accurate distributions are not quite parabolic in shape over the aperture. However, it should be pointed out that the areas under the exact curves and under the approximate distributions are quite close in value. Thus the average energy over the slot is well represented by the Morse and Feshbach approximation even at resonance for the $\phi_0 = 20^\circ$ and $\phi_0 = 25^\circ$ slots.

b) Electric Field in the Slot At Resonance

We now investigate the electric field in the slot at resonance. In Figure 26 we have plotted the real and imaginary parts of the electric field over the slot at $\gamma = 3.830$ for both $\phi_0 = 20^\circ$ and $\phi_0 = 25^\circ$. To facilitate comparison of the behavior of the distribution across the slot we have taken the abscissa as ϕ/ϕ_0 . We have also plotted the corresponding $\phi_0 = 30^\circ$ slot distributions from Figure 41 in S.E.R.A.V. We note that for ϕ/ϕ_0 less than about 0.3

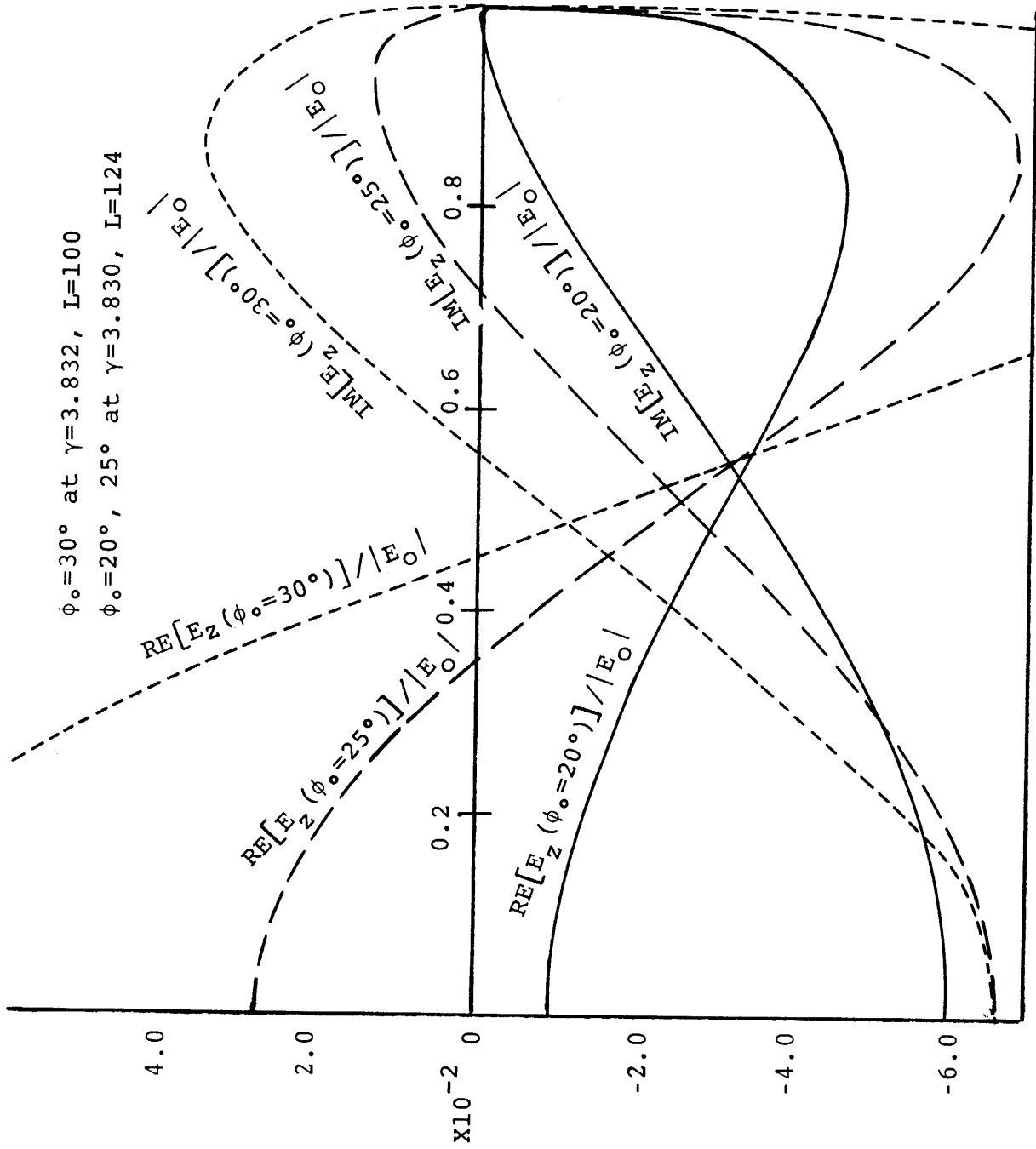


FIGURE 26. Real and Imaginary Parts of the Slot Electric Field Near Resonance

the RE $[E_z]$ is, on the average, considerably larger than the corresponding $\phi = 20^\circ$ and $\phi_0 = 25^\circ$ values. The same relative behavior is seen for $0.65 < \phi < 0.95$. For the same reasons discussed in S.E.R.A.V we conclude that constraint condition I on the real and imaginary parts of the slot electric field at resonance, which holds for the narrow slot, obtains for the $\phi_0=20^\circ$ and $\phi_0=25^\circ$ slot cases studied in this report. We further observe that the lower γ value of 3.830 again indicates the interior resonance has been shifted to lower frequency.

c) Back-Scattering Cross-Section

The final characteristic to be considered is the back-scattering cross-section for the smaller slot angles. Figure 27 is the $\phi_0=30^\circ$ plot of back-scattering cross-section as a function of circumference to wavelength ratio published as Figure 9 in S.E.R.A.V. We have merely superimposed the results obtained for the slot angles $\phi_0=20^\circ$ and 25° , using $L=124$, at $\gamma=1.000, 2.000$ and 3.830 . Not too much new information can be obtained from the curves. One characteristic that seems evident however is that the smaller the slot angle the smaller the back-scattering cross-section seems to be.

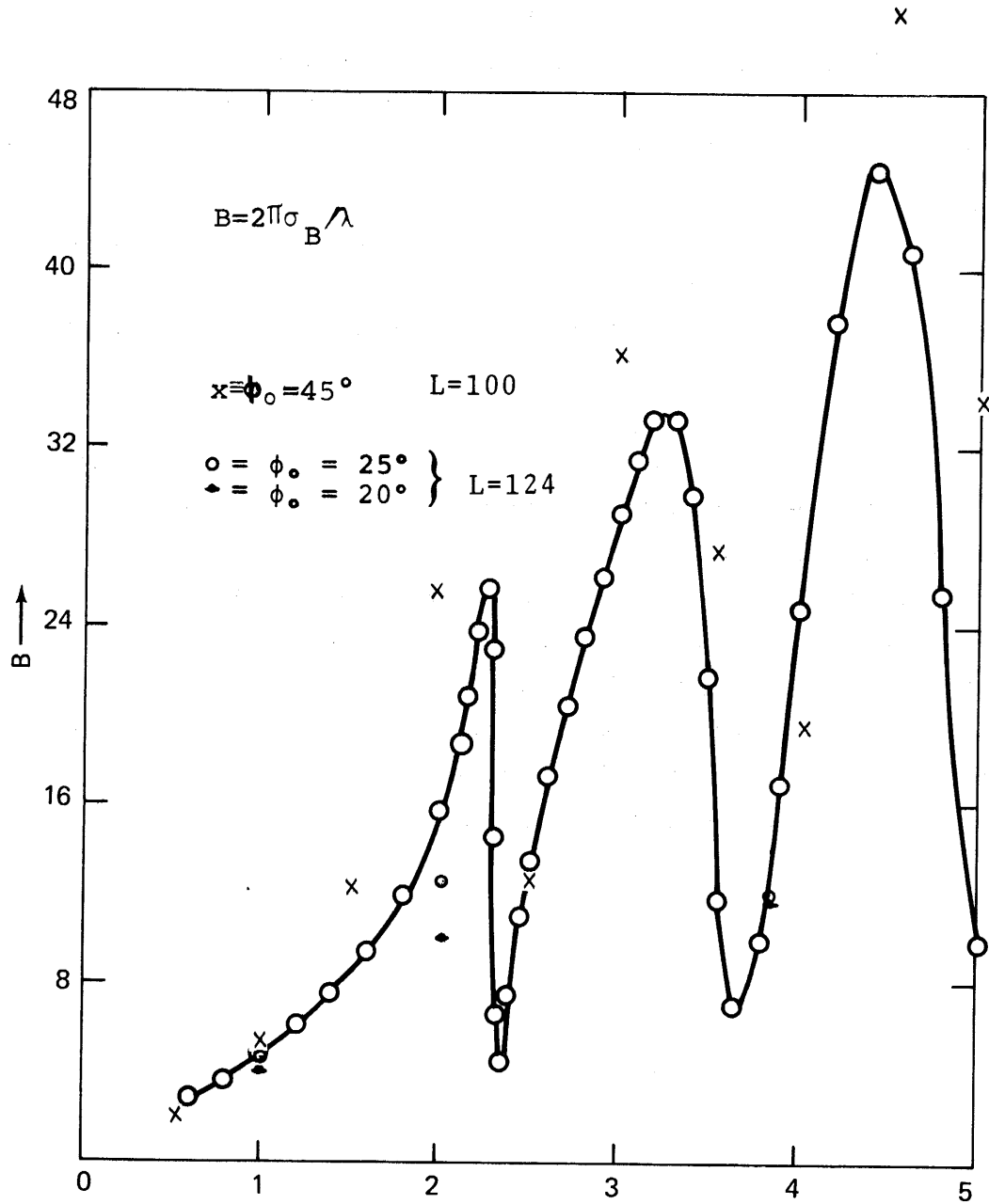


Figure 27. Back-Scattering Cross-Section, $\phi_0 = 30^\circ$

V. COMMENTS ON THE COMPUTER PROGRAM

In performing the calculations reported on in this publication the program STEPS described in S.E.R.A.V was appropriately modified where needed. Only the modifications will be described here. The reader is referred to the earlier paper for the basic discussion of the main computer program. Addition of two subroutines to STEPS constitutes the major change. All the other changes are in the main program itself. They involve reading in additional parameters and calling the new subroutines when they are required.

Essentially, the modified version of STEPS takes the computed values, as determined by the original program, of the electrical field at $\rho=a$ over the cylindrical aperture and then uses them to compute a distribution of the electric field. This distribution is determined along a ray extending outward from the axis of the cylinder. Values of electric field have been obtained along such rays beyond the aperture in the cylinder out to a distance equal to two cylindrical radii from the cylinder itself.

The additional data input required in the modified version of STEPS are

i) RADANG - This specifies the angle from the radial line through the center of the slot aperture to the radial line along which the distribution of the electric field is required. Thus, for example, if the distribution is required along a ray bisecting the aperture RADANG would be assigned the value zero. Again if the electric field was required along a ray passing through the very edge of the slot itself the value assigned to RADANG would be PHIO, an original data input in the unmodified version of STEPS. RADANG can be varied from 0 to 2π .

ii) MLIMIT - This denotes the maximum order of the Bessel functions considered by the subroutine EZROH, described below, which was added to STEPS. The accuracy needed in the calculations required a rather large value for MLIMIT. For most cases treated a value of about 80 proved to be sufficient.

iii) RHOLO - This is the closest value, along any given ray, to the axis of the slotted cylinder for which calculations are to be carried out. It is expressed as either equal to zero or numerically in units of the cylinder radius.

iv) RHODEL - The interval along a ray between successive points at which computation of the electric field is carried out.

v) RHOHI - The largest value along a ray for which field calculations are performed. For radial lines passing through the aperture in the cylinder its maximum value is 2. For rays terminating at the cylinder wall itself the maximum value is unity.

vi) ANGLE - This is just RADANG expressed in degrees. This parameter is used only in conjunction with the Gould Plotter.

vii) PHI 1 - Similarly this is PHIO expressed in degrees for use only in conjunction with the Gould Plotter.

One of the additional subroutines used to augment the basic STEPS program we have dubbed with the identifying title EZRHO. This subroutine effects the calculation of the electric field along radial lines for points within the cylinder where they are at a distance from the center equal to or less than the radius of the cylinder. Two large DO loops are involved. The outer loop considers in turn each discrete point along a given radial line. The inner DO loop cycles through the same type of calculation successively increasing the order of the Bessel functions each time until the value MLIMIT is attained. At that stage output is listed. This output consists of the position along the ray for which the field computations are being performed and the corresponding complex values of the electric field in the form of the amplitude and the phase angle. Upon completion of the calculation of the electric field at all desired points along a given ray the modified version of STEPS plots a curve of amplitude of electric field per unit incident field versus radial position in units of the slotted cylinder radius. One curve is plotted for each input value of ETA (circumference to wavelength ratio), PHIO, and RADANG.

A second subroutine designed to augment the basic program STEPS and called BIGRHO treats positions along a given ray that lie outside of the slotted cylinder. It is called when needed by EZRHO and

provides the changes required to compute the complex electric field in the region exterior to the diffracting, conducting cylinder.

GOULD1, a subroutine called into action by the subrouting EZRHO, is utilized in the modified version of STEPS. This is a standard plotting subroutine used at many computer installations and hence we have omitted any discussion of it from this report. Anyone not having GOULD1 available can use our version of STEPS to obtain the electric field radial distributions by merely suppressing all reference to GOULD1 in our program. This action will in no way affect the calculations.

The modified version of the earlier program STEPS which determines the interior and exterior electric field distributions has not been explicitly included in this report. Those desiring the program should contact the authors and it will be then made available.

VI. CONCLUSIONS AND DISCUSSION

With the publication of this report we will have presented, but for one exception, a nearly complete solution and the corresponding understanding of the scattering characteristics of the infinite, axially slotted, conducting circular cylinder. The exception is the diffraction problem in the case of a very narrow slot in the cylinder. This problem has also been resolved both theoretically and experimentally and the results obtained have been incorporated into a report in this series which shall be subsequently published and disseminated to the community. As has been pointed out in the past the results for this special case are of significant import to merit a report devoted solely to this limit. Nevertheless we now have the interior and slot region exterior electric fields, the surface current distribution over the conductor and the back-scattering cross-section for slot angles that are large enough so that we are dealing with a circular cylindrical strip. These results have been obtained for a range of frequencies that include the lower modes of the system. Thus we have knowledge of the effect of the slot on these resonances as well as the variation of fields and currents from beyond cutoff through the lower resonances as a function of slot angle. Much has been learned about the range of validity of existing approximations for the fields and currents of slotted cylinders.

Having the capability of solving for fields and currents for the slotted cylinder is a considerable advantage. Fortunately sparse matrix techniques have been developed to the point where we can perform a large but not unreasonable number of frequency domain calculations and then appropriately utilize these computer techniques to effect Fourier inversion to desired pulse shapes and thereby attain the time domain response for the slotted cylinder. These numerical methods in fact are one way of obtaining information on the location of resonances for a system and the corresponding line widths. Although the results are not included in this paper determinations of some of these resonances and the linewidths via sparse matrix techniques have been effected. Dependence of these on slot angle has been established also and the results obtained in this way compared

with those obtained in other manners. These shall be reported on in subsequent papers in this series. In the EMP problem area this represents a significant fundamental degree of evolution.

Last but not least the solutions we have obtained for the infinite, axially slotted cylinder scattering problem have considerable potential value for the more complicated problem of the finite length cylinder. We have carried out an extensive program of careful measurement of the fields and currents occurring in the case of a large number of finite cylindrical scatterers with and without apertures. With the infinite cylinder solutions in hand we have examined the limits to which they can be used to approximate the results obtained for the finite cylinders. Numerous situations have been uncovered for which the relatively simpler infinite slotted cylinder either is an adequate approximate solution or serves as a great labor-saving guide to the actual more precise solution in the much more involved finite problem. In view of the fact that a great many real systems are closely approximated by finite cylinders with appropriately sized and located apertures the solution for the infinite axially slotted cylinder has provided us with a tool of tremendous practical value for analyzing quite a large spectrum of real finite scattering problems.

A sequence of reports presenting the experimental results for finite cylinders will follow this one. In these we shall demonstrate the utility inherent in the infinite cylinder case and simultaneously present an experimental technique of considerable versatility which is still undergoing development.

REFERENCES

1. J. N. Bombardt (HDL) and L. F. Libelo "Scattering of Electromagnetic Radiation by Apertures: V Surface Current, Tangential Aperture Electric Field, and Back-Scattering Cross-Section for the Axially Slotted Cylinder at Normal, Symmetric Incidence."
2. A. Sommerfeld, "Partial Differential Equations" p. 29-31 Academic Press, New York, NY 1949.
3. P. M. Morse and Feshbach, "Methods of Theoretical Physics" Part II, p. 1387-1398, McGraw-Hill Book Co., New York, NY 1953.
4. V. N. Koshparenok and V. P. Shestopalov, "Diffraction of a Plane Electromagnetic Wave by a Circular Cylinder with a Longitudinal Slot" Zh. Vychisl. i Mat. Fiz., 11 719-737 (1971).
5. J. J. Bowman, T. B. A. Senior and P. L. E. Uslenghi, eds., "Electromagnetic and Acoustic Scattering by Simple Shapes" p. 92-93, North Holland Publishing Co., Amsterdam, The Netherlands, 1969.
6. R. F. Harrington, "Time Harmonic Electromagnetic Fields" p. 232-234 McGraw-Hill Book Co., New York 1961.
7. M. Kerker, "The Scattering of Light and Other Electromagnetic Radiation" Ch. 6, Academic Press, New York 1969.
8. J. N. Bombardt and L. F. Libelo, "S.E.R.A.:III. An Alternative Integral Equation with Analytic Kernels for the Slotted Cylinder Problem" HDL-TR-1588 Harry Diamond Laboratory, Washington, D.C., August 1972.
9. "Coupling of Plane-Polarized Electromagnetic Waves to Cylindrical Modes", C. L. Andrews, L. F. Libelo, D. P. Margolis, and R. S. Dunbar, Optics News, page 25, Sep 1975.